ALMA MATER STUDIORUM - UNIVERSITÀ DI BOLOGNA

SCUOLA DI INGEGNERIA E ARCHITETTURA

Corso di laurea specialistica a ciclo unico in Ingegneria Edile-Architettura
Dipartimento di Ingegneria Industriale

Tesi di laurea in
Fisica Tecnica Ambientale

Aerogel Incorporated Plasters and Mortars: the case study of precast panels

Candidato
Matteo Calisesi

Relatore
Chiar.mo Prof. Massimo Garai

Correlatore
Prof. Umberto Berardi

Anno Accademico 2016/17
Sessione III

Abstract

The aim of many current studies regarding building envelopes is the improvement of their thermal resistance. In particular, many attempts have been taken to develop highly insulating materials for advanced building envelopes. The present research investigates the possibility to include aerogels in plaster and mortar products. Several samples of Aerogel Incorporated Plaster and Aerogel Incorporated Mortar were prepared by adding granules of aerogel to different types of plasters and mortars. The thermal conductivity of each sample was then measured by means of a heat flow meter apparatus. In the case of the samples of Aerogel Incorporated Mortar, the mechanical strength and the permeability were tested as well. The results showed that the thermal conductivity and the mechanical strength linearly decreased by increasing the quantity of aerogel added to the mixes. For example, while the control mixture of mortar had a thermal conductivity of 0.28 W/mK and a compressive strength of 50.3 MPa, the mixture of mortar with an addition of 36 vol.% of aerogel halved the thermal conductivity to 0.14 W/mK and reduced the compressive strength to 4.1 MPa. Finally, an Aerogel Incorporated Mortar precast panel was designed and the hygrothermal analysis of the panel was carried out by using WUFI Pro software. Results showed that the thermal transmittance of the panel was reduced by 25% compared to traditional precast panels, which suggested that energy savings and reduced costs during the lifetime of the building could be achieved.

L’obiettivo di molte ricerche attuali riguardanti nuove soluzioni costruttive è il miglioramento della loro resistenza termica. In particolare, molti sforzi sono stati fatti per sviluppare materiali altamente isolanti con l’obiettivo di ottenere pacchetti di tamponamento ad elevate prestazioni. La presente tesi si propone di studiare la possibilità di includere particelle di aerogel in intonaci e malte. Campioni di diverse miscele di Aerogel Incorporated Plaster e Aerogel Incorporated Mortar sono stati preparati aggiungendo granuli di aerogel a diversi tipi di intonaci e malte. La conducibilità termica di ogni campione è stata misurata utilizzando un termoflussimetro. Nel caso della miscela di Aerogel Incorporated Mortar è stata testata anche la resistenza meccanica e la permeabilità al vapore acqueo dei campioni. I risultati hanno mostrato che la conducibilità termica e la resistenza meccanica a compressione diminuiscono linearmente all’aumentare della quantità di aerogel aggiunta alle miscele. Per esempio, mentre i campioni di controllo di malta avevano una conduttività termica di 0.28 W/mK e una resistenza meccanica di 50.3 MPa, i campioni di malta con l’aggiunta del 36 vol.% di aerogel hanno dimezzato la conducibilità termica ad un valore di 0.14 W/mK e ridotto la resistenza meccanica a 4.1 MPa. Infine, un pannello prefabbricato di Aerogel Incorporated Mortar è stato progettato e ne è stata fata un’analisi igrotermica utilizzando il programma WUFI Pro. I risultati hanno mostrato che la resistenza termica del pannello è stata ridotta del 25% rispetto ad i tradizionali pannelli prefabbricati, il che suggerisce che possano essere ottenuti risparmi energetici e conseguenti riduzioni dei costi durante la vita dell’edificio.

Acknowledgements

Questa tesi conclude un lungo percorso da studente iniziato molti anni fa, ricco di soddisfazioni e di momenti edificanti.

Nonostante il raggiungimento di questo traguardo sia principalmente frutto del mio impegno, voglio ringraziare gli amici ed i parenti che mi sono stati vicini in questi anni.

In particolare, voglio ringraziare i miei genitori Gabriella e Gianfranco per avermi supportato durante questo percorso e dato la possibilità di studiare in Italia, in Portogallo, ed in Canada. Voglio anche ringraziare le persone care con cui non posso condividere questo momento importante. Un pensiero particolare lo dedico a mio nonno Guido, da cui ho imparato molte cose tra cui la dedizione per il lavoro e la passione per la vita.

List of contents

List of figures

List of tables

List of abbreviations

α	Sound absorption coefficient
$\rho_{aerogel}$	Density of the aerogel
ρ_{air}	Density of the air
ρ_b	Bulk density
α_l	Light absorptance
ρ_l	Normal-hemispherical reflectance
ρ_s	Skeletal density
ρ_{SiO_2}	Density of the silica
AFM	Atomic force microscopy
AIC	Aerogel Incorporated Concrete
AIM	Aerogel Incorporated Mortar
AIP	Aerogel Incorporated Plaster
Al_2O_3	Aluminium(III) oxide (Al_2O_3)
APD	Ambient pressure drying
CASH	Calcium silicate hydrate
CH	Calcium hydroxide
CNTs	Carbon nanotubes
CO_2	Carbon dioxide
d	Gas molecule collision diameter
D_W	Liquid transport coefficient
e	Extinction coefficient
E	Modulus of elasticity
EPS	Expanded polystyrene
EtOH	Ethanol
f_c	Compressive strength
f_t	Tensile strength
FT-IR	Fourier transform infrared spectroscopy
H	Enthalpy of moist building material
HPC	High-performance concrete
HTSCD	High-temperature supercritical drying
h_v	Evaporation enthalpy of water

IARC	International agency for research on cancer
IEQ	Indoor environmental quality
K_n	Knudsen number
LC	Lightweight concrete
LTSCD	Low-temperature supercritical drying
MTR	Mill test report
n	Refractive index
NanoCon	Nano concrete
NHL	Natural hydraulic lime
NIMs	Nano insulation materials
NMR	Nuclear magnetic resonance
Nu	Nusselt number
p	Water vapor partial pressure
PAS	Positron annihilation spectroscopy
PCMs	Phase change materials
P_{cr}	Critical pressure
PEDS-P_x	Polyethoxydisiloxane
PUR	Polyurethane
$q_{w.c}$	Heat flux by convection
$q_{wo.c}$	Heat flux by conduction
SA	Pozzolan (SiO2·Al2O3)
SAXS	Small angle X-ray scattering
SCC	Self-consolidating concrete
SCD	Supercritical drying
SEM	Scanning electron microscope
SiO_2	Silicon(II) oxide
T	Temperature
T_{cr}	Critical temperature
TEMs	Transmission electron microscopes
TEOS	Tetraethoxysilane
TGA	Thermogravimetry analysis
THB	Transient hot bridge
TMOS	Tetraethoxysilane
U	Thermal transmittance
UHPC	Ultra-high performance concrete
u_w	Water content
v	Velocity of a water droplet

V_a	Volume of the aerogel
V_g	Volume of the alcogel
VIPs	Vacuum insulation panels
$V_s\%$	Volume shrinkage
WVDR	Water vapour diffusion resistance WVDR
WVP	Water Vapor Permeability
XPS	Extruded polystyrene
β_c	Coefficient of collision energy transfer efficiency
β_s	Specific extinction
δ	Ratio of insulation material density to the material density
δ_w	Water vapor diffusion coefficient in air
θ	Contact angle of the water droplet on the aerogel surface
λ	Thermal conductivity
λ_{conv}	Gas state convection thermal conductivity
$\lambda_{coupling}$	Second order thermal conductivity
λ_f	Material thermal conductivity factor
λ_{gas}	Gas state thermal conductivity
λ_{leak}	Leakage thermal conductivity
λ_{rad}	Radiation infrared thermal conductivity
λ_{solid}	Solid state thermal conductivity
μ	Vapor diffusion resistance factor of dry material
ρ_w	Density of water
σ	Stefan-Boltzmann constant ($5.67\times10^{-8}W/m^2K^4$)
τ_{ir}	Transmittance of radiation in the infrared range
τ_l	Light transmittance
τ_{vis}	Transmittance of radiation in the visible range
ϕ	Percentage of porosity
φ	Relative humidity

Introduction

1.1 Global necessity of energy savings

Global warming is a huge issue nowadays. The global surface temperature has increased in the last three decades by roughly 0.5 °C due to the concentration of greenhouse gasses in the atmosphere produced by human activities. Moreover, total global emissions grew 12.7% between 2000 and 2005, with an average of 2.4% a year [1]. According to the lowest emission scenario, the global surface temperature will increase by 1.1 to 2.9 °C during the 21st century [2]. The International Energy Agency (IEA) foresees that by 2050 the emissions of CO_2 will double [3]. Models of global energy systems recommend to maintain the stable atmospheric CO_2 concentrations and below 500 ppm [4] to stop the increase of global surface temperature. The global emission growth varies from sector to sector and is dramatically different between developed and developing countries. Moreover, in the last three decades, the world's primary energy demand increased and population growth due to industrial development. Fossil fuels still dominate the market and there are limited energy reserves of not renewable resources.

It is fundamental to undertake appropriate measures to stop this CO_2 emission. Energy saving is the most relevant measure to reach this goal and could be achieved through sustainable technologies and materials. It is necessary that developed countries think about their energy strategy and policy. According to the Kyoto protocol[1], the greenhouse emissions should be reduced by 20% before 2020 compared to the emission levels of 1990. Therefore, an improvement in energy management and optimization of energy consumption might be achieved.

The building industry has a huge impact on energy consumption and greenhouse gas emissions [5]. In 1999, the residential sector's energy consumption in Europe was equivalent to 623 million tons of oil, which was 35% of the overall consumption of energy [2]. Also, in 2005, buildings released more than 30% of the total greenhouse gas emissions in several

[1]Kyoto Protocol to the UNFCCC United Nations Framework Convention on Climate Change adopted at COP3 in Kyoto (Japan), on December 11th, 1997.

developed countries [6]. For these reasons, savings and improvements within the building sector are being investigated to achieve passive houses and zero emission buildings.

1.2 Traditional and superinsulation thermal envelopes

As stated in section 1.1, the reduction of the energy consumption of buildings is necessary in order to reduce the CO_2 emissions. This goal can be achieved by decreasing the thermal losses in buildings and by improving the use of renewable energy. Recent studies have pointed out that insulation improvement measures are more cost-effective than the use of renewable energy solutions, such as solar photovoltaic, solar panels, wind energy, and geothermal energy [7]. Hence, new high performing materials are being developed in order to reduce the heat losses through the envelope of buildings and thus, reducing the size and the energy consumption for heating and cooling. Moreover, a performing thermal insulation in buildings permits to extend the periods of thermal comfort without dependence on heating and cooling systems. Also, insulation is important in terms of the retrofitting of old buildings in order to achieve lower servicing costs during the building lifetime.

The main property of building thermal insulation materials is the thermal conductivity. The cost of the materials is an important parameter to be considered in thermal insulation applications. However, many other properties are very important, e.g. perforation vulnerability, building site adaptability and cuttability, mechanical strength, fire protection, fume emission during a fire, robustness, climate change durability, resistance towards freezing/thawing cycles, water resistance, costs, embodied energy, and environmental impacts. Obviously, a material that fulfills all these properties does not exist. Nevertheless, the main goal is to reach the lowest thermal conductivity with the lowest cost in order to achieve thin and high-performance building envelopes.

Insulation materials for buildings can be classified according to their physical or chemical structure. Examples of common thermal insulation materials for buildings are mineral wool, glass wool, expanded polystyrene (EPS), extruded polystyrene (XPS), cellulose, cork, and polyurethane (PUR). A classification of traditional materials for insulation purposes is given in Fig. 1 and their market share is presented in Fig. 2. Inorganic fibrous materials, such as glass wool and organic foam materials, such as EPS and XPS dominate the market. However, according to current forecasts, by 2020 these traditional materials will start to lose their dominance as a result of superinsulation materials growth. Expanded polystyrene (EPS),

extruded polystyrene (XPS), and polyurethane (PUR) have values of thermal conductivity of about 0.033 W/mK, 0.040 W/mK, and 0.020÷0.030 W/mK [8], respectively. Nevertheless, some of them have low fire resistance or release toxic gasses during fire; for example, polyurethane causes serious health concerns in cases of fire. Furthermore, these traditional materials are used in thicker and multiple layers in order to achieve the required insulation performance. Hence, the application of these materials takes up more space, involves complex building details as well as heavier loads for the building's structure, and implies more architectural restrictions, material usage, and transport volumes.

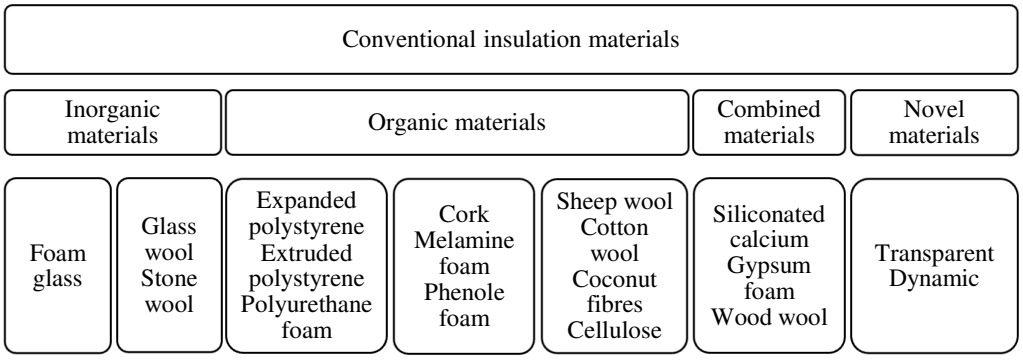

Fig. 1. Classification of traditional buildings insulation materials [2].

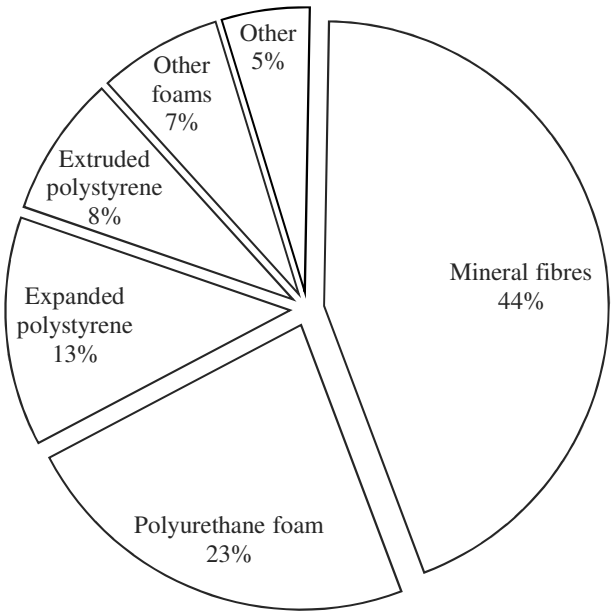

Fig. 2. Market share of traditional buildings insulation materials [2].

The aim of many current research studies is to improve building insulation materials and solutions, which is a crucial need for the insulation market of the future. For this reason, many

attempts have been done in order to develop superinsulation materials and high-performance solutions to optimize building envelopes.

Vacuum insulation panels (VIPs), phase-change materials (PCMs), and aerogel-based materials are the new promising superinsulation materials and solution for building applications. The aim of the studies on these materials is to achieve an improved thermal, sound, and hygrothermal performance as well as a good behavior in case of a fire, a long durability period, and a competitive price. However, these new materials are slowly introduced in the building sector due to the high production costs and traditional materials still offer the best performance per unit cost [7]. Hence, one of the aims of contemporary research studies on superinsulation materials is to improve the performance per unit cost.

1.3 Aerogels in buildings industry

Aerogels are synthetic and highly porous nanostructured materials created by Steven Kistler in 1931 [2]. The term "Aerogel" comes from the fact that they are produced from *gels* in which the liquid component of the *gel* is replaced with a gas. However, despite their name, aerogels are solid, rigid and dry materials. There are three types of aerogels that are obtained by using silica, carbon e alumina. However, silica aerogels are the most common and investigated ones.

Silica aerogels are formed by a cross-linked internal structure of SiO_2 with many small air-filled pores with varying diameters, between 5 nm and 70 nm. They have the highest porosity and specific surface area, as well as the lowest density compared to other known materials. Moreover, they have a translucent structure and a low refraction. Aerogels' most interesting property is their low thermal conductivity [2], attributable to the high porosity and the nano-dimensional size of the pores. On the other hand, they are very brittle due to their low tensile strength and expensive due to the low production volume as well as the high costs of materials involved in the synthesis process. Properties of silica aerogels are deeper discussed in Chapter 2.2.

Nowadays, aerogels have a striking number of applications, including sectors such as building, automotive, electronic, and clothes; for example, they are used as catalysts, thermal insulation materials, particle detectors, supercapacitors, electrodes for capacitive deionization, pesticides, cosmic dust capture, and insulation materials in buildings. The global market of aerogels grew exponentially as well as the number of companies producing aerogels and

patents involving them. In particular, silica aerogels are considered the most promising insulation materials for building applications. In fact, they are a great energy-efficient opportunity as a consequence of their high thermal performance. Thus, they can provide a very good indoor thermal comfort with slimmer envelopes. Furthermore, they have a very low embodied energy compared to traditional materials.

Aerogel-based renders represent one of the most promising solutions to reduce energy losses through envelopes. Moreover, they can be can be a good way to avoid thermal bridges in the building envelopes. In Italy, more than 90% of buildings are not in compliance with the code and need refurbishment. Aerogels represent a possible solution because they can also be a useful tool for the refurbishment and restoration of historical buildings that have to fulfill the new energy codes. Aerogels for building applications have a density between 70 kg/m^3 and 150 kg/m^3 and a very low thermal conductivity. Many efforts are being carried out in order to develop new products based on aerogels and many products have emerged in the market. Opaque aerogel panels and blankets have been developed as insulation layers for building walls and in order to decrease the thermal transmittance of components made of wood and steel. Also, glazing windows which incorporate aerogels are being developed thanks to aerogels' high optical transparency in the range of visible. More recently, some studies employed granular aerogels to develop aerogel-based materials, such as Aerogel Incorporated Plaster (AIP), Aerogel Incorporated Mortar (AIM), and Aerogel Incorporated Concrete (AIC) in order to achieve low density and low thermal conductivity [9]. Fig. 3 summarizes the most relevant aerogel-based products so far.

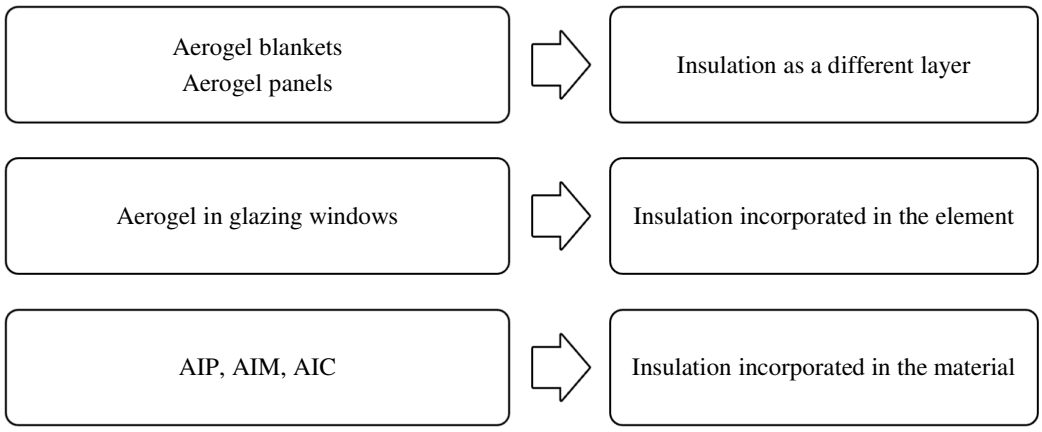

Fig. 3. Most relevant aerogel-based products.

Aerogel-based products already have many applications in roofs, facades, and windows due to their low thermal conductivity and optical transparency. Moreover, they are used as sound

insulation, fire retardant, and permit to achieve transpiration and insulation features as well as space saving [10]. However, aerogels are still expensive compared to traditional insulation materials and their effects for public use will not completely take place until the manufacture costs will be reduced. As a result, aerogels manufacturers have been focusing not only on performance improvements but also on cost reductions.

1.4 Aim of the research

The aim of the study is to develop renders based on aerogel and study their possible applications. Samples of Aerogel Incorporated Plaster and Aerogel Incorporated Mortar were prepared and tested. The thermal conductivity of the samples of Aerogel Incorporated Plaster was evaluated. The same was done for the samples of Aerogel Incorporated Mortar. Moreover, their mechanical strength was tested. Control samples of plaster and mortar were prepared in order to have a point of reference against which the samples of Aerogel Incorporated Plaster and Aerogel Incorporated Mortar were compared. Once characterized the mixtures, a case study of precast panels was developed to test the performance of the materials in a real application.

The following chapter presents the literature review on aerogel and renders based on aerogel. Chapter 3 illustrates the materials, the experimental apparatus, and the procedures used to prepare the samples of Aerogel Incorporated Plaster and Aerogel Incorporated Mortar. Afterward, chapters 4 and 5 present and discuss the results of the tests carried out on the samples of plaster and mortar. Finally, chapters 6 and 7 illustrate the case study of precast panels and complete the research with the conclusions.

Literature review

2.1 Synthesis of the aerogel

Aerogels can be prepared by using different materials such as alumina, chromium, tin oxide, carbon, and silica. However, aerogels based on silica are more common and used for insulation purposes because their production is easier and more cost-effective [11].

Silica aerogels are synthesized by low-temperature *sol-gel* chemistry. The main chemical compounds for the production of silica aerogels are silicon alkoxides. The synthesis of silica aerogels is generally carried out in three phases which are: *gel preparation*, *aging of the gel* and *drying of the gel* [2].

The first step consists of hydrolyzing and condensing alkoxides. Afterward, successive steps remove the alcohol to form aerogels by using methods which permit to preserve the porous texture of the wet phase [6].

The production of aerogels always involves these three general steps. Nevertheless, extra procedures can also be carried out in order to modify the final network; e.g. aerogels are often reinforced with some mechanically stronger material, such as glass fiber, mineral fiber, and carbon fiber. Also, they can be cross-linked with polymers. On the other hand, these extra procedures may increase their thermal conductivity and density [12]. Dorcheh and Abbasi have presented a detailed review on the synthesis of silica aerogels [13].

2.1.1 Gel preparation

The *gel* is obtained through the *sol-gel* process. This procedure permits to obtain a solid material, the *alcogel*, by using nanoparticles, which are dispersed in a solution, the *alcosol*. The solution acts as the precursor that leads to an integrated product structure [2]. Gels are classified according to the solution used: hydrogel for water, alcogel for alcohol and aerogel for air [12].

The *sol* becomes a *gel* when the nanoparticles dispersed in it stick together and form a continuous three-dimensional structure throughout the liquid. As stated before, the mechanical rigidity of the *gel* is improved by increasing the number of cross-linking [12]. *Gel* preparation ends when the *sol* reaches the *gel point*. Brinker and Scherer [2] thoroughly described this process.

The main precursors utilized to produce aerogels are silicon alkoxides. Waterglass or sodium silicate, i.e. Na_2SiO_3, could be used in place of silicon alkoxides as cheaper raw materials in order to produce silica aerogels [6]. The most used silicon alkoxides, as shown in Table 1, are Si $(OCH_3)_4$ (tetraethoxysilane, or TMOS), $Si(OC_2H_5)_4$ (tetraethoxysilane or TEOS) and $SiO_n(OC_2H_5)_{4-2n}$ (polyethoxydisiloxane or PEDS-P_x). Alkoxides are expensive and dangerous materials, therefore, commercialization is not allowed [13]. PEDS and TMOS lead to uniform pores and higher surface area than TEOS [13]. Hence, the thermal conductivity of aerogels obtained by using PEDS and TMOS are lower compared to the thermal conductivity of aerogels obtained by using TEOS. On the other hand, TEOS are used in order to obtain a higher transmittance of radiation within the range of visible light [6]. The PEDS-P_x is obtained as follows:

$$Si(OC_2H_5)_4 + nH_2O \leftrightarrow SiO_n(OC_2H_5)_{4-2n} + 2nC_2H_5OH, \quad \text{for } n \leq 2 \qquad (1)$$

Table 1. Main precursors used to synthesize silica aerogels.

Constituent	Chemical formula	Abbreviation
Tetraethoxysilane	Si $(OCH_3)_4$	TMOS
Tetraethoxysilane	$Si(OC_2H_5)_4$	TEOS
Polyethoxydisiloxane	$SiOn(OC_2H_5)_{4-2n}$	PEDS-Px

Hydrolysis is performed with a catalyst. There are three types of catalysis: acid catalysis, base catalysis and two-step catalysis [13]. They lead to a wider distribution of larger pores and a lower thermal conductivity [2]. Acid hydrolysis usually comports long times. The time interval before the catalyst addition may vary from 0 to 72 h [9].

As stated before, the solid nanoparticles dispersed in the solvent have to stick together in order to withstand the stress caused by the supercritical drying process [9]. This might require the use of an additive to make them stick together.

Silica alcogels based on TEOS are prepared by hydrolysis and condensation of C_2H_5OH (ethanol or EtOH) diluted TEOS, in the presence of water and two catalysts, which are $C_2H_2O_4$

(oxalic acid) and NH_4OH (ammoniumhydroxide) [14]. Different quantities of alkoxides and water yield to different products [13].

Table 2. Chemicals involved in hydrolysis and condensation of alcogels based on TEOS.

Constituent	Formula	Abbreviation
Oxalic acid	$C_2H_2O_4$	
Ethanol	C_2H_5OH	EtOH
Ammoniumhydroxide	NH_4OH	
Water	H_2O	

The chemical reaction which uses TEOS/EtOH-based polymeric silica *sol* to produce common silica aerogels used for insulation purposes is as follows [9]:

Hydrolysis:

$$Si(OC_2H_5)_4 + 4H_2O\ (+ C_2H_2O_4) \rightarrow Si(OH)_4 + 4C_2H_5OH \quad (2)$$

Condensation:

$$Si(OH)_4 + (OH)_4Si\ (+ NH_4OH) \rightarrow (OH)_3Si{-}O{-}Si(OH)_3 + H_2O \quad (3)$$

$$Si(OH)_4 + (OH)_4Si\ (+ NH_4OH) \rightarrow (OH)_3Si{-}O{-}Si(OC_2H_5)_3 + C_2H_5OH \quad (4)$$

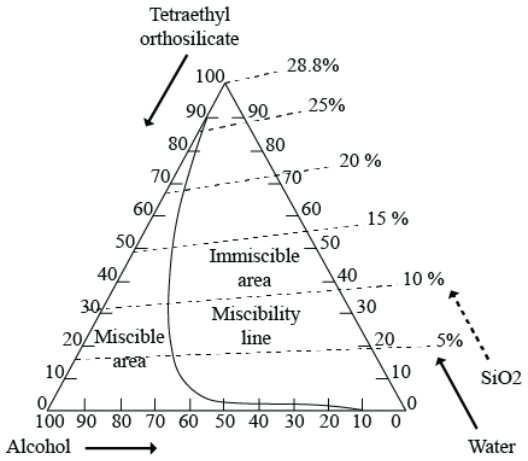

Fig. 4. Phase diagram of the solution TEOS–ethanol–water at 25° C [13].

2.1.2 Aging of the gel

Once a *sol* reaches the *gel point*, it may still contain unreacted alkoxide groups and hydrolysis may continue. For this reason, the *gel* is aged in its mother solution at the ambient temperature in order to complete hydrolysis and prevent the *gel* shrink during the drying process [6],[13].

The aging procedure often requires adding ethanol-siloxane to the *gel*, in order to increase its stiffness and strength [6]. The mechanical and permeability properties of the *gel* depend on the aging time, the temperature and the pH [13]. The aging time is a function of two aging mechanisms. The first one is the reprecipitation of silica dissolved from the particle surfaces onto the necks between particles. The second one is the reprecipitation of small dissolved silica particles onto larger ones. The time required to conclude this process is proportional to the thickness of the *gel* and can be reduced by using aging vessels [12]. In 2004, Reichenauer [13] presented that aging of silica gels in water reduces the shrinkage of the *gel* during the drying.

After the aging of the *gel*, all the water inside the pores must be removed before the drying process. This could be achieved by washing the *gel* with ethanol and heptane [2]. The water that is not removed from the *gel*, will not be removed through the supercritical drying and will make the *gel* much more opaque and dense [15].

2.1.3 Drying of the gel

Aerogels are essentially the three-dimensional networks of the *gel* isolated from the solution [6]. Drying of the *gel* is a critical step. The *gel mother liquid* is removed from the network by using a liquid-to-gas phase change process. Possible shrinkage of the *gel* during drying is determined by the capillary pressure which may reach 100–200 MPa [13]. Three different methods for drying the aerogels are used: supercritical drying (SCD), ambient pressure drying (APD) and the freezing drying.

The first one permits to avoid capillary tension but comports higher costs. On the other hand, the second one is more cost-effective but involves capillary tension which can lead to shrinking and possible fractures [2]. However, high pressure is always required and leads to high costs. At the moment, SCD is generally used for silica aerogels [6].

2.1.3.1 Supercritical drying

Supercritical drying is the most used drying process for aerogels [2]. The liquid comes out of the pores above the critical temperature T_{cr} and the critical pressure P_{cr}. When the liquid

reaches the critical point, it is transformed into a gas without two phases have been present at the same time and the molecules are able to move freely. For this reason, SCD method consents to avoid capillary tension [2],[16].

Two applications of SCD process exist, the *high-temperature supercritical drying* (HTSCD) and *low-temperature supercritical drying* (LTSCD) [6]. In 1931, Kistler [2] has presented a detailed review of HTSCD whereas LTSCD was presented in 1985 by Tewari et al. In HTSCD, methanol reacts with OH groups on the surface to form CH_3O making the silica aerogel partially hydrophobic. LTSCD is used for building applications. During the LTSCD, the solvent is replaced by a liquid that has a critical point close to ambient temperature, such as carbon dioxide (T_{cr} = 304.2 K, P_{cr} = 72.786 atm). Fig. 5 shows the process of the LTSCD.

The process may be divided into three steps. Firstly, the aged *gel* is placed in an autoclave filled with non-flammable liquid dioxide at 4÷10° C until the pressure reaches approximately 100 bar to replace the solvent in the pores of the *gel* with the liquid dioxide. Afterward, the temperature is raised above the critical temperature, which is about to 40° C, while the pressure is kept constant [13]. Secondly, the pressure of the autoclave is isothermally depressurized until it reaches atmospheric pressure. Finally, the autoclave is cooled at ambient pressure to the room temperature [6].

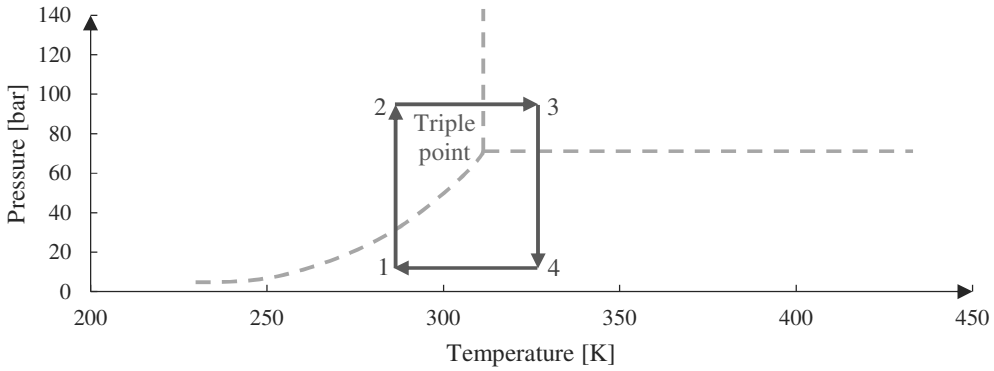

Fig. 5. Representation of the low-temperature supercritical drying cycle [12].

2.1.3.2 Ambient pressure drying

The elevated costs of production due to the great amounts of energy consumed by SCD to create high pressures is limiting the usage of aerogels as a thermal insulation material in buildings. An alternative to the supercritical drying is the ambient pressure drying (APD). This is the most cost effective procedure, compared to supercritical drying. Nevertheless, APD comports capillary tension on the surface of the pores and can cause fractures. The stress

pressure is proportional to the viscosity of the liquid and inversely proportional to the permeability of the wet *gel*. Fractures are likely to occur especially when the pores are small [13].

APD may be divided into two steps. Firstly, the solvent in the pores is chemically altered through substituting hydrophobic functional groups of H from hydroxyl groups in order to obtain hydrophobic aerogels. Secondly, drying is carried out by ambient pressure evaporation allowing the liquid to exit slowly to the exterior. This is the most complex step.

2.1.3.3 Freeze drying

Freeze drying is another possibility to dry gels. The solvent is replaced with a chemical that has a low expansion coefficient and a high sublimation pressure. Subsequently, the liquid in the pores is frozen and then sublimed in a vacuum. This method has many disadvantages: the aging period to stabilize the *gel* network requires a long time and the expansion coefficient of the liquid must be lower than the solvent one whereas its sublimation pressure must be higher [2].

2.2 Properties of the aerogel

Silica aerogels have uncommon solid properties. For this reason, many researchers and companies are interested in improving the high potential of these materials. Table 3, illustrates a summary of the most important properties of silica aerogels that will be examined in the next few chapters. Next sections provide an overview of these properties.

Table 3. Properties of silica aerogels.

Property	Value
Primary particle diameter [nm]	2÷5
Pore diameter span [nm]	2÷100
Mean pore diameter [nm]	20÷40
Percentage of porosity [dimensionless]	85÷99.9
Internal surface area [m^2]	600÷1000
Bulk density [kg/m^3]	3÷350
Bulk density for building purposes [kg/m^3]	70÷150
Volume shrinkage [dimensionless]	<10
Water resistance up to 250°C of superhydrophobic silica aerogel [in air]	Good

Compressive strength [kPa]	300
Tensile strength [kPa]	16
Thermal conductivity [W/mK]	0.004
Thermal conductivity for building purposes [W/mK]	0.013÷0.014
Normal-hemispherical transmittance of radiation [dimensionless]	0.80÷0.93
Longitudinal sound speed [m/s]	100
Temperature stability [°C]	Up to 600
Not-flammable	Yes
Not-reactive	Yes
Not-release toxic gasses during fire	Yes

2.2.1 Pore structure

As stated in the previous chapter, silica aerogels are porous. They consist of a cross-linked internal structure of SiO_2 chains, with many small pores filled with air. Pore network is an open-pore structure where pores are interconnected. Hence, fluids can move from pore to pore and flow through the material. This property makes the aerogels excellent catalysts and catalyst supports [13].

The pores volume occupies from the 85% up to the 99.9% of the total volume of the aerogels. Hence, high porosity and small pores lead to unique physical, thermal, optical and acoustic properties. Nevertheless, they comport low mechanical properties too [6].

Aerogels have a pore diameter of 2÷100 nm and an average pore diameter of 20÷40 nm. IUPAC classification for porous materials defines “micropores” the pores smaller than 2 nm in diameter, “mesopores” the pores with a diameter of 2÷50 nm, and “macropores” those ones with diameters bigger than 50 nm. According to this classification, the majority of the pores are mesopores. However, silica aerogels have pores of all the three sizes [13].

Scanning electron microscopes (SEMs) and transmission electron microscopes (TEMs) are techniques used to investigate the microstructure of the aerogels. However, they comport difficulties correlated to the sample preparation. Moreover, they produce a two-dimensional image which makes harder the information processing, especially in the case of high porous materials such as aerogels. SEMs and TEMs permit to evaluate the pore size as well [13]. Examples of SEMs and TEMs pictures are shown in Fig. 6. Other non-destructive techniques have been used in order to investigate the aerogels, such as the positron annihilation

spectroscopy (PAS), the small angle X-ray scattering (SAXS), the atomic force microscopy (AFM), and the nuclear magnetic resonance (NMR) [13].

The percentage of porosity (ϕ) depends on the bulk density (ρ_b) and the skeletal density (ρ_s), physical quantities defined in the next section. Cuce et al. [2] reported the value of the percentage of porosity from 85% up to 99.9%. According to the ASTM [17], the percentage of porosity is "the ratio of the volumes of the pores in the particles to the volumes enclosed by their envelopes" and is defined by the following formula:

$$\phi = \left(1 - \frac{\rho_b}{\rho_s}\right) \times 100 \tag{5}$$

Aerogels have got a high surface area. The BET[1] internal surface area is 600÷1000 m^2. Just to give an idea, one gram of aerogel flattened out on a surface would cover an area of the size of a football field [18].

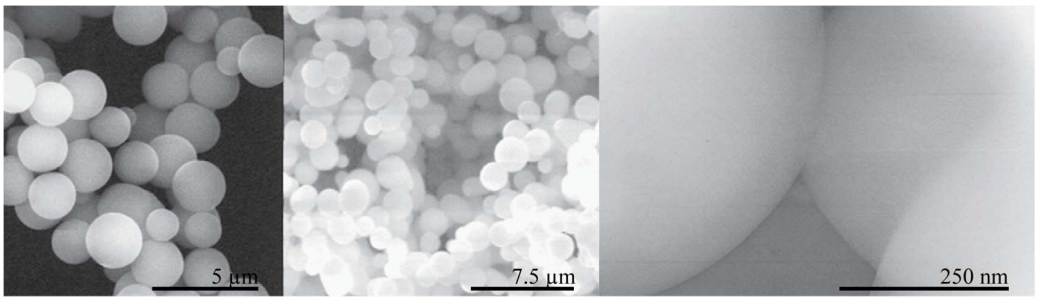

Fig. 6. Pictures of the pores of silica aerogel [13].

2.2.2 Density

As stated earlier, the air-filled pores take from 85% to 99.8% of the total aerogel volume. For this reason, aerogels are the lightest solid materials ever known. They are used to produce catalysts, absorbers, sensors, fuel storage, ion exchange targets for ICF, X-ray lasers, subsea pipelines, space suits, and dust collector in NASA missions due to their porosity and density [19]. The texture of the solid part of the aerogels is composed of ultrafine particles. Silica aerogels have a small fraction of solid silica which value falls between 1% to 10% [13].

[1] Brunauer, Emmett and Teller (BET) method based on nitrogen-adsorption technique in order to measure the specific surface area of a material.

Two different physical characteristics are used to define silica aerogels in terms of density: bulk density (ρ_b) and skeletal density (ρ_s). ASTM D3766 [17] gives the definitions of skeletal and bulk densities. Skeletal density is "the ratio of the mass of discrete pieces of solid material to the sum of the volumes of the solid material in the pieces and closed (or blind) pores within the pieces" [17]. Bulk density is "the ratio of the mass of a collection of discrete pieces of solid material to the sum of the volumes of the solids in each piece, the voids within the pieces, and the voids among the pieces of the particular collection" [17].

In the case of aerogels, where the pore network is an open-pore structure, the skeletal density of the pores in the particles must to be close to that of the bulk solid. The density depends on the procedure used to synthesize the aerogel [20] and is often determined by using helium pycnometer. The density of the aerogel ($\rho_{aerogel}$) is related to the porosity (ϕ) and the density of the air (ρ_{air}) through this formula:

$$\rho_{aerogel} = \rho_{SiO2} - \phi \times (\rho_{SiO2} - \rho_{air}) \quad (0 \leq \rho \leq 1) \tag{6}$$

Woignier and Phalippou [20] have presented a value of the skeletal density around 2200 kg/m^3 by using a helium pycnometer. Skeletal densities of 200÷700 kg/m^3 have been reached afterward. More recently, different studies have found values of skeletal density of 3÷350 kg/m^3 [13]. To have an idea of how lightweight aerogels are, the air has a density of 1.2 kg/m^3. However, aerogel currently used for buildings have an average density of 70÷150 kg/m^3 [6].

2.2.3 Volume shrinkage

The percentage of volume shrinkage (V_s%) is calculated from the volume of the aerogel (V_a) and the change in the volume of the alcogel (V_g) by using the formula:

$$V_s\% = \left(1 - \frac{V_a}{V_g}\right) \times 100 \tag{7}$$

Venkateswara and Bhagat [9] have investigated aerogels based on TEOS and managed to find a value of volume shrinkage smaller than 10%.

2.2.4 Hydrophobicity

Silica aerogels can be either hydrophobic or hydrophilic due to the process used during the synthesis. The silanol polar group in the aerogel network (Si-OH) causes the absorption of water and leads to a hydrophilic behavior [13]. Contact with water could demolish aerogels due to the surface tension in the pores. Moreover, the presence of water inside the pores worsens other proprieties and deteriorates the material with time. For these reasons, in many applications, aerogels should be hydrophobized in order not to absorb water and water vapor.

The hydrophobic property can be improved adding to the pore surface nonpolar side function, such as a silylating agent. The nonpolar side function can be introduced by two different methods illustrated in the next paragraph. Usually, aerogels dried by HTSCD are hydrophobic and those dried through LTSCD by using CO_2 are hydrophilic [13]. In fact, HTSCD results in methoxy groups $(-OCH_3)_x$ on the surface which are hydrophobic, whereas LTSCD forms hydroxyl groups (-OH) on the surface, which are hydrophilic. The surface modification of the aerogels due to the improvement of the hydrophobic property increases mechanical properties as well. Therefore, cracks growth can be significantly reduced in hydrophobic aerogels. On the other hand, it reduces optical transmittance and porosity [21].

Hydrophobic silica aerogels are produced by using two methods: the *co-precursor method* and the *derivatization method*. In the *co-precursor method*, a hydrophobic reagent containing the organic group is added to the *sol* during the *sol-gel* step and afterward, the *gel* is high-temperature supercritically dried from methanol. This method is used in APD methods as well [2]. In the *derivatization method*, the *gel* is immersed in a chemical bath containing the hydrophobic reagent and a solvent. Then, the *gel* is supercritically dried from methanol. Organic groups used either as co-precursors or derivatizing reagents along with the TMOS and the TEOS are organosilane compounds such as methyltrimethoxysilane, phenyltriethoxysilane, dimethylchlorosilane, trimethylchlorosilane, trimethylethoxysilane, and hexamethyldisilazane. Methyltrimethoxysilane can be used as a precursor as well [21].

The hydrophobicity of the aerogels is tested evaluating several parameters. The contact angle of the water droplet on the aerogel surface (θ) is calculated by using the formula:

$$\theta = 2\tan^{-1}\left(\frac{2h}{w}\right) \tag{8}$$

where h is the high and w is the width of the water droplet touching the aerogel surface.

Traveling microscopes are used in order to evaluate the high and the width of the droplet, as shown in Fig. 7. The velocity of a water droplet (v) is evaluated on an inclined hydrophobic surface. The *co-precursor method* leads to aerogels with higher contact angle but which are opaque. On the other hand, the *derivatization method* results in aerogel transparent but with lower contact angle [21].

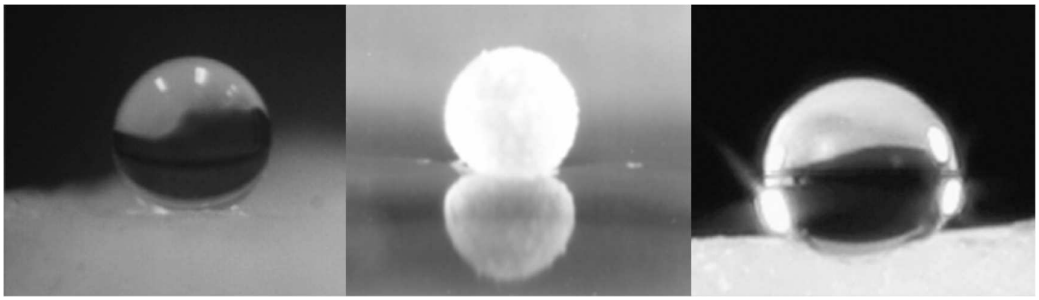

Fig. 7. Picture of a water droplet on silica aerogel [13].

Superhydrophobic and flexible aerogels have been obtained by Venkateswara Rao et al. [21]. Aerogel synthesized by using methyltrimethoxysilane as a precursor led to a value for the contact angle around 175°, which is the highest value ever recorded. The bulk density of this aerogel was around 200 kg/m^3 and the optical transmittance was around 5%. The value of the water droplet velocity is calculated as a function of the angle of inclination of the superhydrophobic aerogel surface. The droplet velocity increases from 0.4 m/s to 1.44 m/s as the angle of inclination increases from 8° to 52°.

One important issue is that the hydrophobic aerogels show hydrophobicity just for a definite period of time. Due to the exposition to air over a long time, they start to absorb water. This is an uncommon property for hydrophobic materials [13].

2.2.5 Mechanical properties

Silica aerogels have a relatively high compressive strength (f_c). The measured values are up to 300 kPa, which is considered a good load bearing. On the other hand, they have very low tensile strength (f_t), around 16 kPa. For this reason, aerogels are very fragile. The challenging issue is to improve their tensile strength by incorporating in the aerogels a fiber matrix [6]. The correlation between tensile strength and compressive strength of Aerogel Incorporated Concrete (AIC), which will be discussed in later chapters, is expressed by the following formula [18]:

$$f_t = A \times f_c^B \quad (9)$$

where A and B are constants material-dependent. Examples of values of A and B constants are reported in section 2.4.

2.2.6 Thermal properties

Before talking about the thermal properties of aerogels, it is necessary to define the thermal properties. Table 4 shows an overview of the thermal properties. Thermal conductivity (λ) is the ability of a substance to conduct heat. It is measured in W/mK. Thermal transmittance (U), also known as U-value, defines the rate of transfer of heat through one square meter of a structure. It is measured in W/m^2K. Thermal resistance (R), also known as R-value, is the opposition to the heat flow due to the elimination of the heat transfer mechanism. It is measured in m^2K/W.

Table 4. Overview of the thermal properties.

Thermal dimension	Symbol	Unit of measure
Thermal conductivity	λ	W/mK
Thermal transmittance	U	W/m^2K
Thermal resistance	R	m^2K/W

Thermal conductivity and thermal resistance are related by the following formula:

$$\lambda = \frac{s}{R} \quad (10)$$

where s is the thickness of the material.

Thermal resistance and thermal transmittance are related by the following formula:

$$R = \frac{1}{U} \quad (11)$$

Thermal insulation materials have low thermal conductivity and thus, retard heat flow. The thermal transmittance is the most used property to evaluate the thermal flow through a partition or a structure. A low thermal conductivity permits the use thin building envelopes with low thermal transmittance.

The heat transport is driven by the difference in temperature between the surfaces of the material. Thermal conductivity is made up of six parts: solid state thermal conductivity (λ_{solid}),

gas state thermal conductivity (λ_{gas}), radiation infrared thermal conductivity (λ_{rad}), gas state convection thermal conductivity (λ_{conv}), second order thermal conductivity ($\lambda_{coupling}$), and leakage thermal conductivity (λ_{leak}) [7]. These properties are added in order to calculate the thermal conductivity, as shown in the following formula:

$$\lambda(T) = \lambda_{solid}(T) + \lambda_{gas}(T) + \lambda_{rad}(T) + \lambda_{conv}(T) + \lambda_{coupling}(T) + \lambda_{leak}(T) \quad (12)$$

Each of the components must be minimized in order to obtain a low overall thermal conductivity. Fig. 8 shows an example which takes into account just solid state thermal conductivity, gas state thermal conductivity, and radiation conductivity. The optimal point from insulation perspective is achieved where the sum of the contributions is at a minimum [2].

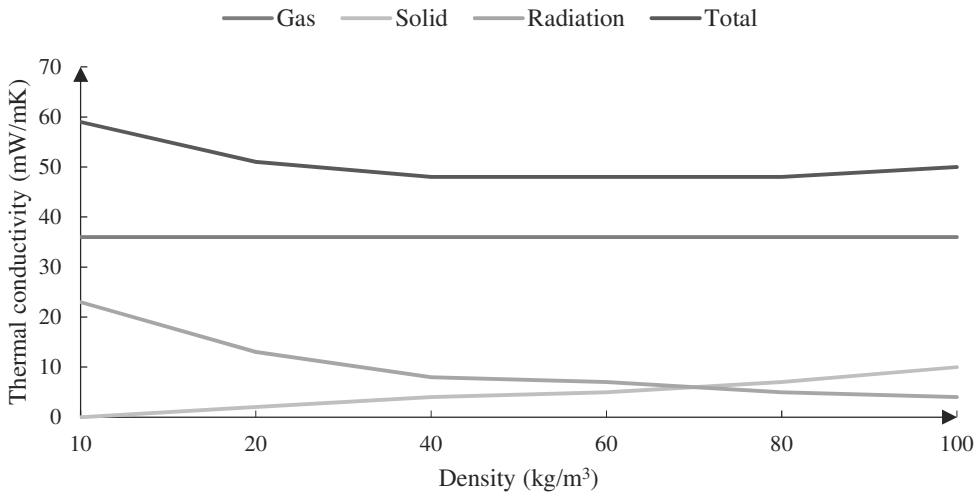

Fig. 8. Thermal conductivity of a porous insulation material [2].

2.2.6.1 Solid state thermal conductivity

The solid state thermal conductivity has a massive impact on the overall thermal conductivity. It is strongly related to the thermophysical properties of the material and increases with the bulk density of the material. It involves the heat transfer between atoms due to the lattice vibrations, that is through chemical bonds between atoms. The equation to calculate the solid state thermal conductivity is [2]:

$$\lambda_{solid} = \lambda_f \delta^2 \quad (13)$$

where λ_f is the material thermal conductivity factor and δ is the ratio of insulation material density to the material density.

2.2.6.2 *Gas state thermal conductivity*

The gas state thermal conductivity is linked to the collision of the molecules which transfer the energy from one to the other. The thermal conductivity of the air is about 0.025 W/mK. It does not depend on the density and leads to a minimum total thermal conductivity around 0.030 W/mK [2]. The gas state thermal conductivity is also related to the pressure [18]. In order to decrease the gas state thermal conductivity, the gas can be substituted with a different one which has lower thermal conductivity. Moreover, another way to reduce the gas state thermal conductivity is to reduce the pore size of the material. This leads to the so-called *Knudsen effect*, which is a typical behavior of aerogels. *Knudsen effect* correlates the gas thermal conductivity to the characteristic pore diameter and the gas pressure in the pores. It is more comprehensively explained in the paragraph 2.2.6.7.

2.2.6.3 *Radiation infrared thermal conductivity*

The radiation infrared thermal conductivity is related to the emittance of electromagnetic radiation from the material. It takes place even though two bodies are separated by a medium that is colder. The net radiation is the difference between the body radiation emitted and received. The radiation effect is relevant for insulation materials with a small amount of solid thus, with a low bulk density [2], and can be neglected at room temperature [18]. A simplified equation to define the radiation thermal conductivity is:

$$\lambda_{rad} = \frac{16\sigma}{3\beta} T^3 \tag{14}$$

where σ is Stefan-Boltzmann constant ($5.67\times10^{-8}W/m^2K^4$), T is the temperature in Kelvin and β_s is the extinction coefficient that is calculated as follows:

$$\beta_s = \rho e \tag{15}$$

where ρ is the material density and e is the specific extinction coefficient.

2.2.6.4 *Convection thermal conductivity of the gas phase*

The convection thermal conductivity of the gas phase involves the movement of air and moisture in two different ways: the air that fills the micropores provides convection inside the pores cells and through the material on a macro scale. Microscale convection does not occur within closed pores, but this is not the case of aerogels which have open-pore structure. Convection in porous materials is defined by the Nusselt number (Nu). This must be greater than one to have natural convection. The Nusselt number is defined by the formula:

$$Nu = \frac{q_{w.c}}{q_{wo.c}} \quad (16)$$

where $q_{w.c}$ is the heat flux with convection and $q_{wo.c}$ is the heat flux with conduction.

2.2.6.5 Leakage thermal conductivity

The leakage thermal conductivity represents an air and wetness leakage driven by a pressure difference. Moisture in nanometer pores has to be avoided otherwise overall thermal conductivity increases considerably. It is normally neglected because the materials are supposed to be dry and without any holes.

2.2.6.6 Second order thermal conductivity

The second order thermal conductivity is the term that takes into account the second order effects between the various thermal conductivities. It is complex to calculate and is normally neglected.

2.2.6.7 Silica aerogels overall thermal conductivity

Air as insulation material has reached its limit and it is necessary to develop new high-performance insulation materials. For this reason, thermal superinsulation materials such as aerogels have being developed in order to meet current requirements [2]. Aerogels are used to develop portable coolers, transport vehicles, pipes, cryogenic, skylights, space vehicles and probes, casting molds, and building insulation materials due to the thermal properties [19].

Silica aerogels are extraordinarily highly insulating materials. Their thermal conductivity is smaller than of the still air and is about 0.004 W/mK [7] when carbon black is used to defeat the radiation thermal conductivity. However, commercial aerogels currently used have a thermal conductivity at an ambient pressure of 0.013÷0.014 W/mK [7]. The reasons why they are such a good insulation materials are low solid state thermal conductivity, low gas state thermal conductivity, and low radiation infrared thermal conductivity.

The low solid state thermal conductivity of silica aerogels is due to the fact that, although the intrinsic solid thermal conductivity of silica is relatively high, aerogels have a small fraction of solid silica. Moreover, the skeleton structure has many ‘dead-ends’ which lead to an ineffective and long tortuous path of heat flow.

The low gas state thermal conductivity of aerogels due to their nanometer open-pore size has great influence on their overall thermal conductivity [6]. Aerogels grid structure does not need to prevent air in order to achieve very low thermal conductivity [8]. In fact, when pores are smaller than 40 nm, the gas thermal conductivity of the air located in the pores becomes very low. Thus, if the solid thermal conductivity of the material is small, the overall thermal conductivity decreases. Moreover, if they are perforated, local thermal bridges are not induced except the ones caused by the perforating agents [8]. To be more detailed, they achieve such a low gas thermal conductivity thanks to the *Knudsen effect* [7]. It occurs when the mean free path of the gas molecules is bigger than the pore diameter. Therefore, it is more likely that a gas molecule placed inside the pore hits the pore wall than other gas molecules. In order to define the gas thermal conductivity, it is necessary to introduce the Knudsen number (K_n) by using this formula [8]:

$$K_n = \frac{k_B T}{\sqrt{2}\pi d^2 p \delta} = \frac{\sigma_{mean}}{\delta} \tag{17}$$

where k_B is the Boltzmann's constant (1.38×10^{-23}J/K), T is the temperature in Kelvin, d is the gas molecule collision diameter in meters, p is the gas pressure in pores in Pa, δ is the characteristic pore diameter in meters, and σ_{mean} is the mean free path of gas molecules in meters.

Therefore, according to the Knudsen formula, the gas thermal conductivity (λ_{gas}) is calculated as follows [8]:

$$\lambda_{gas} = \frac{\lambda_{gas,0}}{1 + 2\beta_c K_n} \tag{18}$$

where $\lambda_{gas,0}$ is the thermal conductivity in the pores at standard temperature and pressure, β_c is the coefficient characterizing the molecule-wall collision energy transfer efficiency (which is between 1.5 and 2.0), and K_n is the Knudsen number.

Low gas state thermal conductivity could be improved by filling the aerogels with a low conductive gas, by decreasing the pores size and by applying vacuum on the aerogel. Biesmans et al. [22] proved that density, pressure, and physical shape affect the thermal performance of the aerogels, as shown in Fig. 9. As it can be observed, gaseous conductivity strongly increases at ambient pressure due to the *Knudsen effect*. Lee et al. [23] analyzed the temperature

dependence of thermal conductivity of polyurea aerogels. They demonstrated, as presented in Fig. 10, that aerogels have improved thermal performance at low operating temperatures.

Low radiation infrared thermal conductivity is due to the low temperature where aerogels are normally employed. However, it has a dominant impact on the overall thermal conductivity at high temperatures. The radiation thermal conductivity lowers with decreasing of pore diameter as the gas state thermal conductivity and the emissivity of the inner pores [8]. The radiation thermal conductivity can be inhibited by adding carbon black to the aerogel.

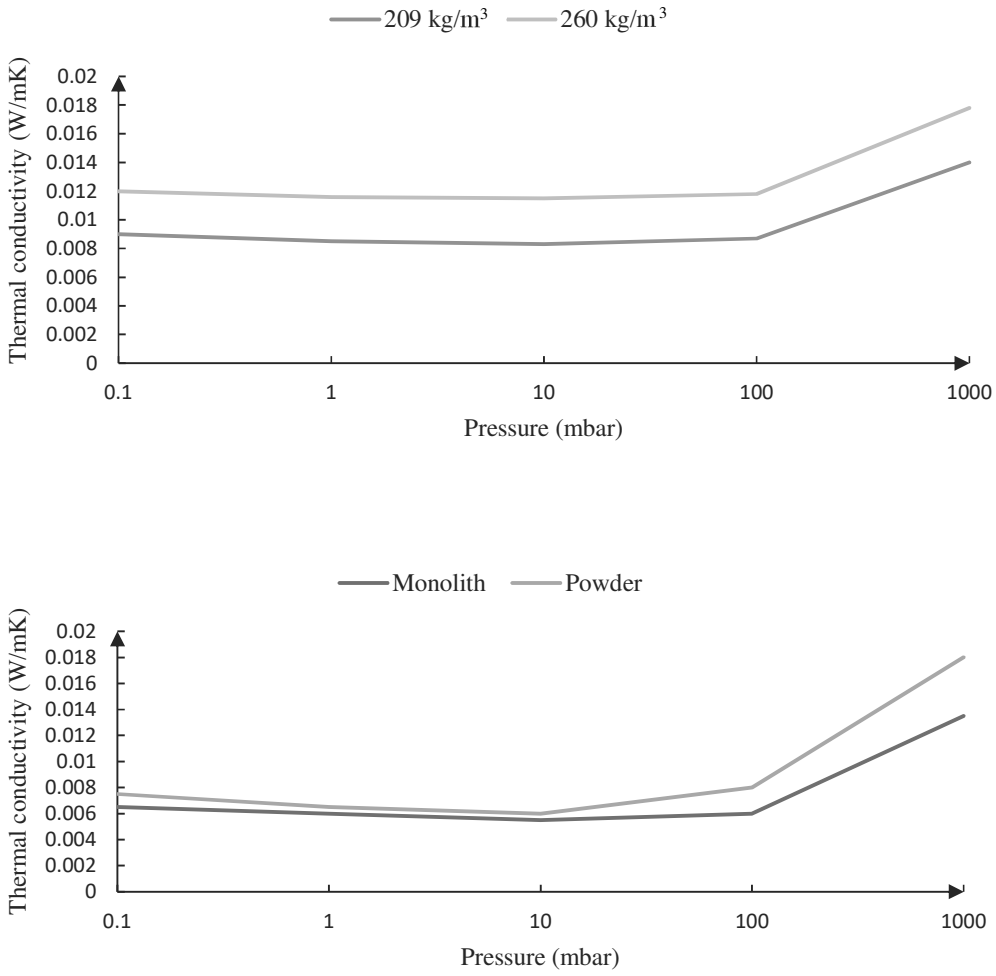

Fig. 9. Thermal conductivity of aerogel as a function of density, pressure, and shape [2].

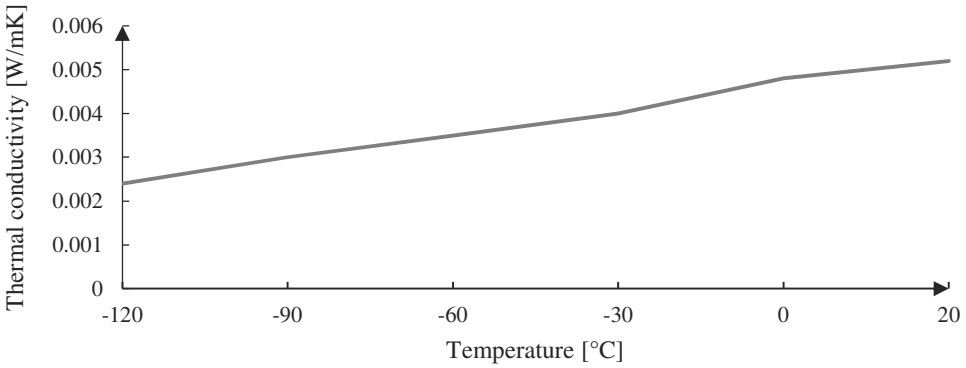

Fig. 10. Thermal conductivity of aerogel as a function of temperature [2].

Finally, to give an idea and compare aerogels with other materials, Table 5 presents an overview of the materials used for insulation purposes sorted by their thermal conductivity [2].

Table 5. Thermal conductivity of traditional materials used for insulation purpose [7].

Material	Thermal conductivity [W/mK]
Cork	0.040÷0.050
Loose-fill cellulose	0.039÷0.042
Foam glass	0.038÷0.05
Mineral wool	0.034÷0.045
Glass wool	0.031÷0.043
Expanded polystyrene (EPS)	0.029÷0.055
Extruded polystyrene (XPS)	0.029÷0.048
Phenolic resin foam	0.021÷0.025
Polyurethane foam (PUR)	0.020÷0.029
Silica aerogels	0.012÷0.020
Organic aerogels	0.012÷0.020
Vacuum insulation panels (VIP)	0.003÷0.011
Vacuum glazing	0.003÷0.008

2.2.7 Optical properties

Aerogels are used to produce Cherenkov detectors, lightweight optics, light guides, special effect optics, and glazing windows due to their optical properties [19]. Optical properties concern the characteristics of a material within the range of visible considering the relative response of the visual system. However, in chapter 2.2.7.2, energetic properties in the infrared spectrum will be considered as well.

The light transmittance (τ_l) is the ratio of the total energy transmitted through a sample to the total energy incident on the surface from a defined direction. The normal-hemispherical reflectance (ρ_l) is the ratio of the total energy reflected from a sample into the subtending hemisphere to the total energy incident on the surface from a defined direction. The light absorptance (α_l) is the ratio of the energy absorbed by a sample to the total energy incident on the surface from a defined direction. These physical quantities are related by the following formula:

$$\alpha_l + \rho_l + \tau_l = 1 \tag{19}$$

Silica aerogels have interesting optical properties, as they can reach a good transparency and visible light transmittance, which is uncommon for porous materials. Hence, they can be produced as opaque, translucent or transparent materials. The transparency depends on their microstructure that has a scale smaller than the wavelength of light and increases with a decrease in the pore and particle size [9]. However, they tend to scatter the transmitted light. Therefore, a slight effect of scattering occurs in the visible with isotropic angular distribution and the quality of the visible light transmitted is reduced. This behavior is described by the *Rayleigh Scattering theory*, that is more comprehensively explained in the paragraph below [13].

2.2.7.1 Optical and scattering properties of aerogels in the visible range

The wavelength of visible range, or visible spectrum, varies between 380 nm and 780 nm. Silica aerogels have high transmittance of radiation in the visible range (τ_{vis}), as Fig. 11 shows [2]. Reim at al. [24] found a value of solar transmittance about 0.88 for a monolith translucent silica aerogel in a 10 mm thick packed bed [24]. Venkateswara Rao et al. [9] presented values of solar transmittance of silica aerogels between 0.80 and 0.90. Moreover, Pierre et al. [25] showed that aerogels made from TMOS in methanol can reach an optical transmittance up to 93% [25]. Cuce at al. [2] proved that monolithic aerogels perform better than granular aerogels due to their higher light transmittance. Adachi et al. [26] synthetized

aerogels with a refractive index greater than 1.03 at a wavelength of 633 nm by using di-methyl-formamide as a solvent in the *sol-gel* process.

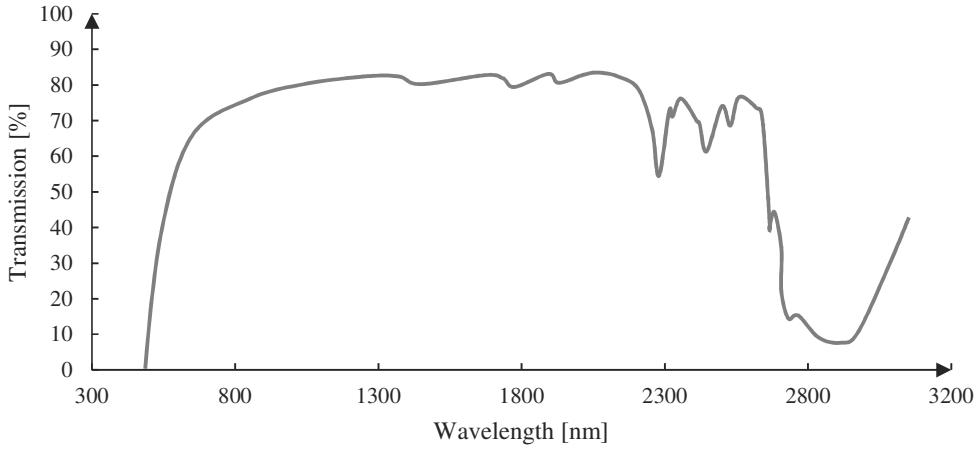

Fig. 11. Transmittance of a silica aerogel in the ultraviolet and visible spectrum [2].

Many parameters can influence the solar transmittance of radiation in the visible length. Water desorption and burning of organic components obtained by heating the aerogels can increase the solar transmittance up to 6% [6]. Also, the parameters of the synthesis process affect the solar transmittance. In glazing applications, a specific treatment of the glass can improve the visible quality. On the other hand, by adding a few vol.% isopropanol or other opacifiers, the transmittance within the visible range can be reduced [6].

Scattering properties of silica aerogel have been considered as well. The scattering is caused by heterogeneities in the nanoporous structure which leads to the so-called *Rayleigh Scattering* [25]. The *Rayleigh scattering effect* is described by using geometrical optics and consists of an isotropic scattering of vertically polarized incident light, an anisotropic scattering of horizontally polarized incident light according to the $cos^2\theta$ formula and a wavelength dependence of scattered light that varies as $1/\lambda^4$. It occurs when dust particles in the pore, with a size similar to the wavelength of the incident light, interacts with the solid parts [6]. The size of the pores effects the efficiency of scattering. However, aerogels exhibit a wavelength independent component of scattering that may not be isotropic and some samples can diverge from Rayleigh angular distribution. As a result, silica aerogels reflect bluish light when observed against a dark background and transmit slightly reddish light, if exposed to direct sunlight [2].

The refractive index (n) is a dimensionless number that defines how the light transmits through a material. It is calculated with the simplified *formula of Clausius-Mosotti*:

$$n = 1 + 0.19\rho \tag{20}$$

where ρ is the density of the silica aerogel.

2.2.7.2 Infrared range

The wavelength of the infrared spectrum varies between 780 nm and 1 mm. Silica aerogels have high transmittance of radiation in the infrared range (τ_{ir}) as well. As stated in chapter 2.2.6.3, the transmittance in the infrared range increases the thermal conductivity, particularly at high temperatures. The transmittance of a silica aerogel in the infrared spectrum is shown in Fig. 12.

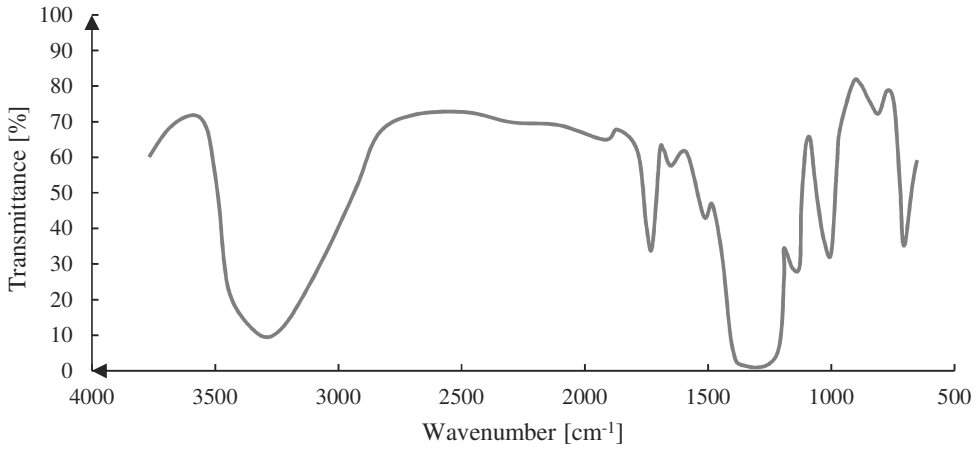

Fig. 12. Transmittance of a silica aerogel in the infrared spectrum [2].

2.2.8 Acoustic properties

Aerogels are good acoustic insulators [25]. Moreover, granular aerogels are great reflectors and have also been proposed as a shock absorbing materials [19]. The acoustic propagation in aerogels depends on their structure, density, and texture. However, the use of aerogel in acoustic comfort is still marginal [27]. The longitudinal sound velocity in monolith aerogels is smaller than 40 m/s, whereas in non-monolith aerogels is about 100 m/s. It decreases to 60 m/s with a particle size of 80 µm [27]. Furthermore, an attenuation of 60 dB can be obtained by combining layers with diverse granular sizes and an overall thickness of 70 mm. M. Schmidt et al. [28] measured the sound absorption coefficient (α) of aerogel particles by using the Kundt's tube. The maximum values of sound absorption are reached at high

frequencies [28]. The maximum value of sound absorption coefficient decreases and moves to lower frequencies with increasing the thickness of the particles layer. Measurements of the acoustical impedance of samples showed that it depends strongly on the geometry and the boundary condition imposed to the samples [2]. Traditional materials at low frequencies show a substantial decrease in sound absorption. However, in the case of aerogel particles, it is not that marked. For these reasons, aerogels can be used to produce architectural and appliance insulation, impedance matchers for transducers, range finders, speakers, and glazing windows [19]. Jérôme Lefebvre et al. [27] developed a hybrid acoustic absorber combining cellulose foam and silica aerogel. According to their research, cellulose permits to improve mechanical and acoustic properties. Moreover, results show remarkable absorption properties, especially at low frequencies.

2.2.9 Health hazards

Aerogel insulation products suffer from dust production. The exposure to crystalline silica dust leads to diseases such as silicosis, chronic obstructive pulmonary, chronic bronchitis, tuberculosis, and lung cancer. However, silica aerogels are amorphous silica, that is almost 0% crystalline. Hence, according to the International Agency for Research on Cancer (IARC), the exposure to silica aerogels is not associated with a risk for lung cancer to humans. US Occupational Safety and Health Administration declared that the exposure limit for the respirable dust of this material is of 5 mg/m^3 [6]. Animal studies in long-term inhalation of high concentrations of amorphous silica showed partially reversible inflammation, emphysema, and granuloma formation, but no progressive fibrosis of the lungs. Moreover, they revealed that amorphous silica can be completely cleared from the lungs. Epidemiological studies of workers with high occupational exposure to synthetic silica confirmed that it does not cause silicosis and fibrosis. However, the available data are limited and a risk of chronic bronchitis, chronic obstructive pulmonary disease or emphysema cannot be excluded with certainty [29]. However, further researches are necessary. The main problem related to the assessment of health effects of amorphous silica is its contamination with crystalline silica.

Aerogels may cause health problems during installation. Table 6 shows a report presented by Aspen Aerogels [30] about the potential health problems caused by aerogels. For this reason, precautions should be taken and *health & safety guidelines* have to been followed. Aerogels should be kept in rubber, plastic or aluminum covers to avoid direct contact with hands. Special breath mask should be used in order to avoid inhalation during installation that may cause irritation of the respiratory tract. Moreover, eyewear and gloves should be used in order to prevent eye and skin damage. Finally, airborne dust during installation may cause allergic

reactions. Hence, people with an allergy should not stay in the installation environment for a long time [2].

Table 6. Potential hazardous effects of aerogel on human health [30].

Incident	Effects
Inhalation	Inhalation of airborne dust may cause mechanical irritation of the upper respiratory tract.
Eye contact	Exposure to material's dust can produce a drying sensation and mechanical irritation of the eyes.
Skin contact	Skin contact with dust from this product can produce a drying sensation and mechanical irritation of the skin and mucous membranes.
Skin absorption	The material is not absorbed through the skin.
Ingestion	If the material is ingested in large quantity, it may produce mechanical irritation and blockage.
Acute health hazards	Dust from this product is a physical irritant and may cause temporary irritation or scratchiness of the throat or itching and redness of the eyes and skin.
Chronic health hazards	The exposure to silica aerogels is not associated with a risk for lung cancer to humans.
Medical conditions aggravated by exposure	Excessive inhalation of dust may aggravate pre-existing chronic lung conditions including bronchitis, emphysema, and asthma; dermal contact may aggravate existing dermatitis.

2.2.10 Fire behaviour

During a fire, some traditional materials cause serious health hazards problems; for example, PUR release hydrogen cyanide and isocyanates, which is very toxic [7]. An important feature of silica aerogels is that they have a very high melting point, which is around 1200°C. Also, they are non-flammable and non-reactive due to their chemical structure. Moreover, they do not release toxic gasses during a fire. For these reasons, they can also be used in buildings as fire-protecting and fire-retarding materials in order to avoid spreading of fire from one place to another [2].

2.2.11 Cost performance

The production cost of aerogels is still very expensive for the cost-sensitive building industry and hinders their use as insulation materials in building applications. According to the analysis presented by Koebel et al. [31], there is a relevant difference between the cost of traditional materials and the cost of superinsulation materials. In fact, the cost for aerogel insulation is twenty times higher than that of traditional insulation and thus, it has to be lowered substantially [31]. Researchers and producers are trying to improve aerogels performance and decrease their production cost. Also, ongoing studies aim to develop new kinds of aerogels. The cost of aerogels is very irregular in the current market but it has been decreasing with time. According to Koebel et al. [31], the price of aerogel could drop below 1500 US$/m^3 by 2020. However, in the case of aerogels, the costs-thermal performance ratio is still not enough competitive. Hence, traditional insulation materials still dominate the insulation market due to their lower cost of production. Nowadays, the main explanation for the use of aerogel insulation systems is related to the space saving, longevity, chemical resistance, and thermal properties [31]. However, as the energy demand and the energy cost are increasing, aerogel products used in building sector are expected to increase in the future. Moreover, the aerogel cost will probably decrease due to improvements in aerogel production and large-scale production [32].

The high price of aerogels is due to the low production volume and the high costs involved in the synthesis process. However, the cost of aerogels is gradually decreasing. In fact, the global market of aerogels is almost tenfold increased since 2003. Moreover, according to the ongoing studies, the cost of a meter cube of aerogel will achieve 50% cost reduction in production within the next few years and will decrease to US$660 by 2050 [2]. Shukla et al. [12] proposed some expedients to reduce the cost of production of aerogels. Firstly, the expenses can be reduced by using cheaper raw materials such as rice husk, clay, oil shale ash, and recycling process materials and by using cheaper processing solvents; for example, water glass as a cheaper silica source is used to reduce the cost of raw materials and synthesis of TEOS is five times cheaper than synthesis of TMOS [9], [13]. Secondly, the price can be decreased by using low-vapour-pressure solvents that do not evaporate during the aging process such as an ionic liquid. Thirdly, the cost of aerogels can be cut down by using APD method instead of SCD, in which the *gel* is dried at atmospheric pressure. Finally, the price can be lowered by using fewer fiber reinforcements.

Koebel et al. highlighted the importance to consider a life-cycle-cost analysis (LCCA) in order to compare aerogel with traditional materials. In fact, it is necessary to consider both the initial

cost of the insulation material and the energy savings over the life cycle of the building; for example, space and energy savings due to the use of aerogels can compensate some of the added costs of production. Excessive insulation leads to high initial investments whereas low insulation comports high energy consumptions. Hence, it is necessary to find the optimum insulation levels that correspond to the value that minimizes the overall life cycle cost. The optimal value depends also on the cost of the aerogel. In fact, as the price of aerogel decrease, the optimal value increases. Cuce et al. [2] compared a brick wall insulated by using glass wool with a brick wall insulated by using aerogel. They carried out an LCCA considering a lifetime of 10 years. The results showed that the required thickness of glass wool to achieve the U-value of 0.3 W/m^2K for modern buildings in the UK, was about of 104 mm. On the other hand, in order to achieve the same insulation performance by using aerogel, only 37 mm of thickness were necessary. As a consequence, the payback period of aerogel was calculated to be about 1 year. Ibrahim et al. [32] carried out a comparison between an aerogel-based mortar with an EPS-based mortar. The estimated payback period in the case of aerogel was about 3.5 years whereas was only about 0.2 years in the case of EPS. Shukla et al. [12] evaluated both aerogel and traditional insulation applications, by referring to the current costs of the materials. They demonstrated that aerogel, for a target U-value of 0.7 m^2K/W, saves about 35% of the costs compared to the fiberglass blanket solution. Moreover, for a target U-value of 1.41 m^2K/W, the aerogel method is more cost-effective compared to traditional insulation methods, excluding the fiberglass. Finally, for a target U-value of 2.11 m^2K/W, the aerogel method cost is much higher than for fiber and foam insulation.

Energy savings and payback depend also on the climate. In fact, the thickness or the percentage of aerogel should be optimized for different climates by doing a cost analysis over the lifetime of the building. As the climate gets colder, the thickness or the percentage of aerogel in a mixture increase. For the hottest climates, the payback period can be more than 10 years [3].

2.2.12 Embodied energy

The embodied energy is the overall energy required to produce a material and is measured in MJ/kg. In order to assess the overall energy used throughout the manufacturing process of a material, it is necessary to consider its entire life energy cycle analysis. In order to compare the different material, Cuce et al. [2] considered the thickness necessary to reach a U-value of 0.3 W/m^2K, which is the required U-value for modern buildings in the UK. The embodied energy of aerogel is around 200 MJ/kg, which is in general low compared to traditional materials; for example, the embodied energy of EPS is around 300 MJ/kg, of cork and foam

glass is around 400 MJ/kg, and of XPS and PUR is about 200 MJ/kg. Only the embodied energy of glass wool is 20 MJ/kg lower than the aerogel embodied energy.

2.3 Aerogel Incorporated Plaster (AIP)

Materials currently used in buildings can be grouped into four general categories. The first one consists of materials that have low bulk density and thus, low compressive strength as well as low thermal conductivity. They are used for thermal and sound insulating purposes. Rock wool, glass wool, expanded polystyrene, extruded polystyrene, and mineral fiber belong to this category. On the other hand, the second group includes materials that have high bulk density and thus, high compressive strength as well as high thermal conductivity due to the high solid state density. These materials are used for structural purposes in order to bear loads. Mortar, concrete, and steel belong to this category. The third group consists of those materials which have to bear some loads as well as to have an adequately low density and low thermal conductivity. Lightweight concretes belong to this category and are examined in section 2.4. Finally, the last group includes materials used as finishing layer, such as plaster. They usually are lightweight materials.

Nano insulation materials (NIMs) represent an opportunity to develop new high performing materials in the field of render composites due to their economic, ecologic, mechanical, and thermal features. Producing, handling, and processing cement-based materials are responsible for 5% to 8% of worldwide CO_2 emissions [1]. Hence, it is necessary to investigate new materials which permit to combine good mechanical and thermal-igrometric performance [33]. Aerogels renders represent a possible alternative due to their low density, low overall thermal conductivity, and high hydrophobicity. For example, replacing normal aggregates in the concrete by aerogel particles or adding aerogel to standard plasters, improves the thermal resistance and leads to lightweight materials as well as good fire and acoustic resistances.

The AIP has been investigated by Kim et al. [10], in 2013, and Buratti et al. [34], in 2016. The literature review on AIP is presented in the following sections. Table 7 summarizes the properties of the most suitable mixtures of AIP presented in the literature so far.

Table 7. Properties of the most suitable mixtures of Aerogel Incorporated Plaster.

Reference	Kim et al. [10]	Buratti et al. [34]
Parameter	Value	
Density [kg/m^3]	Undefined	125
Thermal conductivity [W/mK]	0.13	0.16
Compressive strength [MPa]	5.9	Undefined

2.3.1 Kim et al. research on AIP, 2013

In 2013, Kim et al. [35] studied the insulation properties of AIP as a non-structural component. They prepared various samples of aerogel cement by using aerogel powder and cement and also by using aerogel, cement, and pozzolan. Different percentages of aggregates with respect to the mixture were considered. Pozzolan ($SiO_2 \cdot Al_2O_3$ or more simply SA, according to the Berzelius nomenclature) is composed of silicon(II) oxide (SiO_2) and aluminum(III) oxide (Al_2O_3). Pozzolan reacts with the calcium(II) hydroxide ($Ca(OH)_2$ or more simply CH, according to the Berzelius nomenclature) formed during the hydration of the cement. The result of this reaction, as shown in formula (21), is calcium silicate hydrate (CASH, according to the Berzelius nomenclature). The CH has a solid crystalline structure whereas the SA has to be amorphous and finely ground in order to make the reaction sufficiently rapid. This reaction permits to replace the CH, which is not water resistance, with the CASH, which is water resistance. Moreover, it is a non-exothermic reaction and, hence, it reduces the hydration heat that is important in order to reduce the detrimental expansion of the cement.

$$\begin{gathered} \text{CH + SA} \leftrightarrow \text{CASH (according to the Berzelius nomenclature)} \\ \text{calcium(II) hydroxide + pozzolan} \leftrightarrow \text{calcium silicate hydrate} \end{gathered} \tag{21}$$

The materials used by Kim et al. to prepare the mixture were:

- ordinary Portland cement;
- powder-type hydrophobic silica aerogel with a density of 50 kg/m^3, a porosity of 95%, and thermal conductivity of 0.02 W/mK;
- methanol;
- water;
- pozzolan.

They prepared different samples according to ISO 679 with a percentage of aerogels ranging from 0.5 wt.% to 2 wt.% and a water/cement ratio about 0.5. Also, in some samples, 20% of

pozzolan was substituted for cement. The methanol was used to mix the hydrophobic aerogel with cement paste, to reduce pores between hydration particles and thus, to maintain compressive and flexural strength. The aerogel-methanol ratio adopted was 1.43. However, it is important to highlight that the use of methanol for construction purposes should be avoided [18]. Aerogels were directly mixed with cement paste. After the casting process, molds were covered with polyethylene films and kept at 20°C and RH of 90% for 24 hours. Finally, samples were cured in water at 20°C for 28 days.

Afterward, Kim et al. tested the properties of the samples. The thermogravimetry analysis (TGA) was performed in order to check the thermal stability of the aerogel at high temperatures. The Fourier transform infrared spectroscopy (FT-IR) and the scanning electron microscope (SEM) analyses were executed in order to analyze the chemical and physical stability of aerogel in the cured cement. Thermal conductivity tests were carried out by using the TCI apparatus developed by C-Therm. The samples were tested for mechanical properties by using a Universal Test Machine. Flow tests were carried out as well. Finally, the absorption of water due to the porosity was calculated according to the following formula:

$$abs.\% = (W_{sat} - W_{dry}) / W_{dry} \quad (22)$$

where W_{sat} is the weight of the samples saturated in water, and W_{dry} is the weight of specimens dried by heating to 120°C and later cooled into a chemical desiccator.

The TGA analysis showed that the aerogel is very stable up to 1150°C, thus it can be used as a fire-resistance insulation material without emitting toxic gasses and deforming. The FT-IR spectroscopy showed that the treatment with methanol reacted very well and helped to the formation of cement composite. Moreover, no chemical molecule changes of aerogel on the process were found. The SEM photographs showed that aerogel particles were stably settled in the cured mix and no chemical and physical deformation occurred. The thermal conductivity decreased with increasing the aerogel contents, especially in the case of the samples without pozzolan. It decreased to 75% of regular concrete when 2 wt.% of aerogel was added. With an addition of 0.5 wt.% of aerogel, a thermal conductivity about 0.32 W/mK was measured. Table 8 shows the thermal conductivities of the different mixtures. The compressive strength was tested in function of the aerogel content and by adding 0.5, 1, and 2 wt.% of aerogel it decreased from 26.3 MPa to 13.1 MPa, 8 MPa, and 5.9 MPa respectively. The flexural strength was tested in function of the wt.% aerogel content as well. By adding 0.5, 1, and 2 wt.% of aerogel, it decreased from 6.6 MPa to 4.4 MPa, 3.6 MPa, and 2 MPa respectively. Finally, they

proved that aerogel does not have a substantial effect on flow tests. However, the flow of fresh aerogel cement was sharply dropped due to the presence of methanol.

Table 8. Mixtures of Aerogel Incorporated Plaster produced by Kim et al. [35].

Aerogel cement paste				
Aerogel content [%]	0	0.5	1	2
Thermal conductivity [W/mK]	0.51	0.32	0.27	0.13
Compressive strength [MPa]	23.6	13.1	8	5.9
Flexural strength [MPa]	6.6	4.4	3.6	2
Percentage of decrease [%]	-	26	47	75
Aerogel cement paste with pozzolan				
Aerogel content [%]	0	0.5	1	2
Thermal conductivity [W/mK]	0.56	0.45	0.33	0.10
Percentage of decrease [%]	-	9	29	72

2.3.2 Buratti et al. research on AIP, 2016

In 2016, Buratti et al. [10] carried out a research on Aerogel Incorporated Plasters. Three mixture were prepared by mixing natural calk with granular aerogel in different percentages. The first mixture had a percentage of aerogel between 80% and 90% in volume, the second one between 91% and 95%, and the last one between 96% and 99%. Moreover, a control mixture without aerogel was prepared. Parallelepipeds with an edge length of 300 mm were cast in order to test the thermal conductivity. Furthermore, cylindrical samples with diameters of 29 mm and 100 mm were produced to test the acoustic properties of the mixtures.

The thermal properties were tested by using the heat flow meter *Fox 314 HFM* apparatus. The parallelepipeds were placed between two flat plates controlled to a specified constant temperature and the thermal conductivities of the samples were obtained. The acoustic properties were preliminarily tested by using a *Kund's Tube.* The normal incidence absorption coefficient was measured with two microphones by using the transfer function method.

The density of the plasters was found to fall when aerogel particles were added to the mixtures. Values between 115 kg/m^3 and 300 kg/m^3 were found. Also, the thermal conductivity of the samples decreased by adding aerogel particles. Values between 0.014 W/mK and 0.05 W/mK were found. Table 9 summarizes the results of the tests. The acoustic tests showed that the aerogel-based plaster layer moderately influences the absorption coefficient.

Table 9. Test results on the samples of plaster produced by Buratti et al. [34].

Sample	Percentage of aerogel [%]	Density [kg/m^3]	Thermal conductivity [W/mK]
Mix1	-	2200	0.50
Mix2	80÷90	300÷275	0.050÷0.045
Mix3	91÷95	136÷126	0.021÷0.019
Mix4	96÷99	125÷115	0.016÷0.014

Buratti et al. carried out a comparison between AIP and traditional solutions for building refurbishment. Traditional plasters usually have values of thermal conductivity that vary between 0.29 W/mK and 0.70 W/mK. Different existing buildings were refurbished by using the AIP in order to evaluate the *in-situ* performance. The aerogel coating was found to be very effective for a stone wall with a thickness of 60 cm and both an internal and an external coating of natural lime. The thermal resistance of the wall dropped from 2.14 W/m^{2}K to 1.73 W/m^{2}K by applying 5 mm of aerogel based-plaster.

Finally, *in-situ* infrared thermography analysis was carried out on the northern façade of a multi-family house located in Pordenone (Italy). A decrease of about 2 °C due to the application of the aerogel-based plaster was measured. Moreover, they evaluated the additional cost of the aerogel plaster compared to conventional materials. The price for the natural plaster without aerogel was about 2 €/m^2. The price for the AIP was about 10 €/m^2, considering a thickness the coat of just 1 mm.

2.4 Aerogel Incorporated Mortar (AIM) and Aerogel Incorporated Concrete (AIC)

Lightweight concretes have many applications due to their porosity which leads to higher heat insulation as well as to fewer loads on the bearing structure. Nowadays, they have many applications due to their high strength-weight ratio and high heat insulation features. For instance, they are used as a screed for floors and roof slabs, as covering for architectural purposes, to realize partition walls, panel walls in framed structures, and precast elements. Lightweight concrete is prepared by substituting partially or totally the aggregates of concrete with lightweight materials. Traditional light aggregates are pumice, diatomite, volcanic cinders, perlite, and light expanded clay. More advanced solutions use expanded polystyrene (EPS). Is it important to select which aggregates are better to be used in order to avoid

interactions with the binder phase [10]. Air-entraining admixtures are used to obtain light concrete as well.

Concrete has a thermal conductivity of 1.7÷2.5 W/mK [33], which is very high. Moreover, concretes are often used along with rebars and thus, the thermal conductivity gets much higher. As a consequence, concrete building envelopes have to include thermal insulation layers in order to reach an adequate overall low thermal transmittance and get thicker.
As stated earlier, lightweight concrete permits to achieve both thermal insulation and load-bearing properties. However, even when lightweight concrete is used, the application of thermal insulation layers is often required to achieve the requisite of thermal conductivity. Moreover, the lightweight materials with low thermal conductivity have usually a compressive strength smaller than 4.7 MPa [36]. Hence, these materials are not available for multi-storey building and others with high compressive strength combined with external thermal insulation layers are preferred. Thermal insulation can be achieved with different materials. For example, mineral wool has good thermal properties and adequate sound absorption performance at high frequencies but shows a significant decrease at frequencies below 800 Hz.

Expanded polystyrene incorporated concrete has usually a density of 95÷750 kg/m^3, a compressive strength between 2.9 MPa and 5.8 MPa, and a thermal conductivity of 0.23-0.26 W/mK, depending on the quantity of EPS employed. However, EPS incorporated concrete has many cons: it is not fire-resistant and releases toxic gasses during the fire. Also, it is likely to be damaged as a result of the external impacts, and its mechanical properties are not enough for many structural requirements. Moreover, in presence of water or vapors, its thermal properties worsen significantly. Therefore, traditional materials are often used in multiple layers and lead to a thicker and more complex building details and less net floor area.

The purpose of the ongoing researches on aerogels-incorporated mortars and concretes is to design new mixtures which guarantee both adequate compressive strength and thermal insulating performance. As a consequence, their application is important when the thermal building's insulation would be improved with a slight increase of the thickness of the walls. That is, single leaf exterior walls of the multi-storey building without any other thermal insulation layer can become a reality [10]. Moreover, hydrophobic aerogels are very stable materials against water. This is important in order to keep their thermal insulation properties and avoid water absorption that changes the volumetric composition and the properties of the concrete mix [18]. Moreover, the improved thermal conductivity reduces the building energy consumption by heating and cooling and improves the indoor environmental quality (IEQ) by avoiding mold and condensation on the interior walls. Finally, aerogel-based renders are fire-

resistant and do not release toxic gasses during the fire. Hence, the possibility to use aerogel-based renders in buildings might be a way forward. Three possible applications of NIMs in buildings' envelopes are shown in Fig. 13. Table 10 proposes a comparison between the two most used traditional materials, which are rockwool and EPS, and the aerogel.

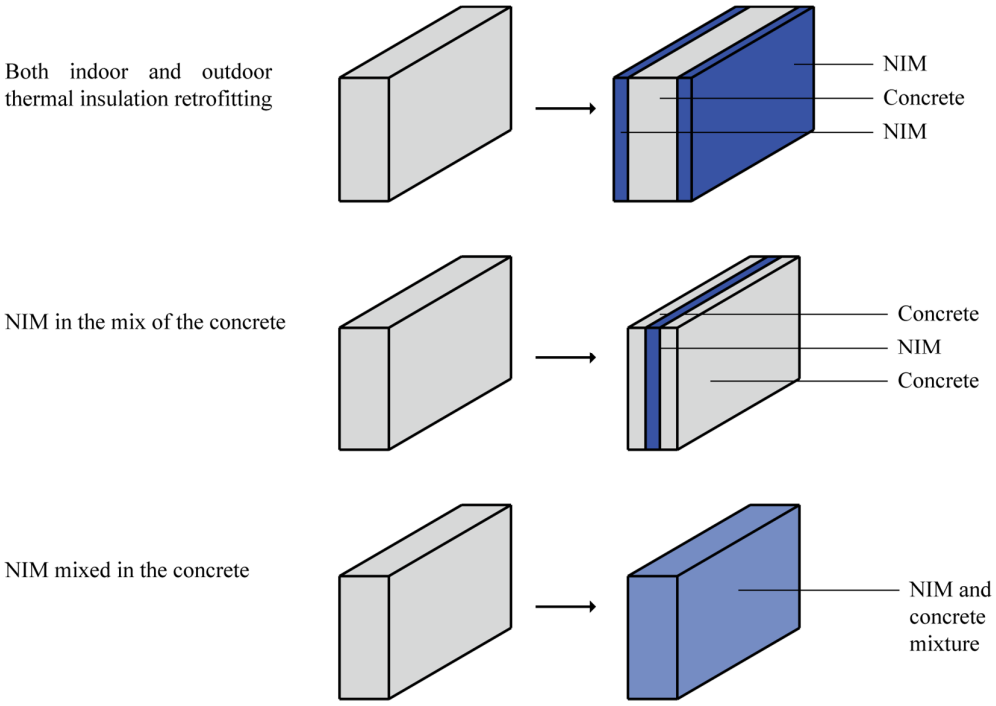

Fig. 13. Application of nano insulation materials in envelopes.

Table 10. Comparison between the properties of rock wool, EPS, and aerogel.

Property	Rockwool	EPS	Aerogel
Density [kg/m^3]	40÷200	16÷35	3÷100
Thermal conductivity [W/mK]	0.037	0.037÷0.038	0.012÷0.020
Max service temperature [°C]	-240÷800	100	600
Acoustic properties	High	Low	High
Fire resistance	Good	Poor	Good
Cost	Low	Medium	High

The preparation of AIC has been investigated by Ratke et al. [37], in 2008, Gao et al. [18], in 2014, Fickler et al [36], in 2015, and Serina et al. [33], in 2015. Those studies and the state-of-the-art of AIC are presented in the next sections. A restricted number of studies are available due to the high production cost of the aerogel and many properties of the aerogel-based renders have not been investigated yet. Table 11 summarizes the properties of the most suitable mixtures of AIM presented in the literature so far. The aim of many investigations is to

combine thermal and insulation properties into a single building material to obtain a minimal thickness. Serina et al. [33], envisioned that in the future it will be possible to use NanoCon (Nano Concrete) as a new material with structural properties similar to the concrete, low thermal conductivity, and low negative environmental impacts. For this purpose, they proposed to join NIMs with CNTs (carbon nanotubes) in order to reach low thermal conductivity due to the presence of NIMs and large tensile strength due to the presence of CNTs. CNTs have very high thermal conductivity but, on the other hand, surpass the tensile strength of steel rebars by two orders. In fact, the tensile strength was measured to be about 63000 MPa, even if the theoretical limit is 300000 MPa. For this reason, the impact of this material may be huge compared with the steel rebars which have a typical tensile strength of 500 MPa or concrete without rebars which usually has a compressive strength of 30 MPa and a tensile strength of only 3 MPa. Moreover, NanoCon within a foreseeable future may also be imagined without steel rebars as well. That means that problems of corrosion of rebars in concrete may be avoided. This scenario would have a huge impact on the buildings industry.

Table 11. Properties of the most suitable mixtures of Aerogel Incorporated Mortar.

Reference	Gao et al. [18]	Serina et al. [33]	Fickler et al. [36]
Parameter		Value	
Density [kg/m^3]	1000	Undefined	860
Thermal conductivity [W/mK]	0.26	0.55	0.17
Compressive strength [MPa]	8.3	20	10
Flexural tensile strength [MPa]	1.2	4.5	2.7
Fire resistance	Undefined	Undefined	Undefined
Manufacture cost	High	High	High

2.4.1 Gao et al. research on AIM, 2014

In 2014, Gao et al. [18] prepared and tested lightweight and thermal insulating Aerogel Incorporated Mortar. They investigated the influence of the vol.% of silica aerogel granules embedded in the cement matrix by preparing different mixtures of mortar. A good balance between the mechanical strength and the thermal performance has been considered during the mixing design process. They highlighted the importance to improve the AIM manufacture procedure as, for example, the alkali-silica reaction during the hydration of the cement may destroy the aerogel particles. The procedure proposed by Gao et al. does not require pre-treatment with methanol.

They investigated samples of AIM prepared by using a standard Hobart 2-litre mixer and containing cement, sand, silica fume, superplasticizer, hydrophobic aerogel particles, and water. More specifically, the raw materials used to prepare the samples were:

- CEM I 52.5R with a density of 3140 kg/m^3;
- natural sand from Finland, with a particle density of 2600 kg/m^3, selected by using a sieve with a size of 0.5÷2 mm;
- silica fume Elkem Microsilica Grade 940 with a density of 2200 kg/m^3;
- acrylic polymer superplasticizer Dynamon SP130;
- hydrophobic aerogel granules ISOGEL 800 with a density of 100 kg/m^3 and a thermal conductivity of 0.02 W/mK;
- distilled water with a water-binder ratio of 0.4.

Silica fume and superplasticizer were used in order to modify the characteristics of the mortar. The binder was considered as the sum of cement and silica fume where the amount of silica fume was 10.8 wt.% of the binder phase. The volume of aggregates and aerogel was 60 vol.% of the mortar sample. The superplasticizer content was 1 wt.% of the binder phase. The air void was set as 2 vol.% for all samples. Cement, sand, silica fume, superplasticizer, hydrophobic aerogel particles were mixed before through a dry mixing process and afterward, superplasticizer and water were added slowly. The resulting slurry was poured into in a prism-shaped mold and an electric vibrator was used for about 3 seconds to avoid segregation. Finally, the sample was held at a vapor saturated environment at room temperature for 24 hours, then de-molded and maintained in the same water saturated environment for 28 days. Table 12 shows the mixtures of the AIM produced [18].

Table 12. Mixtures of Aerogel Incorporated Mortar produced by Gao et al. [18].

Sample	Cement [g]	Sand [g]	Silica fume [g]	Super pl. [g]	Aerogel [g]	Water [g]	Aerogel [vol.%]
2Ref	117.8	405	14.3	1.32	0	49.76	0
2A10	117.8	338	14.3	1.32	3.07	50.10	10
2A20	117.8	271	14.3	1.32	6.14	50.43	20
2A30	117.8	203	14.3	1.32	9.21	50.76	30
2A40	117.8	136	14.3	1.32	12.28	51.10	40
2A50	117.8	68	14.3	1.32	15.36	51.43	50
2A60	117.8	0	14.3	1.32	18.47	51.76	60

The AIM samples were tested immediately after the curing process in order to reduce the effects of hydration or moisture contents. As Fig. 14 shows, when the aerogel content

increases, the resulting mortar density decreases. The values reported were a result of the arithmetic mean of nine individual measurements. According to the formula (6), the difference between the measured and the calculated values is due to the water absorption by aerogel particles, the reaction of aerogel with hydroxides, the breakage of aerogel particles during the mixing process, and the higher void-valued content than the assumed 2 vol.%. Considering a density of compact silica about 2196 kg/m^3, a density of air about 1.2 kg/m^3, and a density of aerogel about 100 kg/m^3, the porosity calculated was about 95.5%. The density of the obtained mortar samples with the aerogel content of 60 vol.% was about 1000 kg/m^3. Hence, a reduction of almost 50% compared to the density of the reference plain mortar of 1980 kg/m^3 was measured.

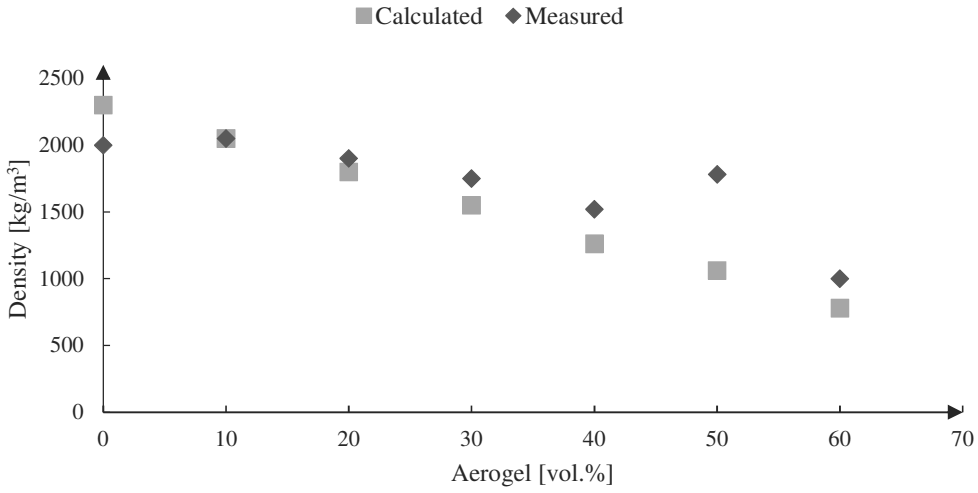

Fig. 14. Aerogel volume content vs. density in mortar, Gao et al. [18].

The values of thermal conductivity were found by using a hot-disk thermal constants analyzer model *TPS 2500S* and a disk-type *Kapton sensor 5465*. Values around 0.26 W/mK for the mortar sample with the aerogel content of 60 vol.% and of 1.86 W/mK of the reference plain mortar were found. Results are reported in Fig. 15. Gao et al. also calculated the thermal conductivity of the AIM (λ_{AIM}), according to the following equation obtained by using the two-phase mixture model:

$$\lambda_{AIM} = \frac{1}{4} \times \left\{ (3x_A - 1)\lambda_A + (3x_M - 1)\lambda_M + \left[\left((3x_A - 1)\lambda_A + (3x_M - 1)\lambda_M \right)^2 + 8\lambda_A \lambda_M \right]^{0.5} \right\} \quad (23)$$

where λ_A and λ_M are the thermal conductivities of the aerogel and the mortar matrix, and x_A and x_M are the volume fractions of the aerogel and the mortar matrix.

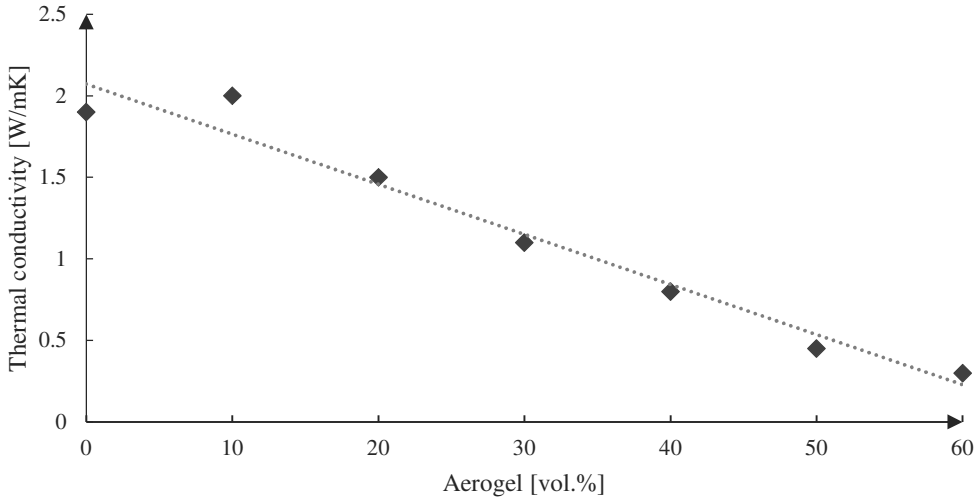

Fig. 15. Aerogel volume content vs. thermal conductivity in mortar, Gao et al. [18].

The mechanical properties were found as a result of the arithmetic mean of three individual measurements for the tensile strength and six individual measurements for the compressive strength. As Fig. 16 shows, when the aerogel content increases, the resulting mortar compressive strength decreases. A value of compressive strength around 8.3 MPa was found with the aerogel content of 60 vol.%, while the compressive strength of the reference mortar was about 55 MPa. Finally, according to equation (9), Gao et al. established the values of the constant A and B as follows:

$$f_t = 0.277 \times f_c^{0.795} \tag{24}$$

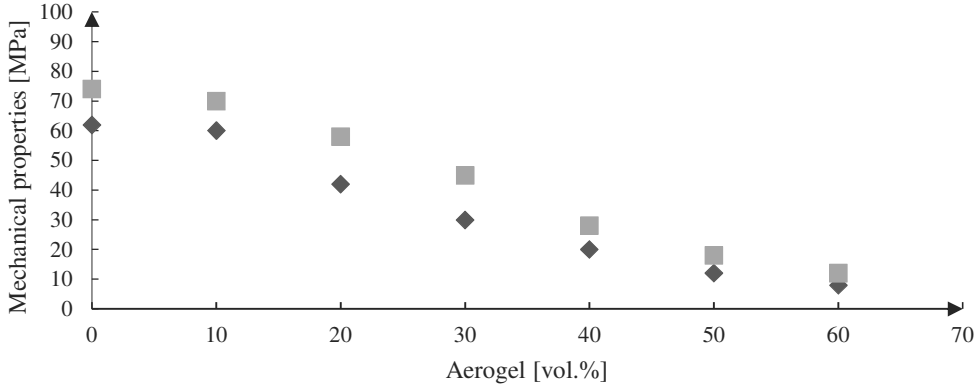

Fig. 16. Aerogel volume content vs. compressive strength in mortar, Gao et al. [18].

The AIM samples had fewer air voids than the mortar samples of reference. In fact, the aerogel particles affect the air flow by gas diffusion due to the microporous nature and the large surface

area of aerogel particles. Moreover, the carbon dioxide (CO_2) absorbed by aerogel particles had reacted with calcium(II) hydroxide to form calcium carbonate ($CaCO_3$) which change the microstructure of the mortar. Furthermore, they verified that aerogel particles are stable during the hydration of the cement. Finally, after the mechanical tests, the resulting pieces were used for morphology characterization by using a field emission scanning electron microscopy (FE-SEM). The morphology characterization showed that aerogel particles are not destroyed by the mixing and cure process as well as by the alkaline environment due to the hydration process. Therefore, aerogels particles are stable during the hydration of cementitious materials and are not degraded by the process of hydration. Finally, Gao et al. found the superior stability of aerogel compared to silica fume particles, due to their hydrophobic nature and a silicate layer produced through the reaction with surrounding cement that acts as protection.

As stated before, density, thermal conductivity, and mechanical strength depend on the aerogel content. When the aerogel content increases, density, thermal conductivity, and compressive strength decrease. Gao et al. found that density is an intrinsic and independent parameter to characterize the properties of AIM. Consequently, they proposed two relations between thermal conductivity (λ_{AIM}) and density (ρ) and between compressive strength (f_c) and density (ρ), expressed by the following equations:

$$\lambda_{AIM} = 0.038e^{0.0019\rho} \tag{25}$$

$$f_c = 0.5e^{0.0023\rho} \tag{26}$$

2.4.2 Serina et al. research on AIM, 2015

In 2015, Serina et al. [33] presented an experimental investigation of ultra-high performance concrete (UHPC) modified Aerogel Incorporated Mortar designed by using a UHPC recipe. The aim was to improve the mechanical properties while maintaining constant the thermal ones. Due to the weakness in mechanical properties of the AIM designed by Gao et al. [18], they investigated new mixtures to achieve better properties. Normally, the mechanical properties of concrete are improved by reducing the water/cement ratio or by using UHPC mixtures which contain micro-fine aggregates and very low quantity of water, and high amount of cement and silica fume. Cement and silica fume improve packing thanks to the nano size dimension of its particles and the bond between the cement and the aggregate particles. Afterward, a comparison between UHPC modified AIM samples and AIM samples was carried out.

The materials used by Serina et al. were:

- Anlegg cement (Norcem AS, Brevik/Norway);
- quartz fines (QF, M4000, Sibelco, Rud/Norway) used as filler;
- silica fume (SF, Grade 940U from Elkem Micro- silica, Kristiansand/Norway) used to increase the density in the UHPC and avoid alkaline silica reaction between the aerogel and the mortar matrix;
- silica aerogel P100 with a particle size between 0.01 mm and 4 mm, an average density of 100 kg/m^3, and an average conductivity of about 0.021 W/mK;
- dispersing polymer NRG-700;
- superplasticizer;
- deionised water.

Table 13. Chemical composition of the cement used by Serina et al. [33].

Characteristic	Anlegg cement [%]	Quartz fine [%]	Silica fume [%]	Aerogel [%]
Cao	63.2	0.01	-	-
SiO_2	20.4	99.5	>90	>97
Al_2O_3	4.58	0.20	-	-
Fe_2O_3	3.56	0.03	-	-
MgO	2.26	-	-	-
SO_3	3.84	-	-	-
Na_2O_{eq}	0.71	0.05	-	-
LOI	2.14	-	<3.0	-

The samples were prepared by mixing the dry powders of cement, silica fume, norm sand and quartz fines with a standard Hobart 2-litre mixer. Mixtures with different aerogel loadings between 20 vol.% and 80 vol.%. were produced. A water/cement ratio of 0.2 and a silica fume cement ratio of 0.16 were utilized. The samples of AIM similar to those presented by Gao et al. were prepared with a water/cement ratio of 0.6. Afterward, water and superplasticizer were added. Finally, the mortar was homogenized, cast in metal molds, vibrated, stored at a relative humidity of 100% for 24 hours, and cured in water for 28 days.

The samples were analyzed for their thermal conductivity, flexural strength, compressive strength, density and finally by using SEM imaging. The thermal conductivity was measured by using a *Hotdisk Thermal Constants Analyzer TPS 2500S* and the *Kapton sensor*. All the specimens were measured immediately after curing to reduce the effects of hydration as Gao et al. have done in their research.

When 20 vol.% aerogel was added, the compressive strength decreased from 120 MPa to 70 MPa. An aerogel loading of 50 vol.% led to a compressive strength of about 20 MPa and a thermal conductivity of about 0.55 W/mK, as Fig. 17 shows. Hence, UHPC modified AIM is still unsuitable as a unique system for insulating purposes. However, the improved thermal conductivity permits to use fewer insulation materials and obtain thinner envelopes. Finally, when 80 vol.% of aerogel was added to the mixture, the compressive strength was about 4 MPa. Therefore, a maximum of 70 vol.% of aerogel should be added to the mix. Serina et al. stated that the loss in strength of AIM samples was due to the absence of binders in the system, especially at higher aerogel contents. Furthermore, the low content of water could be another reason. Finally, they observed that the quantity of water affects more the properties below 60 vol.% of aerogel.

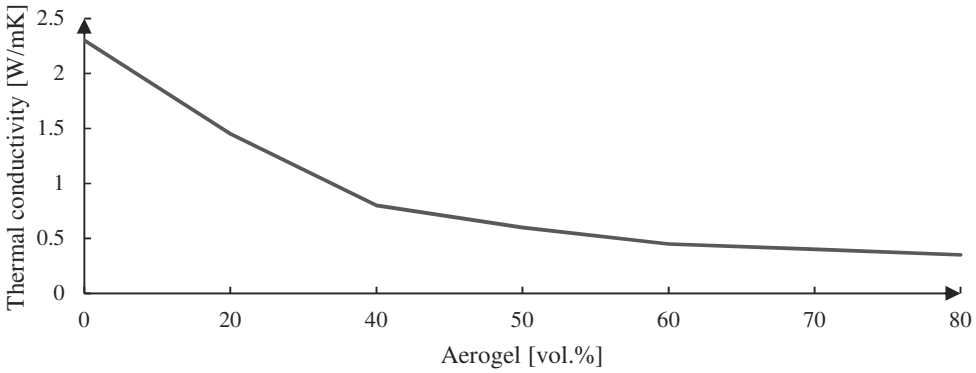

Fig. 17. Aerogel volume content vs. thermal conductivity in mortar, Serina et al. [33].

The density measured was higher than expected. There may be two reasons: firstly, the difference might be caused by the crashing of some aerogel granules during the mixing process that increased the thermal conductivity due to the less nanoporous material and the consequent decreasing of the Knudsen effect. Secondly, it might be ascribed to further hydration of the AIM samples after 28 days. However, density, flexural strength, and compressive strength decreased with increasing of the aerogel loading as it was demonstrated through the previous investigations. In UHPC samples, an important factor in determining the strength was found to be the packing density and the amount of binder in the mix, i.e. cement and silica fume.

The thermal conductivity of the AIM samples decreased from 2.3 W/mK, when no aerogel was present, to 0.31 W/mK when 80 vol.% aerogel was added to the mix. Once again, the thermal properties were modified by the crashing of aerogel granulates during the mixing

process. However, the amount of binder and variation in density did not seem to affect the thermal conductivity.

A comparison between UHPC modified AIM samples and AIM samples similar to those ones presented by Gao et al. was carried out. The compressive strength and the thermal conductivity of the UHPC modified AIM samples were much higher than that of AIM samples made of cement and silica fume. Unhydrated silica fumes have been observed in the AIM samples. Moreover, UHPC modified AIM samples presented better packing than AIM sample and thus, much higher compressive strength (35 MPa versus 11 MPa). However, UHPC modified AIM samples presented a thermal conductivity of 0.74 W/mK, almost twice that of the AIM ones, which was about 0.47 W/mK. According to equation (9), Serina et al. established the values of the constant A and B for UHPC modified AIM samples and AIM samples as follows:

$$f_t = 0.485 \times f_c^{0.745} \tag{27}$$

$$f_t = 0.379 \times f_c^{0.730} \tag{28}$$

The A and B constants found for the AIM samples were very different from those found by Gao et al. It might be caused by the nature, type, and quantity of the materials. The resulting tensile strength of UHPC modified AIM samples with a compressive strength of 20 MPa resulted in being around 2.7 MPa.

Serina et al. finally suggested improving AIM samples, maintaining a maximum aerogel content of 50÷60 vol.%, in order to achieve the required mechanical properties. Further improvements of the insulation and mechanical properties may be obtained by incorporating other binder material with a lower thermal conductivity and amphiphilic materials or fiber.

2.4.3 Fickler et al. research on AIC, 2015

In 2015, Fickler et al. [36] carried out a research in which silica aerogels were mixed with high strength cement matrix in order to obtain high-performance concrete (HPC), ultra-high-performance concrete (UHPC), and lightweight concrete (LC). They tested many samples of Aerogel Incorporated Concrete with a distribution of aerogel between 60 vol.% and 70 vol.%. The bulk density and the compressive strength were lower than conventional concrete when 70 vol.% of aerogel was added. The compressive strength increased by decreasing the percentage of silica aerogel to 60 vol.%. Fickler et al. tested 25 mixtures made of different concentrations of additives, concrete liquefier, micro silica and Portland cement. Superhydrophobic silica aerogel granules embedded in a matrix of ultra high-performance

concrete were used in order to prepare samples of UHPC. The particle size of aerogel granules was between 0.01 mm and 4 mm, the porosity higher than 90% and the density between 120 kg/m³ and 150 kg/m³. The cement used were CEM II 32.5 R, CEM I 42.5R and CEM I 52.5R. The overall thermal conductivity was measured with the transient hot bridge (THB) measurement principle and concrete cubes with an edge length of 0.15 m were tested to measure the compressive strength. The investigation of three concrete cubes for each mixture and each type of storage was necessary. Moreover, the samples were tested at a concrete age of 7 days and 28 days. Thus, 18 specimens for each kind of mixture were produced. The hydration heat of the aerogel concrete was tested by introducing a temperature sensor in the core of each concrete cube. After 5÷8 hours the maximum temperature was reached and after 26 hours the hydration ended.

Furthermore, Fickler et al. investigated three type of storage and the influence of different heat treatments on the compressive strength. The three different kinds of storage tested were the dry storage, the mix storage, and the heat treatment. The dry storage was carried out at an ambient temperature of 20°C. The mixed storage consisted of six days storage in water at 20°C and a dry storage at an ambient temperature of 20°C for the following 12 days. The heat treatment consisted in a storing in a dry cabinet for 24 hours at an ambient temperature between 84°C and 93°C. The influence of the heat treatment on the compressive strength was negligible.

The AIC obtained with the aerogel content of 70 vol.% had a density between 400 kg/m^3 and 570 kg/m^3 and values of thermal conductivity about 0.06÷0.1 W/mK. However, the compressive strength was about 1.4÷2.5 MPa for the mixtures with a density of 500÷620 kg/m^3. Also, samples with compressing strength between 3 MPa and 23.6 MPa were evaluated and values of thermal conductivity between 0.16 W/mK and 0.37 W/mK were found. Fickler et al. presented the thermal conductivity as a function of the compressive strength, as shown in Fig. 18. The most performing mix obtained had a compressive strength of 10 MPa, a density of 860 kg/m^3 and a thermal conductivity of 0.17 W/mK. Further results showed that the AIC had a high frost resistance and a low coefficient of thermal expansion. On the other hand, they revealed a low modulus of elasticity (E), a high volume shrinkage, and a low bond stress.

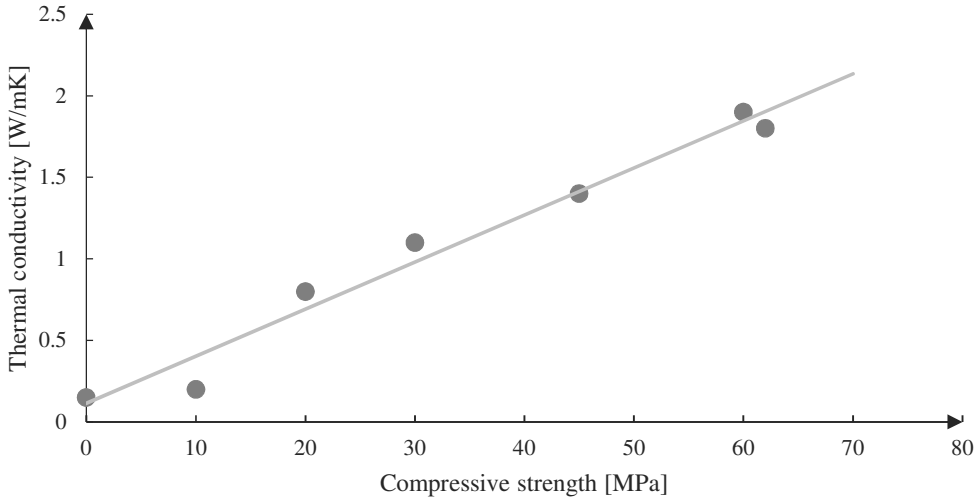

Fig. 18. Compressive strength vs. thermal conductivity in mortar, Fickler et al. [36]

Methodology

3.1 Materials characterization

3.1.1 Aerogel characterization

To produce the samples of AIP and AIM were used the *Cabot Aerogel Particles P300* [38] shown in Fig. 19, which consists of almost 97% of hydrophobic synthetic amorphous silica. This aerogel is highly porous, water repellent, UV stable, lightweight, non-combustible, and inert [39]. Moreover, it has a good sound absorption, thermal insulation, and light transmission. Table 14 present the properties of *Cabot Aerogel Particles P300*. Furthermore, Cabot aerogel is proved to be safe for human and ecological systems and has not relevant impacts on the environment. Fig. 20 presents the thermal conductivity performance of *Cabot Aerogel Particles P300*. Hydrophobic synthetic amorphous silica is chemically similar to other amorphous silica products used in personal care products, such as lotions and cosmetics. As stated in chapter 2.2.9, the exposure to silica aerogels is not associated with a risk for lung cancer to humans. It does not contain crystalline silica and is neither carcinogenic nor mutagenic. Aerogel may be irritating to eyes and skin, and for this reason, specific breath masks and glasses were used during the preparation of the samples.

Fig. 19. Cabot Aerogel P300.

Table 14. Properties of Cabot Aerogel P300 [38].

Property	Value
Physical state	Solid
pH	3.0÷6.5
Melting point/freezing point [°C]	1700
Boiling point [°C]	2230
Decomposition temperature [°C]	>300
Flammability	Not flammable
Particle size range [mm]	1.2÷4.0
Pore diameter [nm]	20
Porosity [%]	90
Particle density [kg/m^3]	120÷180
Bulk density at 20 °C [kg/m^3]	65÷85
Surface chemistry	Hydrophobic
Surface area [m^2/g]	600÷800
Oil absorption [g DBP/100g particle]	540÷650

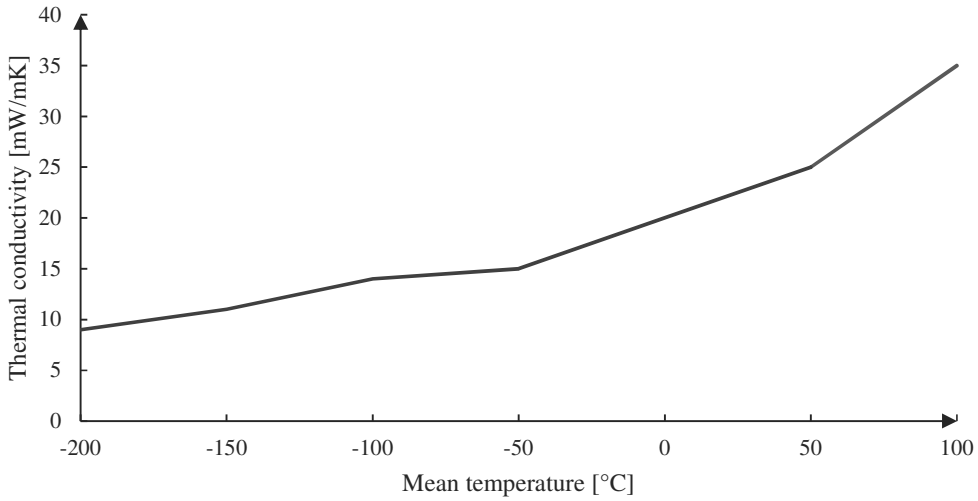

Fig. 20. Thermal conductivity of Cabot Aerogel Particles P300 [38].

3.1.2 Lime characterization

Two different types of hydraulic lime were utilized to prepare the samples of plaster. *Calce idraulica NHL 3.5* produced by *CHIRAEMA s.r.l.* and *Saint Astier NHL 3.5* produced by *TransMineral USA, Inc.* Moreover, samples of plaster were produced by using *Fixit 222 Aerogel high-performance insulating plaster* which is produced by *Fixit AG*. This hydraulic lime already contains particles of aerogel. The sections below describe in details these materials.

3.1.2.1 Fixit 222 Aerogel high-performance insulating plaster

Fixit 222 Aerogel high-performance insulating plaster [40] is produced by *Fixit AG* since 2013. It contains aerogel granules provided by the Cabot company, light mineral aggregates, and additives, i.e. water retaining agent, air-entraining agent, and a hydrophobic agent. The binder consists of natural hydraulic lime NHL 5, calcium hydroxide, and white cement. The range of applications of *Fixit 222* includes the renovation of old buildings and historical buildings. It should be applied to the substrate with a machine specially equipped for use with insulating plaster. Brickwork, sand-lime bricks, natural stonework, quarry stone walls as well as raw shuttered concrete are all suitable base surfaces. The thermal conductivity of *Fixit 222* is around 0.028 W/mK. Due to its mineral-based composition and high water vapor permeability, mold and mildew attacks are prevented. Moreover, *Fixit 222* is non-flammable and guarantees fire safety of buildings. Table 15 summarizes the properties of the *Fixit 222*.

Table 15. Properties of Fixit 222 Aerogel high-performance insulating plaster [40].

Property	Value
Thermal conductivity [W/mK]	0.028
Bulk density [kg/m^3]	220
Water vapour diffusion resistance coefficient μ	4÷5
Flammability	Not flammable
Possible thicknesses [mm]	30÷80
Allows an exact copy of the original wall to be made	Yes
Indoor use	Yes
Outdoor use	Yes

3.1.2.2 Calce idraulica NHL 3.5

Calce idraulica NHL 3.5 is a natural hydraulic lime produced by *CHIRAEMA s.r.l.* It is prepared at a temperature of about 1000° C from a clayey limestone. It does not contain cement or clinker compounds. It can be used with bricks, tuff, stones and in all masonry building as well as in historical monuments. Table 16 gives a summary of the features of *Calce idraulica NHL 3.5*.

Table 16. Properties of Calce idraulica NHL 3.5 [41].

Property	Value
Mechanical strength [MPa]	3.5
Bulk density [kg/m^3]	600
Residue at 0.09 mm	2.50
Residue at 0.20 mm	0.30
CaO [%]	40.0
SO_3	0.60
Colour	White
Expansion [mm]	< 2

3.1.2.3 Saint Astier natural hydraulic lime NHL 3.5

Saint Astier NHL 3.5 [42] is a natural hydraulic lime (NHL). It has been in production for over 150 years by *TransMineral USA, Inc*. The characteristics of the raw materials consist of an undisturbed layer of calcareous rock infiltrated mainly by silica with only traces of other minerals. It is recommended when moderate strengths and better freeze-thaw resistance are required. For this reasons, it is used as base coat and for stone works. It can be mixed in cement mixers and sprayed by using guns. The binder/aggregates ratio recommended is between 1:1.5 and 1:3. Table 17 presents the main features of *Saint Astier NHL 3.5*.

Table 17. Properties of Saint Astier NHL 3.5 [42].

Property	Value
Mechanical strength [MPa]	3.5
Bulk density [kg/m^3]	650
Surface cover [cm^2/g]	9000
Residue at 0.09 mm [%]	9.50
Whiteness index	72
Expansion [mm]	< 1

3.1.3 Cement characterization

The cement utilized to produce the samples of mortar was Portland cement General Use (type GU) produced by CRH Canada Group Inc. Table 18 and Table 19 present the Mill Test Report (MTR) of the physical and chemical properties of the cement carried out in compliance with *CSA-A3001-13 General Use Portland Cement* [43]. The density of the cement was 3150 kg/m^3.

Table 18. Physical properties of the cement used to produce the samples [44].

Physical properties	
Fineness 45 µm sieve retained [%]	7
Autoclave expansion [%]	0.03
Sulfate Expansion [%]	0.012
Initial Time of Set [min]	120
Blaine [m^2/kg]	394
Air Content [%]	7
Compressive Strengths at 1-day [MPa]	19.2
Compressive Strengths at 7-day [MPa]	35.2
Compressive Strengths at 28-day [MPa]	40.6

Table 19. Chemical properties of the cement used to produce the samples [44].

Chemical properties	
Chemical components	Percentage [%]
Loss on Ignition (LOI)	2.4
Insoluble Residue	0.48
SO_3	4.0
MgO	2.6
SiO_2	19.2
Al_2O_3	5.1
Fe_2O_3	2.6
CaO	62.1
Free lime	0.8
C_3S	53
C_2S	15
C_3A	9
C_4AF	8

3.1.4 Aggregates characterization

Natural aggregates were utilized to prepare the samples of mortar. The maximum diameter of the aggregates was set to 4.75 mm to avoid more costs due to the sieving of the aggregates. Table 20 presents the report of the chemical characteristics of the aggregates used to prepare the samples produced by LafargeHolcim [45]. The density of the aggregates was around 2650 kg/m^3.

Table 20. Report of the composition of the aggregates used to produce the samples [45].

Chemical components	Percentage [%]
Loss on Ignition (LOI)	20.05
SiO_2	42.57
CaO	22.74
Al_2O_3	5.99
MgO	2.26
Fe_2O_3	2.07
Na_2O	1.6
K_2O	1.06
TiO_2	0.241
SO_3	0.08
Mn_2O_3	0.079
P_2O_5	0.074
SrO	0.034
Cl	0.024
Cr_2O_3	0.014
ZnO	0.002

3.1.5 Additives characterization

Additives are the constituents of concrete other than cement, water, and aggregate. They are added to the mix in order to modify the properties of the concrete and improve its performance. Moreover, they are used to guarantee the quality of concretes during mixing, transporting, placing, and curing. In this research, two different additives were used to prepare the samples of mortar, i.e. an *air-entraining admixture* and a *superplasticizer*.

Air-entraining admixtures are used to generate a highly stable air void system for increased protection against damage from freezing and thawing, severe weathering, or de-icer chemicals.

Also, they improve the resistance to the action of frost and de-icing salts as well as sulfate, sea and alkaline waters. In this study, the air-entraining admixture adopted was the *Grace Darex AEA EH*. It was used to produce the control samples of the mixture of *Mortar + air entraining*, described in chapter 3.3. *Darex AEA EH* is a complex mixture of organic acid salts in an aqueous solution and complies with *ASTM C260 Standard Specifications for Air-Entraining Admixtures for Concrete* [46]. It is supplied ready-to-use and does not require pre-mixing with water. *Darex AEA EH* entrains air effectively with micro silica concrete and with fly ash concrete. Air is incorporated into the concrete by the mechanics of mixing and stabilized into millions of discrete semi-microscopic bubbles. These air bubbles act like flexible ball bearings increasing the mobility or plasticity and workability of the concrete. This can permit a reduction in mixing water with no loss of slump. Hence, also placeability is improved and bleeding, plastic shrinkage and segregation are minimized.

Superplasticizers, or *high range water reducing admixtures*, are used to reduce the amount of water while maintaining a certain level of consistency and workability. The use of superplasticizers may produce high strength concrete. Superplasticizers can also be utilized in producing flowing concrete used in inaccessible areas due to, for example, the presence of the steel rebars. In this study, the superplasticizer admixtures adopted was the *Grace ADVA CAST 575*. It was used to produce the mixtures of Aerogel Incorporated Mortar described in chapter 3.3. *Grace ADVA CAST 575* is a high efficiency, low addition rate polycarboxylate-based high-range water reducer designed for the production of a wide range of concrete mixes, from conventional to *self-consolidating concrete*. It is a plant-added superplasticizer that is formulated to obtain improved workability to the concrete and achieve high early compressive strength as required by the precast industry. *ADVA Cast 575* can be used to produce self-consolidating concrete (SCC) or may be used in conventional concrete production. Moreover, *ADVA Cast 575* may be used to produce concrete with very low water/cementitious ratio concrete to achieve extreme workability without segregation to the concrete. *ADVA Cast 575* meets the requirements of *ASTM C494* [47] as a Type A and F, and *ASTM C1017* [48] Type I plasticizing. It is supplied as a ready-to-use liquid and does not contain intentionally added chlorides.

3.2 Experimental apparatus

In this chapter, is presented the experimental apparatus used to prepare and test the specimens described in chapter 3.3. A weighting device, a glass graduates, a mixer, a trowel, a release agent, and specimen molds were used during the preparation of the samples. The thermal conductivity of the specimens was tested according to the *ASTM C518* [47] by using the *NETZSCH Heat flow meter - HFM 436 Lambda*. The compressive strength was tested according to the *C109/C109M – 16* [49] that references to the *ASTM standards* by using a compressive machine.

3.2.1 Heat flow meter

The thermal conductivity of the samples was tested in the Building Science Laboratory of the Ryerson University of Toronto. The tests were carried out in compliance to *ASTM C518* [47]. The specimens utilized were parallelograms with an edge length of 150 mm and a thickness of 20 mm. A frame made of expanded polystyrene was used to test the samples in order to reduce the thermal bridges, as Fig. 21 shows.

Fig. 21. Frame made of expanded polystyrene used to test the samples.

The high precision instrument used for testing the samples was the *NETZSCH Heat flow meter (HFM) 436/6/1 Lambda*. This device offered a wide variety of thermal conductivity testing

instruments covering almost all possible applications and temperature ranges. The heat flow meter produced a one-dimensional heat flux through the sample that was placed between two parallel plates at constant but different temperatures. The heat flow created by the defined temperature difference was measured with a heat flux sensor. Fourier's law of heat conduction was used to calculate the thermal conductivity and the thermal resistance. Test results were available within short periods, with outstanding accuracy and repeatability. *HFM 436 Lambda* allowed to apply a precise thermal load on the specimen and ensured the plates contact with the sample across the entire surface in order to produce a minimal and uniform contact resistance. The samples were placed between the two heated plates, controlled to a user-defined mean sample temperature and temperature drop. The plate temperatures were controlled by bidirectional heating/cooling Peltier systems, coupled with a closed loop fluid flow with an integrated forced air heat exchanger. Thermocouples fixed in the plates measured the temperature drop across the specimen and thermal flux meters embedded in each plate measured the heat flow through the specimen. Data were continuously acquired, processed and stored by the integrated electronics, and upon completing the test, all relevant results were printed out. The thermal conductivity of the specimens was calculated according to the following formula:

$$\lambda = \frac{Q \times s}{\Delta T} \tag{29}$$

where Q is the heat flux [W/m^2], s is the thickness of the specimen [m], and ΔT is the temperature difference across the specimen [K].

A schematic design of the *NETZSCH HFM 436 Lambda* is presented in Fig. 22. The instrument was calibrated with an NIST-certified reference standard sample of known thermal conductivity in order to obtain the precise correlation between the signal output of the transducers and the actual heat flow. The accuracy of the machine was set to 0.1%. Table 21 presents the main features of the *HFM 436/6/1*.

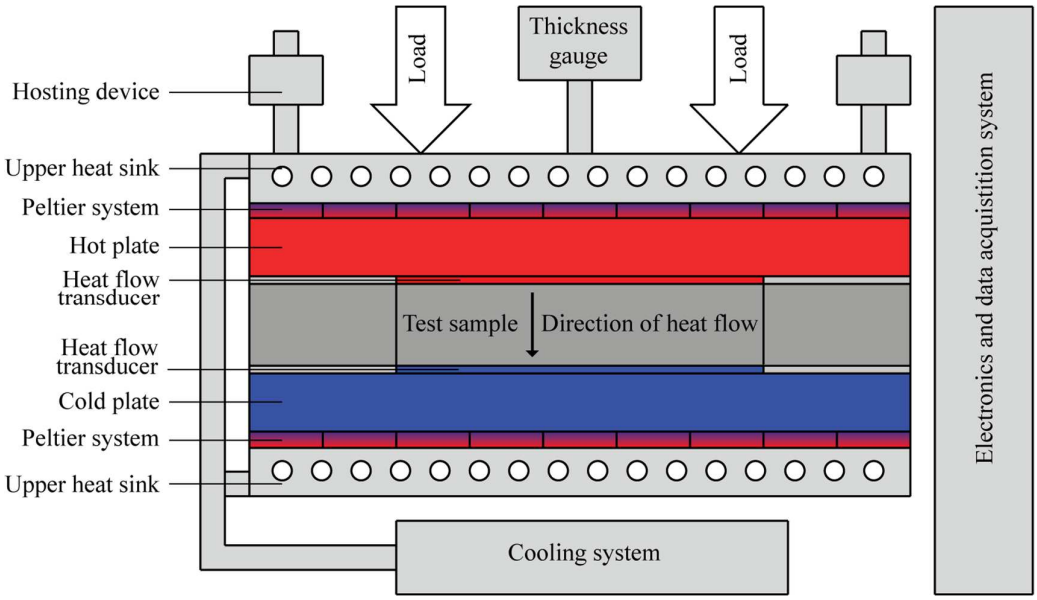

Fig. 22. Schematic design of the heat flow meter used to test the plasters and mortars.

Table 21. Main features of the heat flow meter used to test the samples [50].

Feature	Value
Plate temperature ranges [°C]	Variable, -40 to 100
Cooling system	External chiller
Plate temperature control	Peltier system
Thermocouple precision [°C]	± 0.01
Number of programmable temperatures	10
Specimen size [mm × mm × mm]	610 × 610 × 200
Thermal insulance range [m^2K/W]	0.1 to 8.0
Thermal conductivity range [W/mK]	0.002 to 1.0
Repeatability [%]	0.25
Accuracy [%]	±1 to 3

3.2.2 Compressive machine

The compressive strength of the mortar samples was tested in the Civil Engineer Laboratory of the Ryerson University of Toronto. The tests were carried out in compliance to the *ASTM C109/C109M – 16* [49], that provides a method to determinate the compressive strength of hydraulic cements and other mortars. The specimens utilized were cubes with an edge length of 50.8 mm. The compressive strength was tested by using the *Riehle Crusher*, a hydraulic type compressive machine. A schematic design of the *Riehle Crusher* compressive machine is given in Fig. 23.

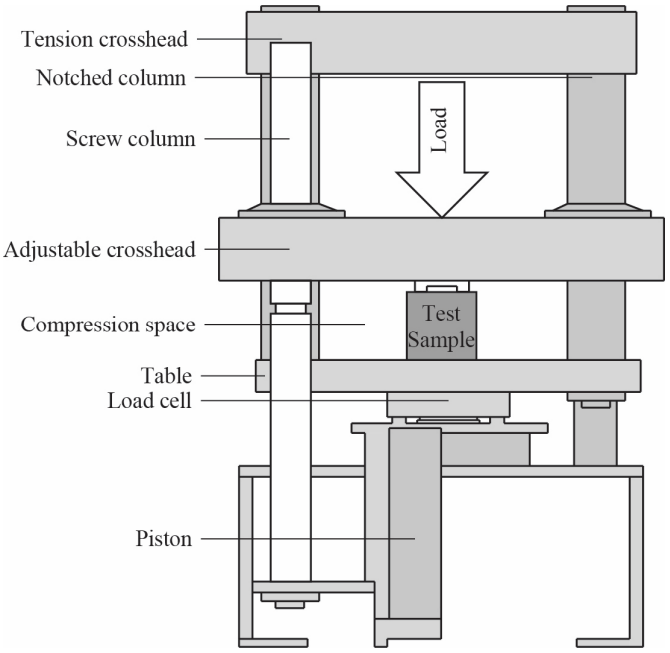

Fig. 23. Schematic design of the compressive machine used to test the mortars.

3.3 Recipes formulation and samples preparation

The following sections introduce the mix designs adopted to prepare the samples of plaster and mortar. Furthermore, the procedure utilized to produce the samples and the international standards of reference are presented.

3.3.1 Aerogel Incorporated Plaster (AIP)

3.3.1.1 Recipes formulation

Different samples of Aerogel Incorporated Plaster were cast considering the previous studies discussed in chapter 2.3. Three kinds of hydraulic lime were used and overall, eleven different types of plaster were produced. The raw materials utilized to produce the samples of plaster are presented in Fig. 24Table 23. The percentage of water added to the samples varied from 20 vol.% to 26 vol.%. For each type of plaster, a control mix was prepared by mixing the hydraulic lime with only water. The mixtures of Aerogel Incorporated Plaster were prepared by adding different quantities of aerogel.

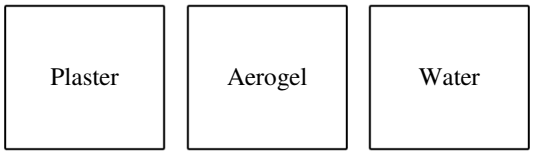

Fig. 24. Materials utilized to produce the mixtures of plaster.

Table 22 summarizes all the different mixtures which were prepared. The author highlights the fact that *Pure Fixit* already contained a quantity of aerogel around 50 vol.%. For this reason, only 15 vol.% and 25 vol.% of aerogel was added to the *Pure Fixit* to produce *Fixit + 15% aerogel* and *Fixit + 25% aerogel* mixtures, respectively. One the other hand, *Calce Idraulica* and *Saint Astier Plaster* were two different kinds of pure lime. Hence, similar percentages of aerogel were added to the mixes to produce comparable samples of Aerogel Incorporated Plaster. 25 vol.%, 50 vol.%, and 70 vol.% of aerogel particles were added to *Calce Idraulica* to produce *Calce Idraulica + 25% aerogel, Calce Idraulica + 50% aerogel* and *Calce Idraulica + 70% aerogel*. Similarly, mixes of *Saint Astier Plaster + 25% aerogel, Saint Astier Plaster + 50% aerogel,* and *Saint Astier Plaster + 70% aerogel* were produced. The quantities of materials added to the mixtures were measured in liters, which is the common procedure to prepare plasters. It permits to save time when plasters are prepared on the site because is faster than the weighing of materials. On the other hand, this procedure leads to less accuracy.

Table 22. Mix design of the mixes of plaster.

Mix	Plaster [l]	Aerogel [l]	Water [l]	Aerogel [vol.%]
Pure Fixit	5.5	0	1.534	0
Fixit + 15% aerogel	4	0.8	1.355	15
Fixit + 25% aerogel	4	1.6	1.579	25
Pure Calce Idraulica	6	0	2.174	0
Calce Idraulica + 25% aerogel	5	2.5	2.7	25
Calce Idraulica + 50% aerogel	2	3.5	1.26	50
Calce Idraulica + 70% aerogel	0.4	1.5	0.3	70
Pure Saint Astier Plaster	6	0	1.5	0
Saint Astier Plaster + 25% aerogel	5	2.5	2.7	25
Saint Astier Plaster + 50% aerogel	2	3.5	1.26	50
Saint Astier Plaster + 70% aerogel	0.4	1.5	0.3	70

3.3.1.2 Sample preparation

For each mix, parallelograms with an edge length of 150 mm and a thickness of 20 mm were produced to test the thermal conductivity. The wooden molds used to cast the samples were sprayed by using a release agent. To prepare the control samples, the plaster and the water were mixed together in a bucket by using a drill and a paddle, as shown in Fig. 25 and Fig. 26.

Fig. 25. Equipment used to prepare and cast the samples of plaster.

Fig. 26. Preparation of a mixture of plaster.

Afterward, the mixture was poured into the molds and cast, as shown in Fig. 27. To prepare the samples of Plaster Incorporated Aerogel, the aerogel and the plaster were firstly mixed together in a bucket and then the water was added. Subsequently, the mixture was poured into the mold. The molds were hit by using a plastic hammer during the casting process in order to avoid air voids. The samples were held at ambient temperature and covered with a plastic sheet for one day and then demolded. Table 23 presents the number of samples produced for each kind of plaster.

Fig. 27. Casting of a sample of plaster.

Table 23. Number of samples of plaster produced.

Mix	Number of samples
Pure Fixit	7
Fixit + 15% aerogel	7
Fixit + 25% aerogel	6[1]
Pure Calce Idraulica	7
Calce Idraulica + 25% aerogel	6[1]
Calce Idraulica + 50% aerogel	7
Calce Idraulica + 70% aerogel	3[2]
Pure Saint Astier Plaster	7
Saint Astier Plaster + 25% aerogel	6[1]
Saint Astier Plaster + 50% aerogel	7
Saint Astier Plaster + 70% aerogel	3[2]

[1] One sample broke during the demoulding process.
[2] Only three samples were cast due to the high quantity of aerogel involved in the production.

3.3.2 Aerogel Incorporated Mortar (AIM)

3.3.2.1 Recipes formulation

Various samples of Aerogel Incorporated Mortar were produced considering the previous studies presented in section 2.3.1. Two control mixtures and three samples of AIM were prepared by using the material described in chapter 3.1 and presented in Fig. 28. Overall, five mixtures were tested. One control mix was a standard mortar and the other was a standard mortar with the addition of the air entraining admixture. The samples of aerogel incorporated mortar were produced by adding a quantity of aerogel from 30% to 36% of total volume.

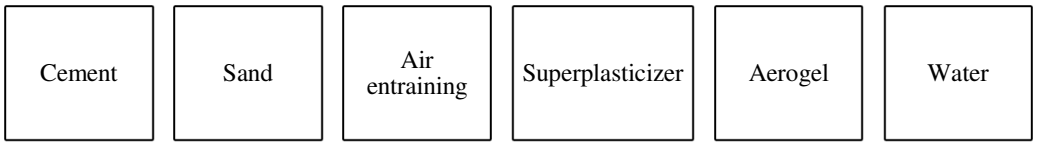

Fig. 28. Materials utilized to produce the mixtures of mortar.

Table 24 and Table 25 illustrate the mix designs that were adopted to produce each batch. The quantities of materials added to the mixes were measured by mass. Table 26 shows the water/cement ratio and the aerogel/sand ratio adopted for each mixture. Moreover, it shows the increments on aerogel/sand ratio. The water/cement ratio adopted for all the mixture was 0.54. The aerogel/sand ratio was linearly increased in order to achieve a higher aerogel volume content. Table 27 presents the percentage of aerogel added to the mixtures that ranges from 30 vol.% to 36 vol.%.

Table 24. Mix design of the mixes of mortar.

Mix	Cement [kg]	Sand [kg]	Water [kg]	Aerogel [kg]
Standard mortar	2.667	8	1.443	-
Mortar + air entraining	2.667	8	1.443	-
Mortar + 30% aerogel	2.667	8	1.443	0.352
Mortar + 33% aerogel	2.667	6.31	1.443	0.352
Mortar + 36% aerogel	2.667	5.21	1.443	0.352

Table 25. Admixtures added to the mixes of mortar.

Mix	Air entraining [ml]	Superplasticizer [ml]
Standard mortar	-	-
Mortar + air entraining	5.33	-
Mortar + 30% aerogel	-	200
Mortar + 33% aerogel	-	200
Mortar + 36% aerogel	-	200

Table 26. Water/cement and aerogel/sand ratios adopted to produce the mixes of mortar.

Mix	w/c	a/s	Increase in a/s
Standard mortar	0.54	-	-
Mortar + air entraining	0.54	-	-
Mortar + 30% aerogel	0.54	0.04400	-
Mortar + 33% aerogel	0.54	0.05575	0.01175
Mortar + 36% aerogel	0.54	0.06750	0.01175

Table 27. Percentage of aerogel added to the mixtures of Aerogel Incorporated Mortar.

Mix	Cement [l]	Sand [l]	Water [l]	Aerogel [l]	Aerogel [vol.%]
Mortar + 30% aerogel	0.84	3.019	1.443	2.34	30
Mortar + 33% aerogel	0.84	2.381	1.443	2.34	33
Mortar + 36% aerogel	0.84	1.966	1.443	2.34	36

The first control sample, *Standard mortar*, is a standard mortar prepared by using cement, sand, and water, as shown in Fig. 29. The second one, *Mortar + air entraining*, is a lightweight mortar prepared by using cement, sand, water, and air entraining admixture. The samples of *Mortar + 30%, 33%,* and *36% aerogel* were prepared by using cement, sand, water, aerogel, and superplasticizer. The superplasticizer was necessary in order to improve the workability of the mortar. The cement/water ratio was kept constant whereas the aerogel/sand mass ratio was linearly increased. The dosage rate of superplasticizer adopted was 200 mL, according to the recommended values between 130 and 650 mL/100 kg of cement.

Fig. 29. Cement, sand, and water utilized to produce *Standard mortar*.

3.3.2.2 Sample preparation

For each mixture, nine cubes with an edge length of 2 inches (50.8 mm) were produced to test the compressive strength and four parallelograms with an edge length of 150 mm and a thickness of 20 mm were cast to test the thermal conductivity. Table 28 summarizes the number of samples of each kind of mortar produced.

Table 28. Number of samples of mortar produced.

Mix	Number of samples
Standard mortar	9 cubes + 4 parallelograms
Mortar + air entraining	9 cubes + 4 parallelograms
Mortar + 30% aerogel	9 cubes + 4 parallelograms
Mortar + 33% aerogel	9 cubes + 4 parallelograms
Mortar + 36% aerogel	9 cubes + 4 parallelograms

The mold utilized to produce the specimens are shown in Fig. 30. The procedure described in the *ASTM C109/C109M-16* [49] was used to produce the samples. As shown in Fig. 31, a thin coating of release agent was applied to the interior faces of the molds by using a brush or an impregnated cloth. Then, the mold faces were wiped with a cloth to remove any excess of release agent and achieve a thin coating on the interior surfaces.

To prepare the control mixes, the dry paddle and the dry bowl were placed in the mixing position and the water was placed in the bowl. Then, the cement was added to the water and the mixer was started at the low speed for 30 seconds. Afterward, the entire quantity of sand was slowly added over a period of 30 seconds while mixing at slow speed and, at the end of

this process, 30 seconds more at medium speed for 30 seconds. Subsequently, the mixer was stopped and the mortar was let stand for 30 seconds. During the first 15 seconds of this step, the mortar collected on the side of the bowl was scraped down into the batch. Finally, the mixer was started again at the medium speed for 60 seconds. To prepare the *Mortar + air entraining*, the air entraining admixture was mixed up with water and the same procedure was carried out.

Fig. 30. Mold utilized to produce the samples of mortar.

Fig. 31. Release agent applied to the interior faces of a mold.

To prepare the batch of Aerogel Incorporated Mortar, the cement and the aerogel were firstly mixed in a bucket. Afterward, the dry paddle and the dry bowl were placed in the mixing position, the superplasticizer admixture was mixed up with water and placed in the bowl. Subsequently, the cement mixed with aerogel was placed in the bowl and the mixer was started

at the low speed for 30 seconds. Afterward, the same procedure adopted in the case of the control mixtures of mortar was carried out.

The specimens were molded within a total elapsed time of not more than 150 seconds after completion of the original mixing of the mortar batch. A layer of mortar was placed in all of the cube compartments and tamped thirty-two times in four rounds, each round at right angles to the other and consisting of eight adjoining strokes over the surface of the specimen, as illustrated Fig. 32. The tamping pressure was just sufficient to ensure uniform filling of the molds. When the tamping of the first layer in all the cube compartments was completed, the compartments were filled with the remaining mortar and tamped as specified for the first layer. On completion of the tamping, the mortar was smooth off the cubes by drawing the flat side of the trowel, with the leading edge slightly raised. The same procedure was adopted to cast the parallelograms to test the thermal conductivity.

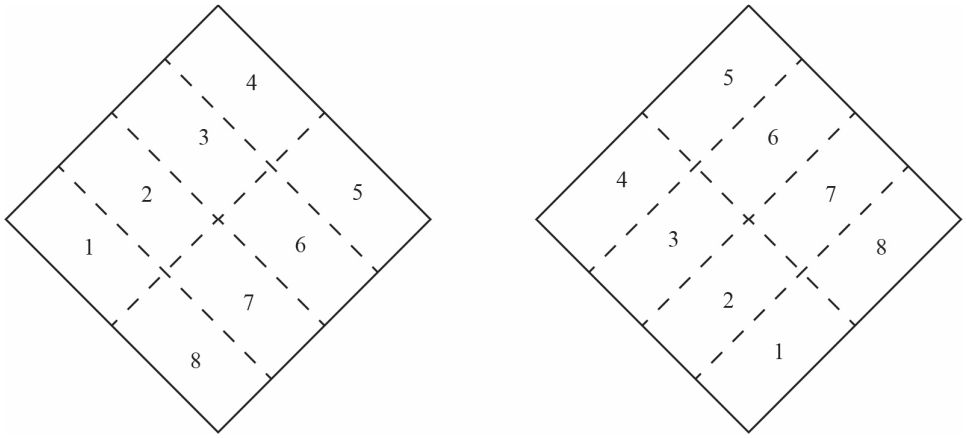

Fig. 32. Tamping rounds process to produce the samples of mortar [49].

The samples were held at a vapor saturated environment for 24 hours, then de-molded and maintained in the same water saturated environment for 28 days. For each batch of mortar three cubes were tested one day after the preparation, three cubes at the seventh day of cure, and the last three after twenty-eight days. The parallelograms were held at a vapor saturated environment for 24 hours, then de-molded and maintained in the same water saturated environment for 7 days. Afterward, when they got dry, the thermal conductivity was tested. For each batch of mortar, at least two parallelograms were tested. The density of the samples was measured after the curing until it was found stable. The weight of the control mixtures permitted to estimate the level of air in the control mix *Mortar + air entraining*.

Experimental Results

4.1 Results on Aerogel Incorporated Plaster (AIP)

The samples of Aerogel Incorporated Plaster were tested in the Building Science Laboratory of the Ryerson University of Toronto. The overview of the test results is presented in the following sections and discussed in section 5. The results of all the tests are included in the Appendix. By increasing the quantity of aerogel less water was necessary in order to achieve a good workability. Moreover, the samples with the highest quantity of aerogel resulted in being brittle and breakable. The samples of plaster produced to test the thermal conductivity are shown in Fig. 33, Fig. 34, and Fig. 35.

Fig. 33. Samples of AIP with *Calce Idraulica* produced to test the thermal conductivity.

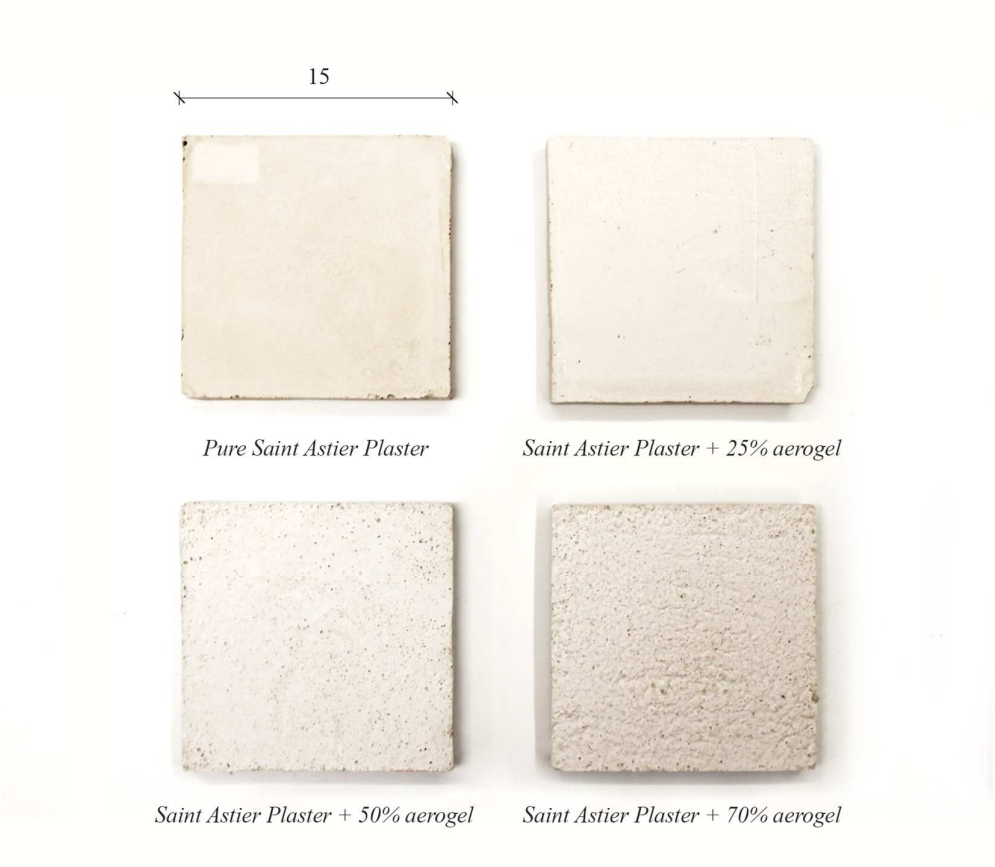

Fig. 34. Samples of AIP with *S.A. plaster* produced to test the thermal conductivity.

Fig. 35. Samples of AIP with *Fixit* produced to test the thermal conductivity.

4.1.1 Density

Table 29 illustrates the mean values of the weight and the density of each mixture. Table 37, in Appendix 1, shows the weight and the density of the samples of plaster used to calculate the data presented in Table 29. The dry weight was the stable value found after the drying process. The density of the samples was calculated by considering a mean volume of the samples of 450 cm^3 since the variation of the thickness of the samples was neglectable.

Table 29. Mean weight and density of the mixtures of plaster.

Mixture	Dry weight [g]	Dry density [kg/m^3]
Pure Fixit	108.6	241.3
Fixit + 15% aerogel	91.7	203.8
Fixit + 25% aerogel	89.7	199.3
Pure Calce Idraulica	499.4	1109.8
Calce Idraulica + 25% aerogel	331.0	735.6
Calce Idraulica + 50% aerogel	225.4	501.0
Calce Idraulica + 70% aerogel	117.3	260.7
Pure Saint Astier Plaster	500.0	1111.1
Saint Astier + 25% aerogel	325.0	722.2
Saint Astier + 50% aerogel	232.9	517.5
Saint Astier + 70% aerogel	138.0	306.7

4.1.2 Thermal conductivity

The values of thermal conductivity, thermal resistance, and thickness at 23.9 °C of each mix of plaster are presented in Table 30. For each mixture, two samples were tested by using the heat flow meter. The accuracy of the heat flow meter was set to 0.1%. The thermal conductivity of each sample was tested at the mean temperatures of 10 °C, 20 °C, and 30 °C with a delta of 20 °C. Hence, the temperature of the plates varied between 0 °C and 40 °C. According to the *ASTM C518* [47], the value of the thermal conductivity at 23.9 °C of each mixture was calculated by doing a linear regression of the thermal conductivities at the three different temperatures mentioned above. The final value of thermal conductivity of each mixture was the mean of the thermal conductivities at 23.9 °C of the two tested samples of the same mixture. As an example, a comparison between the thermal conductivities of two different samples of the same mixture is given in Fig. 36. The two curves represent the thermal

conductivities of *Fixit + 25% aerogel #2*[1] and *Fixit + 25% aerogel #1*. Since they are similar, no more tests were carried out in this case. Similarly, the thermal resistance of each mixture was calculated at 23.9 °C.

Table 30. Properties at 23.9 °C of the mixtures of plaster.

Mixture	Thickness [cm]	Thermal conductivity [W/mK]	Thermal resistance [m^2K/W]
Pure Fixit	2.0623	0.0323	0.6394
Fixit + 15% aerogel	2.1002	0.0276	0.7625
Fixit + 25% aerogel	2.0487	0.0275	0.7484
Pure Calce Idraulica	2.1104	0.2032	0.1373
Calce Idraulica + 25% aerogel	2.0483	0.1151	0.1803
Calce Idraulica + 50% aerogel	2.0242	0.0687	0.2938
Calce Idraulica + 70% aerogel	1.9934	0.0311	0.6427
Pure Saint Astier Plaster	2.1285	0.1906	0.1121
Saint Astier + 25% aerogel	2.0913	0.1176	0.1790
Saint Astier + 50% aerogel	2.0606	0.0712	0.2885
Saint Astier + 70% aerogel	2.0240	0.0356	0.5712

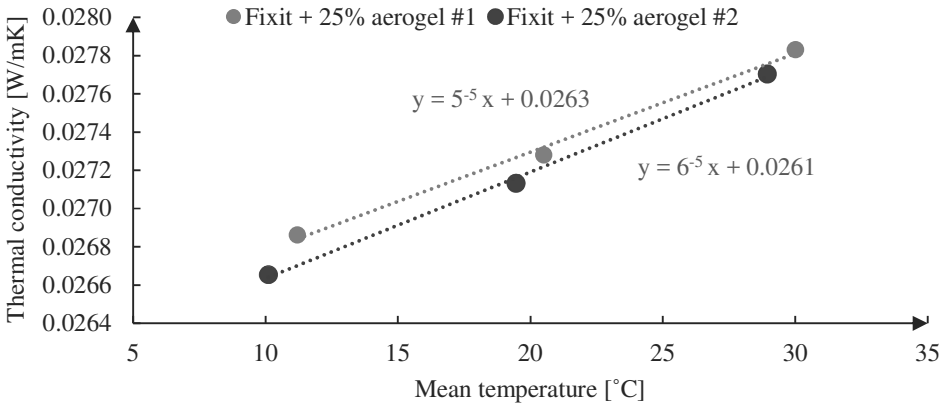

Fig. 36. Linear regressions of the thermal conductivity of two different mixtures of plaster.

The values of thermal conductivity and thermal resistance of the samples at 23.9 °C were calculated by doing a linear regression. Table 38, in Appendix 2, shows the results of each test which was carried out to obtain the data in Table 30.

[1] Samples of the same mixtures were numbered and identified by using hashtags.

4.2 Results on Aerogel Incorporated Mortar (AIM)

The samples of Aerogel Incorporated Mortar were tested in the Building Science Laboratory and the Civil Engineer Laboratory of the Ryerson University of Toronto. Similar tests to the case of plasters were carried out. Moreover, compressive tests were done. The overall results of the tests are presented in the following sections and are discussed in section 3. Specific results are reported in the Appendix. In a similar manner to the case of plasters, by increasing the quantity of aerogel less water was necessary to achieve a good workability. The samples of mortar produced to test the thermal conductivity and the mechanical strength are presented in Fig. 37 and Fig. 38, respectively. The first two samples are the control mixtures. The percentage of aerogel increases from the samples on the top left to the ones on the bottom right.

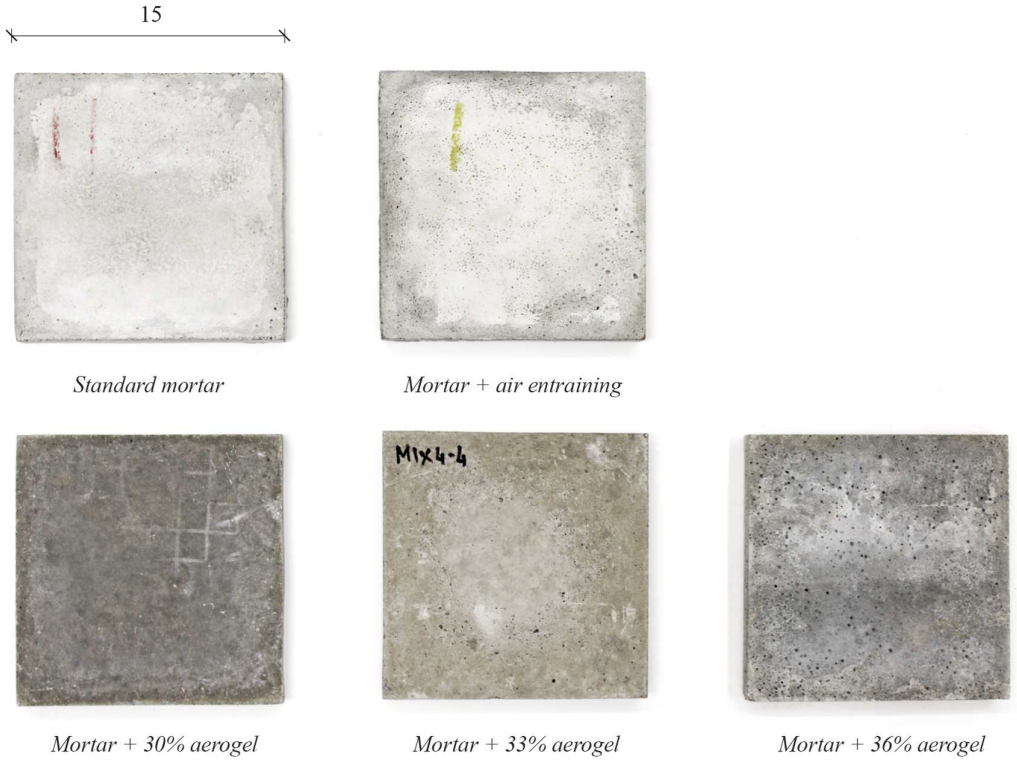

Fig. 37. Samples of mortar produced to test the thermal conductivity.

Fig. 38. Samples of mortar produced to test the mechanical strength.

4.2.1 Density

The cubes were weighed seven days after the casting process to observe the density changes during the cement hydration process. Moreover, the parallelepipeds were removed after seven days of curing and weighed twenty-eight days after the casting process, when they were already dry. The densities of the cubes and the parallelograms were calculated by considering a volume of 131.1 cm^3 and 513.3 cm^3, respectively. Table 31 presents the mean values of the density of each mixture. The first column represents the densities of each mixture at the age of seven days, calculated by using the cubes. The second column shows the dry density of each mixture, calculated by using the parallelograms.

Table 31. Density of the mixtures of mortar.

Mixture	Density day 7 [kg/m^3]	Density dry [kg/m^3]
Standard mortar	2320.22	2065.85
Mortar + air entraining	2025.25	1803.85
Mortar + 30% aerogel	1688.60	1532.10
Mortar + 33% aerogel	1553.03	1334.38
Mortar + 36% aerogel	1386.82	1229.19

Table 31 was plotted in Fig. 39. The weight and the density of all the samples of mortar are reported in Table 39 and Table 40, in Appendix 3. The quantity of air added to the control mix *Mortar + air entraining* compared to the *Standard Mortar* was around 13%.

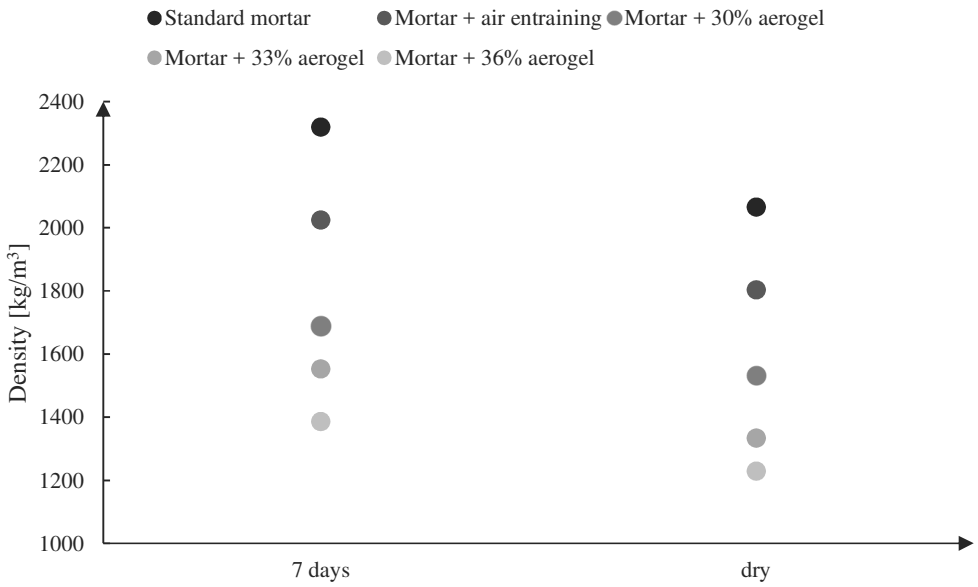

Fig. 39. Density of the mixtures of mortar.

4.2.2 Thermal conductivity

The same procedure of the case of plasters was utilized to measure the thermal conductivity of the samples of mortar. Hence, the reader can reference to section 4.1.2. However, a brief description and an example are given in the present section as well. The samples used to test the thermal conductivity were taken off the room seven days after the casting process and tested when got dry. The values of thermal conductivity, thermal resistance, and thickness at 23.9 °C of each mixture are presented in Table 32. For each mixture, two samples were tested by using the heat flow meter with the accuracy set to 0.1%. According to the *ASTM C518* [47], the values of thermal conductivity at 23.9 °C of each mixture was calculated by doing a linear regression of the thermal conductivities at 10 °C, 20 °C, and 30 °C. A comparison between the thermal conductivities of the two samples of the same mixture is shown in Fig. 40. The two curves are the thermal conductivities of *Mortar + 36% aerogel p#1* and *Mortar + 36% aerogel p#4*. The final value of thermal conductivity and thermal resistance of each mixture was obtained by calculating the mean of the thermal conductivities at 23.9 °C of the two tested samples. As an example, Table 33 present the results of the thermal tests run to characterize *Mortar + 36% aerogel p#1*. The same procedure was utilized to characterize the other samples. Table 42, in Appendix 5, shows the results of all the tests carried out to obtain Table 32.

Table 32. Properties at 23.9 °C of the mixtures of mortar.

Mixture	Thickness [cm]	Thermal conductivity [W/mK]	Thermal resistance [m^2K/W]
Standard mortar	2.2470	0.2844	0.0789
Mortar + air entraining	2.3221	0.2522	0.0921
Mortar + 30% aerogel	2.2773	0.2365	0.0919
Mortar + 33% aerogel	2.2413	0.2009	0.1118
Mortar + 36% aerogel	2.2493	0.1488	0.1519

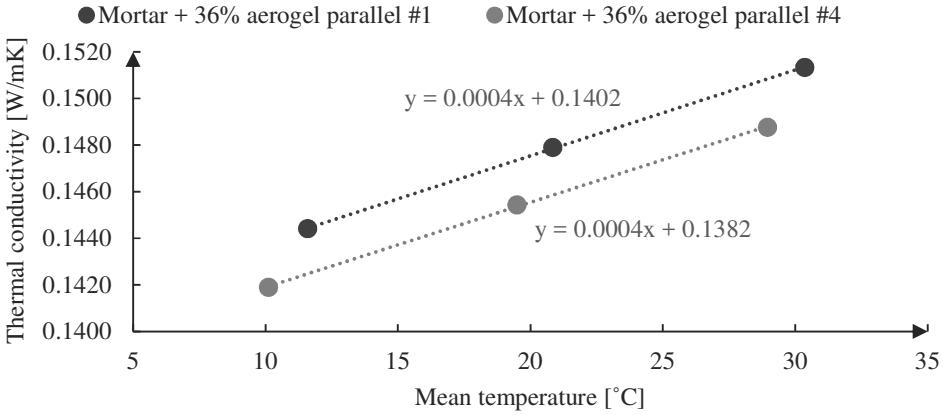

Fig. 40. Linear regressions of two different samples of the same mixture of mortar.

Table 33. Characterization of *Mortar + 36% aerogel p#1* at 23.9 °C.

Sample	*Mortar + 36% aerogel p#1*		
Date	December 17nd, 2016		
Mean temperature [˚C]	11.59	20.85	30.3
Delta [˚C]	21.47	21.32	21.10
Thermal Conductivity [W/mK]	0.1444	0.1479	0.1513
Thermal Resistance [m^2K/W]	0.1550	0.1517	0.1488
Thickness [cm]	2.2385	2.2442	2.2519
Temperature Gradient [K/m]	958.93	949.88	937.15
Test duration [hh:mm]	01:41	01:36	01:33
Mean thermal conductivity at 23.9 °C [W/mK]	0.1498		
Mean thermal resistance at 23.9 °C [m^2K/W]	0.1516		
Mean thickness at 23.9 °C [cm]	2.2466		

4.2.3 Compressive strength

The compressive strength of the samples was tested in the Civil Engineer Laboratory at the Ryerson University. Nine cubes of each mixture with an edge length of 2 inches (50.8 mm) were tested. Three cubes were broken one day after the demoulding process, three more after seven days, and the last three after twenty-eight days.

Table 34 shows the mean values of the compressive strength of each mixture after one, seven, and twenty-eight days. The results are plotted in Fig. 41. Table 41, in Appendix 4, shows the compressive strength of all the samples produced. Those results were utilized to calculate the mean values of compressive strength reported in Table 34.

Table 34. Compressive strength of the mixtures of mortar.

Mixture	Compressive Strength [MPa]		
	Day 1	Day 7	Day 28
Standard mortar	19.823	46.686	50.302
Mortar + air entraining	17.860	21.234	25.092
Mortar + 30% aerogel	5.583	9.955	11.183
Mortar + 33% aerogel	2.487	4.856	5.144
Mortar + 36% aerogel	0.893	3.027	4.109

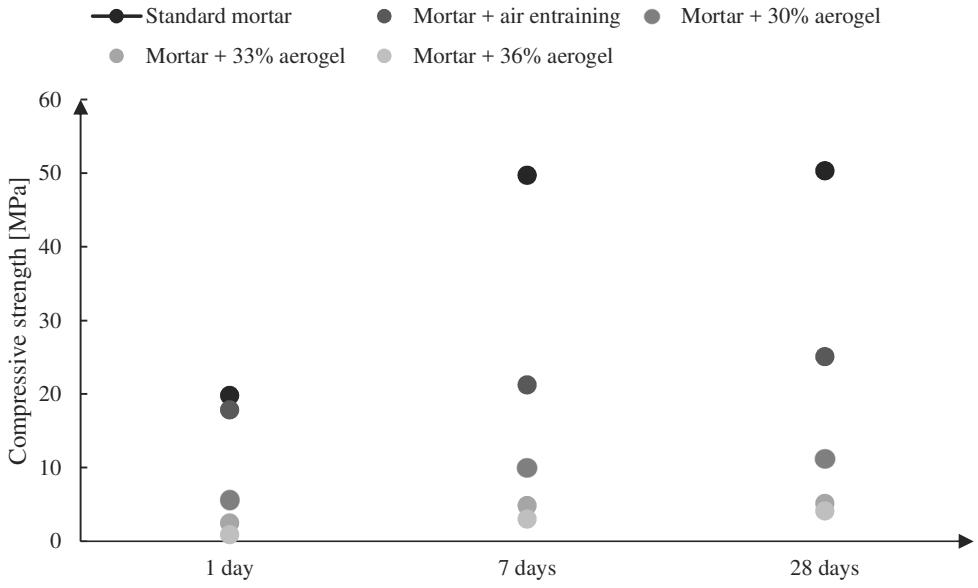

Fig. 41. Compressive strength of the mixtures of mortar.

4.2.4 Permeability

The water vapor permeability of some samples of mortar was tested and the results are presented in this chapter. The water vapor permeability is defined as the time rate of water vapor transmission through unit area of flat material of unit thickness, induced by unit vapor pressure difference between two specific surfaces under specified temperature and humidity conditions. It is measured in gm/hm^{2}Pa, where g is grams, m is meters, h is hours, and Pa is Pascals. The water vapor permeability is related to the moisture, which can be transferred through a material and is an import factor since moisture could create mold, rotting, and corrosion. Moreover, it influences the comfort of the human beings [51].

Many standards define different methods to test the vapor permeability, such as *ASTM E96*, *ASTM 1868*, *ISO 15496*, *ISO 2528*, and *ISO 11092*. The methods can be divided into two groups: the *gravimetric methods* and the *sweating hot plate methods*. The *gravimetric methods* are the most commonly used. They can be carried out according to three different procedures: the *desiccant method*, the *water method*, and the *inverted water method.* In the *desiccant method*, the vapor is passed out from the environment to inside of a cup, where dry calcium chloride or silica gel are placed. In the *water method*, the vapor is passed out from inside of a cup where water is placed in the environment. The *inverted water method* is similar to the *water method* but the cup is turned upside down and the water is in contact with the sample. The three methods are presented in Fig. 42.

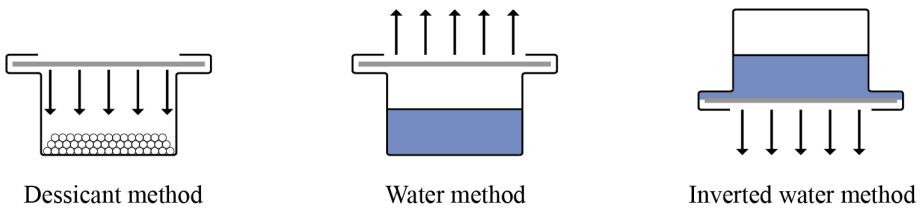

Fig. 42. Gravimetric methods to calculate the water vapor permeability.

The *water method* was used in this research. A cup was filled with water and the sample tight covered to it, in order to achieve a relative humidity of 100% inside the cup. Afterward, it was placed in a controlled environment with a constant relative humidity of 50%. Under the action of the difference of pressure between the water vapor inside and outside of the cup, a vapor transfer occurred through the sample to the environment and the total weight of the cup decreased. The water vapor permeability (WVP) is calculated according to the following formula:

$$WVP = G \times \frac{h}{t \times A \times \Delta P} \tag{30}$$

where G is the weight change of the cup in grams, h is the thickness of the sample in meters, t is the time during which the weight change occurred, A is the surface of the sample in meters squared, and ΔP is the difference in pressure between the two sides of the specimen.

The permeability of three mixtures of mortar was tested: *standard mortar*, *Mortar + 30% aerogel,* and *Mortar + 36% aerogel* were tested. For each mixture, only one sample was tested. However, the results showed no relevant weight changes in cups and hence, a G values too small to calculate an accurate value of permeability. It could be justified by the fact that only small aggregates were used in the mixtures of mortar which resulted in having really compact and not very permeable materials.

Discussion

5.1 Aerogel Incorporated Plaster (AIP)

The density and the thermal conductivity of the mixtures decreased by increasing the quantity of the aerogel. The thermal conductivity of the samples increased linearly with the temperature. As stated in the previous section, the samples resulted in being more brittle by increasing the quantity of aerogel. Moreover, a smaller ratio water/plaster was necessary to achieve a good workability by adding aerogel to the mixes. The time span necessary to dry the samples was between three and seven days, dependently on the amount of water and aerogel added to the mixture and the type of plaster. *Fixit* needed about seven days to dry, more than the other mixtures.

Pure Fixit resulted in being the best balance between thermal conductivity and strength. However, better results in terms of thermal conductivity were achieved by adding aerogel to *Pure Fixit*. The thermal conductivity of the samples of *Pure Fixit* was slightly reduced by adding 15 vol.% of aerogel. However, by adding 25 vol.% of aerogel to *Pure Fixit,* no more improvements on thermal properties were observed. The thermal conductivity and the density of the samples of *Pure Fixit* were similar to the ones of the samples of *Calce Idraulica + 70% aerogel* and *Saint Astier Plaster + 70% aerogel.* The density and the thermal conductivity of *Italian Plaster* and *Saint Astier Plaster* in function of the percentage of aerogel added to the mixtures are presented in Fig. 43 and Fig. 44, respectively. They linearly decreased by adding aerogel and were roughly reduced by a 'factor of three' compared to the control mixture by adding 70 vol.% of aerogel.

The density in function of the amount of aerogel in the mixtures is reported in Fig. 43. As stated before, a linear dependence between the percentage of aerogel and the density was observed. The density of the samples of *Calce Idraulica* and *Saint Astier Plaster* were around 1100 kg/m^3. The density of the samples was reduced by more than 70% by adding aerogel. The lowest density of 260.74 kg/m^3 was achieved by adding 70 vol.% of aerogel.

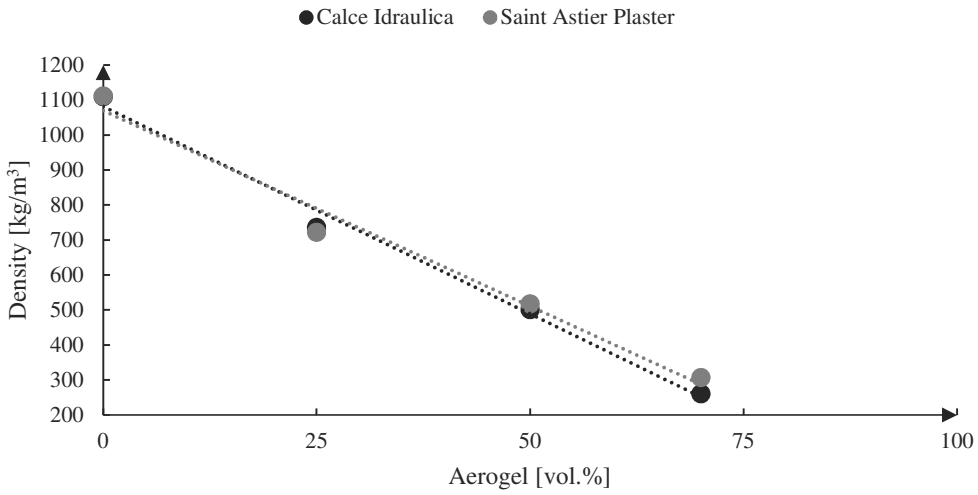

Fig. 43. Aerogel volume content vs. density in plasters.

The thermal conductivity in function of the amount of aerogel in the mixtures is reported in Fig. 44. It decreased linearly by increasing the quantity of aerogel. The thermal conductivity of the samples of *Calce Idraulica* and *Saint Astier Plaster* was about 0.2 W/mK. The lowest thermal conductivity was reached by adding 70 vol.% and was 0.0311 W/mK. Hence, the aerogel permitted to reduce the thermal conductivity by more than 80%.

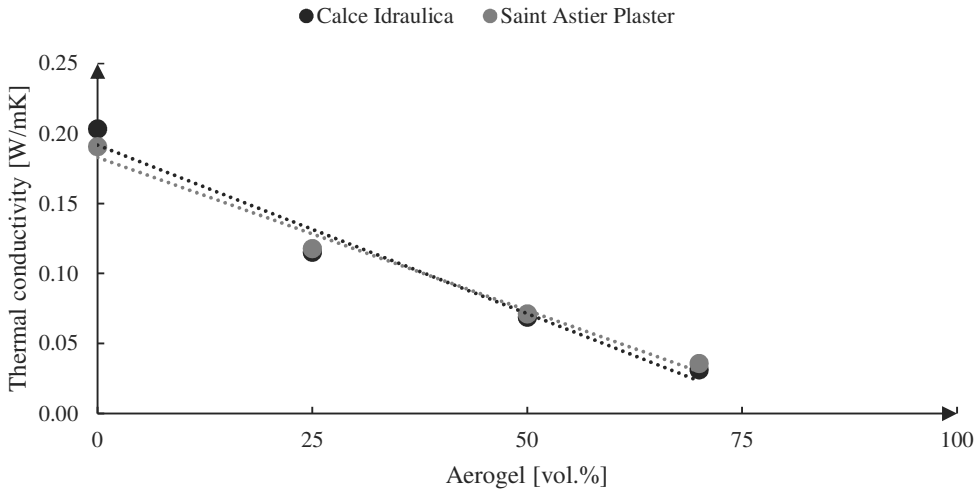

Fig. 44. Aerogel volume content vs. thermal conductivity in plasters.

A comparison between the mixes developed in this study and the ones discussed in the literature review is presented in Fig. 45. The dry density and the thermal conductivity of the mixtures of plaster are reported on the axes. The developed samples did not reach similar performance to the ones presented in the literature review. The plaster developed by Buratti et al. in 2016 [10], had a density of 125 kg/m^3 and a thermal conductivity of 0.16 W/mK. In this

research, the samples with the same thermal conductivity had a density greater than 900 kg/m^3. Hence, the thermal conductivity still has the chance to be improved while maintaining a compact material.

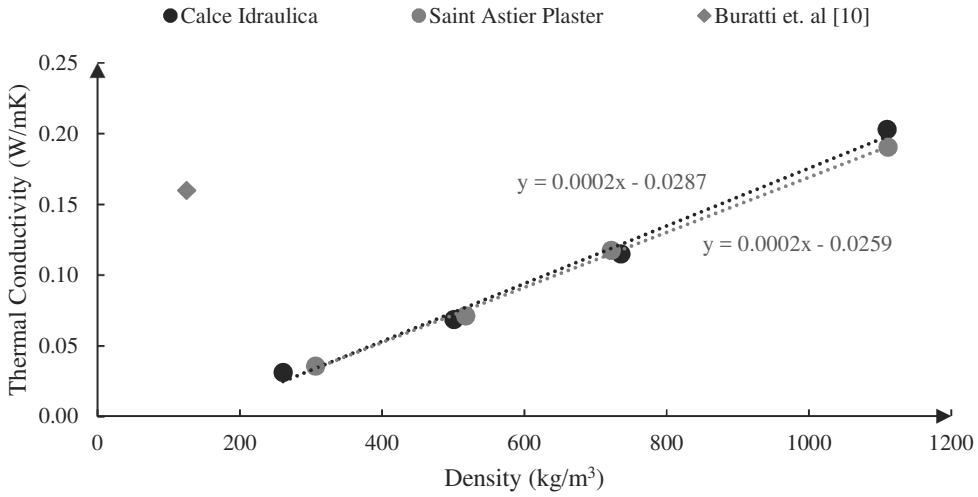

Fig. 45. Density vs. thermal conductivity in plasters.

5.2 Aerogel Incorporated Mortar (AIM)

The density and the thermal conductivity of the samples of mortar decreased by increasing the quantity of the aerogel added to the batches. Similarly, the compressive strength decreased by increasing the quantity of aerogel. The most performing mixture was found to be the *Mortar + 30% aerogel*, as it is explained in the following paragraphs. The samples were compact in the case of the *Mortar + 30% aerogel* and *Mortar + 33% aerogel*. On the other hand, the samples of *Mortar + 36% aerogel* were much more porous and likely to exfoliate. However, the batch of *Mortar + 36% aerogel* was much waterier than what expected due to the reduction of sand. This suggested that improvements in compactness and compressive strength can be achieved by reducing the water/cement ratio. On the other hand, improvements on thermal conductivity could be achieved by adding more aerogel to the mixture and maintaining the same water/cement ratio of the mixture. Moreover, due to the excessive amount of water, the samples of *Mortar + 36% aerogel* presented segregation. As Fig. 46 shows, the surfaces of the same sample of *Mortar + 36% aerogel* look different. The aerogel particles rose to the surface and created an irregular and crumbly surface whereas the heavier aggregates settled to the bottom and formed a smooth and compact surface.

Lower surface *Upper surface*

Fig. 46. Surfaces of a sample of *Mortar + 36% aerogel* which show segregation.

A linear dependence of the thermal conductivity and the temperature was observed, as Fig. 40 in section 4.2.2 showed. The same behavior was observed in the case of the thermal resistance. As Fig. 41 in section 4.2.3 showed, due to the presence of aerogel, the samples of AIM presented flat curves of compressive strength during the curing process. Moreover, a linear dependence of the just mentioned properties and the quantity of aerogel added to the mixes was noticed, as Fig. 47, Fig. 48, and Fig. 49 show.

The density in function of the amount of aerogel in the mixtures is reported in Fig. 47. As stated before, a linear dependence between the percentage of aerogel and the density was observed. The density of the control mix of *Standard mortar* was about 2065.85 kg/m^3. The air entraining and the aerogel reduced the density up to 13% and 40%, respectively. Thus, the density of the samples of mortar almost halved by adding 36 vol.% of aerogel, as Fig. 47 shows. The density of the mixture of *Mortar + 30% aerogel* was about 1530 kg/m^3 and the lowest one of *Mortar + 36% aerogel* was 1229.19 kg/m^3.

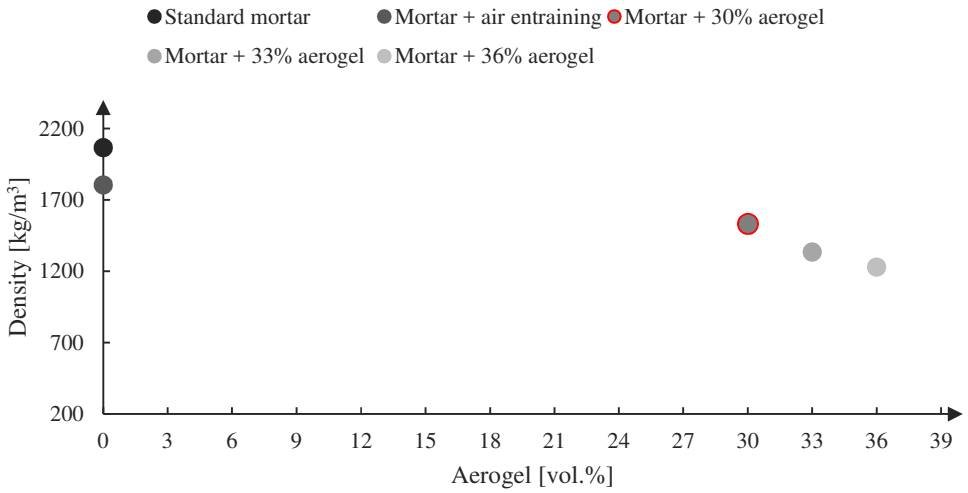

Fig. 47. Aerogel volume content vs. density in mortars.

The thermal conductivity as a function of the amount of aerogel in the mixtures is reported in Fig. 48. Once again, the thermal conductivity decreased linearly by increasing the quantity of aerogel. The samples of mortar almost halved the thermal conductivity by adding 36 vol.% of aerogel, as the mixtures of mortar with aerogel show. The thermal conductivity of *Mortar + 30% aerogel* was 0.2365 W/mK and the lowest one of *Mortar + 36% aerogel* was 0.1488 W/mK. Despite the quantity of air-entraining could not be increased, more aerogel can be added to the mixes in future investigations to decrease the thermal conductivity.

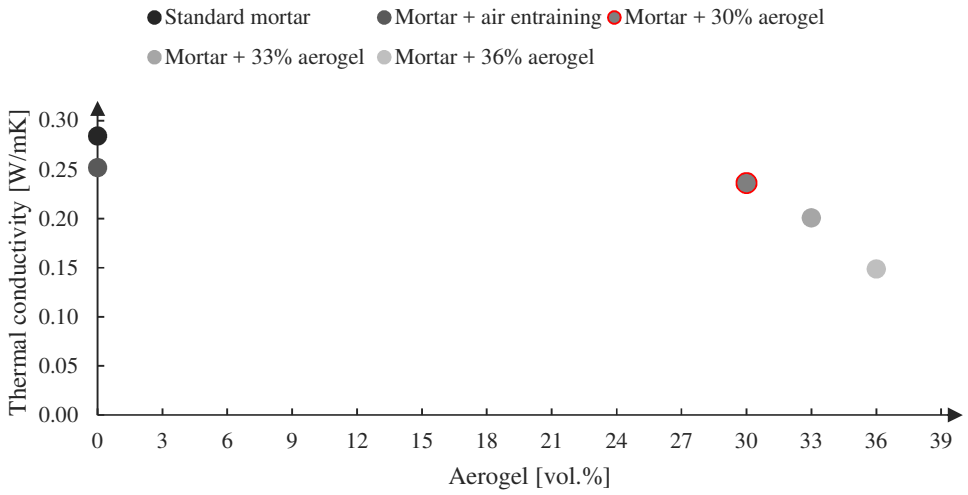

Fig. 48. Aerogel volume content vs. thermal conductivity in mortars.

The compressive strength in function of the amount of aerogel in the mixtures is reported in Fig. 49. It linearly decreased by increasing the quantity of aerogel. However, an improved compressive strength could have been achieved by reducing the quantity of the water in some mixtures which were found to be watery. The compressive strength of the samples of *Standard mortar* was around 50 MPa and halved by adding the air entraining admixture. The compressive strength of the samples of *Mortar + 36% aerogel* decreased by a factor of ten compared to the control sample of *Standard Mortar*. The mixture of *Mortar + 30% aerogel* had a compressive strength of 12 MPa and resulted in being suitable as lightweight mortar.

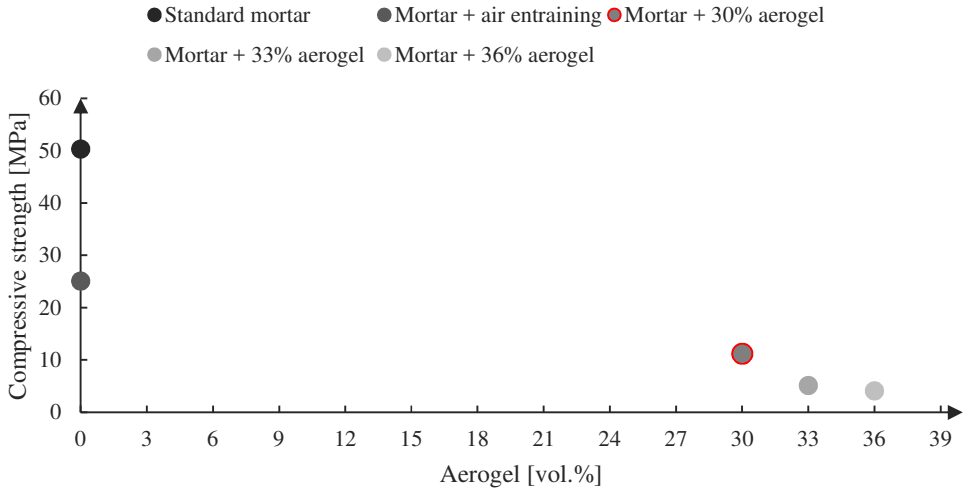

Fig. 49. Aerogel volume content vs. compressive strength in mortars.

A comparison between the mixes developed in this study and the ones discussed in the literature review is presented in Fig. 50 and Fig. 51. As stated before, the most performing mix obtained was the *Mortar + 30% aerogel*, which had a low thermal conductivity as well as was compact and light. In Fig. 50, the dry density and the thermal conductivity of the mixes are reported on the axes. The thermal conductivity linearly increased when the density of the mixtures increased. The density of *Mortar + 30% aerogel* reached low values of density, around 1530 kg/m^3, but still greater than the values presented in the literature.

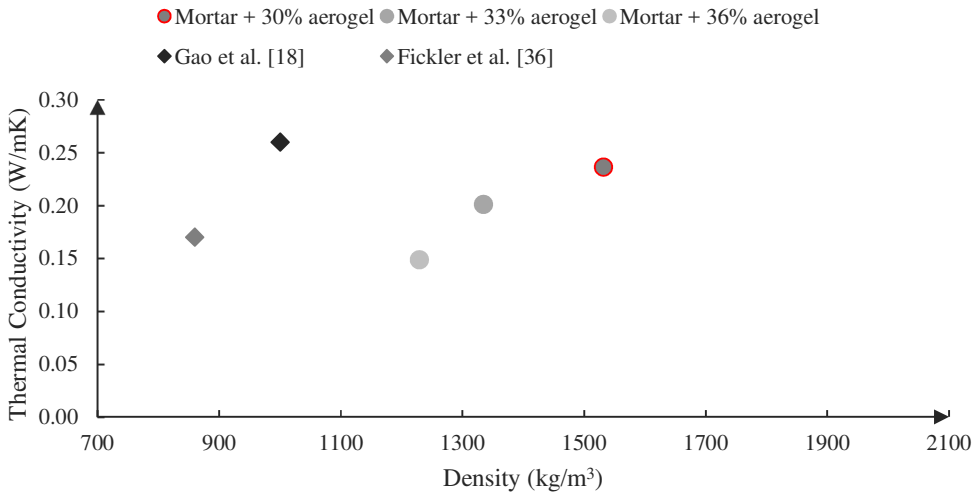

Fig. 50. Density vs. thermal conductivity in mortars.

In Fig. 51, the compressive strength and the thermal conductivity of the mixes are reported on the axes. *Mortar + 30% aerogel* presented a very good balance between thermal conductivity and compressive strength. The thermal conductivity of the mixture of *Mortar + 30% aerogel* was reduced by the 17%, respectively, compared to the control mixture of *Standard mortar.* The thermal conductivity was about 0.24 W/mK and the compressive strength reached 11.1 MPa. This is the most interesting result of the study. In fact, the mixture of *Mortar + 30% aerogel* reached a lower thermal conductivity and a higher compressive strength than the most performing mixture presented by Gao et al. [18], as Fig. 51 shows. The thermal conductivity was reduced by almost 0.03 W/mK and the compressive strength was increased by almost 3 MPa. Moreover, the *Mortar + 30% aerogel* had a compressive strength greater than the one presented by Fickler et al. [36] although, in this case, the thermal conductivity was slightly higher.

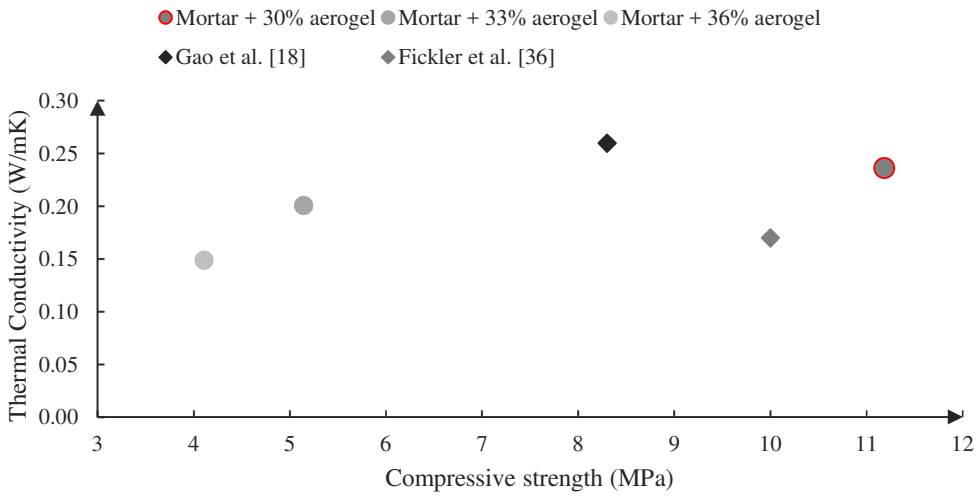

Fig. 51. Compressive strength vs. thermal conductivity in mortars.

As stated in chapter 4.2.4, the results showed G values too small to calculate an accurate value of permeability. It is justified by the fact that only small aggregates were used in the mixtures of mortar which resulted in being really compact and not very permeable.

The case study of a precast panel

6.1 WUFI® Pro 6.0 software

The present chapter introduces WUFI® Pro 6.0 software [52], which was used to run the hygrothermal simulations of a proposed panel with AIM.

The hygrothermal analysis is important since it influences the performance and the durability of the building. Damp can lead to unwanted effects, such as:

- reduction of thermal insulation;
- increased dust contamination, algae or mold growth;
- mechanical stresses due to swelling and shrinking caused by changes in humidity or by salt crystallization;
- damages due to frost, rotting or corrosion;
- incomplete hydration because of drying too rapidly;
- delayed maturing of screed topping because of drying too slowly.

WUFI® Pro is a software designed to calculate the simultaneous heat and moisture transport in building envelopes. It performs hygrothermal analysis on building component cross-sections, considering built-in moisture, driving rain, solar radiation, longwave radiation, capillary transport, and summer condensation. It also takes into account real climate conditions to achieve the accurate design of building components. Results of temperature, relative humidity, and water content are given through temporal and spatial distribution at critical positions of the hygrothermal conditions. A user interface allows a simple set-up of input data and gives graphs and animations of results.

Starting from specified initial conditions, WUFI Pro computes the temporal evolution of the temperature and moisture distributions in the building components. This evolution is determined not only by the transport equations which govern the processes in the component but, also by the heat and moisture exchange with the environment.
The surface transfer coefficients indicate to which extent the conditions in the surroundings affect the building component, especially the heat and moisture flows through its surfaces.

In the calculation of heat transport, WUFI takes into account the thermal conduction, the enthalpy flows through moisture movement with phase change, the short-wave solar radiation, and the night-time long-wave radiation cooling. The vapor transport mechanisms included in WUFI are vapor diffusion and solution diffusion. On the other hand, the liquid transport mechanisms taken into account are capillary conduction and surface diffusion. The convective heat transport by air flows is neglected since it is usually difficult to quantify and would not be very useful in a one-dimensional analysis. Similarly, the convective vapor transport by air flows is ignored. Also, seepage flow through gravitation, hydraulic flow through pressure differentials, as well as electrokinetic and osmotic effects are not included in WUFI analysis.

6.1.1 The calculation model

Different hygrothermal simulation models which provide reliable results has been developed so far. The model which WUFI uses is presented below. The non-steady heat and moisture transport processes in building components are described by the following coupled one dimensional differential equations:

Heat transport equation:
$$\frac{\partial H}{\partial T}\frac{\partial T}{\partial t} = \frac{\vartheta}{\partial x}\left(\lambda \frac{\partial T}{\partial x}\right) + h_v \frac{\partial}{\partial x}\left(\frac{\delta}{\mu}\frac{\partial p}{\partial x}\right) \qquad (31)$$

Moisture transport equation:
$$\rho_w \frac{\partial u_w}{\partial \varphi}\frac{\partial \varphi}{\partial t} = \frac{\partial}{\partial x}\left(\rho_w D_w \frac{\partial u_w}{\partial \varphi}\frac{\partial \varphi}{\partial x}\right) + \frac{\partial}{\partial x}\left(\frac{\delta_w}{\mu}\frac{\partial p}{\partial x}\right) \qquad (32)$$

where D_W [m²/s] is the liquid transport coefficient, H [J/m³] is the enthalpy of moist building material, h_v [J/kg] is the evaporation enthalpy of water, p [Pa] is the water vapor partial pressure, u_w [m³/m³] is the water content, δ_w [kg/msPa] is the water vapor diffusion coefficient in air, T [°C] is the temperature, λ [W/mK] is the thermal conductivity of moist material, μ [%] is the vapor diffusion resistance factor of dry material, ρ_w [kg/m³] is the density of water, and φ [%] is the relative humidity.

The left-hand sides of both equations consist of the storage terms. Heat storage comprises the heat capacity of the dry material and the heat capacity of the moisture present in the material. Moisture storage is described by the derivative of the moisture storage function mentioned above. The right-hand sides of the equations consist of the transport terms. Heat transport is the sum of moisture-dependent thermal conductivity and vapor enthalpy flow. This heat transport by vapor enthalpy flow is due to water evaporating in one place and thereby absorbing latent heat from this place, and then diffusing to a different place, condensing there

and releasing latent heat. This kind of heat transport is often called latent heat effect. Liquid transport through surface diffusion and capillary conduction due to a gradient of relative humidity shows only a relatively minor temperature dependence. Vapor diffusion, on the other hand, is strongly affected by the temperature field, since the saturation vapor pressure increases exponentially with temperature. The differential equations are discretised by means of an implicit finite volume method and are iteratively solved. The accuracy of the numerical solution depends on the mesh widths of the numerical grid, the size of the time steps and the choice of the convergence criteria. Usually, the numerical solution is sufficiently accurate so that the effect of numerical parameters can be ignored in comparison with the effects of the physical parameters like material and climate data.

6.1.2 Data input and data output

The data input required by WUFI to run a simulation are:

- geometry and orientation of the component;
- material data for each layer which may be entered by hand or taken from the material database;
- initial conditions of the temperature and moisture;
- surface transfer coefficients for heat, vapor and liquid transport, orientation and inclination;
- climate conditions which may be entered by hand or taken from the climate database;
- the time span for which the calculation shall be carried out entering the starting date and the number of time steps.

After the calculation is ended, WUFI gives three types of results:

- courses, which describe the temporal evolution of quantities taken at specified locations or as mean values over specified layers. The quantities given as courses are the heat flux densities through the interior and exterior surface, the temperature, and relative humidity at monitoring positions, the mean moisture content of each layer, and the total moisture content of the entire building component;
- profiles, which show the distribution of a quantity across the building component at a specified point in time. The quantities given as profiles are the temperature across the building component, the relative humidity across the building component, and the moisture content across the building component;
- films of the calculation.

WUFI automatically records the initial and final states as profiles but it is possible to specify additional points in time. The results are presented through graphics functions that allow to view the computed courses and profiles, edit and print the graphs.

6.1.3 Material data

The heat and moisture fluxes permeating the building component are not only determined by its present and past conditions and the boundary conditions but also and foremost by the conductive and capacitive properties of the individual materials. There are basic data which are indispensable for a calculation. Other data may be optional, depending on the material and on the purpose of the calculation.

The basic material properties that should be specified are:

- Bulk density [kg/m³];
- Porosity [m³/m³];
- Thermal capacity [J/kgK];
- Thermal conductivity [W/mK];
- Diffusion resistance factor [%].

WUFI can also include air layers in the building components but does not simulate the air convection, which would not make much sense in one dimension anyway. It considers the air layer as a resistance to heat and moisture flows. However, the additional transport phenomena can be included by adjusting the heat conductivity and the diffusion resistance so that the correct heat and vapor flows result from the calculation.

6.1.4 Climate data

Starting from specified initial conditions, WUFI computes the temporal evolution of the temperature and moisture distributions in the building component. This evolution is determined not only by the underlying transport equations which govern the processes in the component but also by the heat and moisture exchange with its surroundings. Since WUFI has been developed specifically for application in building, the surrounding medium is the ambient air, which can be outdoor or indoor air. The surrounding conditions are described in terms of meteorological parameters like temperature, relative humidity, and solar radiation.

WUFI needs the following climate data for each time step:

- rain load vertically incident on the exterior surface [l/m²h];
- solar radiation vertically incident on the exterior surface [W/m²];
- temperature of the exterior air [°C];
- relative humidity of the exterior air [%];
- temperature of the interior air [°C];
- relative humidity of the interior air [%];
- barometric pressure [hPa];
- long-wave atmospheric counter radiation [W/m²].

The weather file may contain measured weather data or synthetic but realistic weather data, such as the Test Reference Years, or artificial data which describe, for example, a laboratory experiment.

As mentioned above, WUFI needs the rain load and the radiation load incident on the wall or roof surface under investigation. Since rain and radiation are directed quantities, these loads depend on the orientation and the inclination of the individual building component. Unfortunately, in conventional weather measurements, they are usually only recorded for horizontal surfaces. It is possible, however, to compute them from conventional weather data. WUFI performs these conversions automatically and the user only needs to supply the conventionally measured weather data.

6.2 Introduction to precast panels

Wall panels are used in concrete structures and steel structures for exterior enclosure design and internal partitions. Design and detailing panels push the experience limits of architects and engineers and requires different interrelated steps.

Wall panels can be classified, according to the following criteria, as:

- non-loadbearing or loadbearing elements;
- precast or cast-in-place elements.

Precast panels used as cladding elements are a common choice. The main advantages of such items are the rapid construction capability, the low cost of the system, and the aesthetic value. Formworks are not necessary and panels can be placed quickly leading to a significant reduction in construction time and costs. Precast panels are usually produced with a standard width of 2.5 m and a maximum height of 13 m, due to the transportation process. The typical thermal transmittance of a precast panel is between 0.34 W/m^2K and 0.50 W/m^2K. Precast panels rely on thickness, density, and mass for weather protection between the exterior and the interior space. Applied exterior weather-resistant coatings can be used, although they alter the finished exterior appearance. Concrete thickness and properties, exterior climate, interior temperature, and humidity conditions influence the design for moisture and vapor transmission. The required structural reinforcements provide tensile strength and are often made of steel bars and, more rarely, of fibers. The joints between two different panels and between the panels and the slabs are complex issues that must be solved with engineers and illustrated in the structural drawings. Opening for windows, louvers, and doors as well as conduits for electrical and lighting items must be evaluated and designed with engineers as well. They are potential weak spots for air and water that can infiltrate through the concrete and near the weather-proofing interfaces of the openings. Seals to provide weather protection should be realized, often doing two distinct lines of sealant. However, achieving a continuous thermal and waterproof envelope is usually difficult due to the connections and hence, panels should be designed to allow drying towards the exterior and interior faces.

Precast panels can be classified as

- horizontal or vertical panels;
- standard or thermal-break panels.

Horizontal panels are connected to the pillars and permit to realize strip windows. Vertical panels are connected to the beams and permit to design windows only in the center. Thermal-

break panels lead to excellent performance under mechanical and thermal resistance profiles. They allow reduced energy costs, meeting the highest standards of thermal efficiencies and reducing the life-cycle costs of the building due to the energy savings. The inner layer of thermal insulance material can be achieved with EPS and provides an improved thermal resistance. On the other hand, thermal-break panels result in being thicker than standard panels and can be up to 40 cm thick. In the following section, the description and the preliminary drawings of the proposed panel are presented. An example of a building which was build using precast panels is given in Fig. 52. It is the Hepworth Art Gallery in Wakefield (UK) designed by David Chipperfield and built in 2011.

Fig. 52. Hepworth Art Gallery in Wakefield (UK) designed by David Chipperfield [53].

6.3 The case study of a precast panel

The proposed panel is precast with thermal break. It is also a vertical and non-loadbearing element. Its overall thickness is 22 cm and involves traditional materials used in thermal break panels, such as EPS. The typical layers of concrete are substituted with a layer of Aerogel Incorporated Mortar, which permits to achieve improved thermal performance. *Mortar + 30% aerogel* is the mixture which was used to run the simulations of the panel since it was found to be the most suitable one, as discussed in chapter 5.2. It was developed in this study and had a density of 1530 kg/m^3, a thermal conductivity of 0.24 W/mK, and a compressive strength of about 11 MPa. More details related to *Mortar + 30% aerogel* were presented in chapters 3, 4, and 5. The U-value of the panel was calculated and compared to the one of the same panel made of concrete C 12/15 instead of Aerogel Incorporated Mortar. The results of the simulations are presented in chapters 6.5.

The precast panel comprises of:

- a weather resistant coating 2 cm thick to protect the panel from external agents and improve its durability;
- an AIM layer 6 cm thick to bear the dead loads;
- an EPS layer 6 cm thick to increase the thermal resistance of the panel;
- an AIM layer 8 cm thick to bear the dead loads.

The wall performance can be improved with an additional interior wall, which is built after that the precast panel is placed and connected to the slabs. An interior wall is proposed in this study. It has an overall thickness of 16 cm and involves traditional material, such as mineral wool and gypsum boards. The overall thickness of the wall is 38 cm. The U-value and the hygrothermal simulations of the wall are presented in chapters 6.5 and 6.6.

The interior wall placed after the precast panel comprises of:

- an air-gap 6.5 cm thick to achieve a double wall and hence, the discontinuity between the interior and the exterior environments;
- an aluminium stud frame to bear the load of the gypsum boards filled with mineral wool 8 cm thick;
- gypsum boards 1.5 cm thick used as interior finishing.

Table 35 characterizes the Aerogel Incorporated Mortar precast panel. The plan, section, and elevation of the wall, as well as two details, are given on the following page. The drawings are a preliminary design of the panel. The height and the width of the panel were chosen referring to typical dimensions of panels. As it can be observed, the precast panel is 6.3 m high, 2.5 m large, and 22 cm thick. However, as stated before, the overall thickness that considers the precast panel and also the interior wall is 38 cm. The weight of the panel was calculated according to the densities presented in the previous chapters and in the literature review.

Table 35. Characterization of the AIM precast panel.

Feature	Characterization
Dimensions [m x m]	6.3 x 2.5
Thickness [cm]	22
Thickness of the insulation layer [cm]	8
Weight [kg/m^2]	240[1]

[1] The density of the EPS used to calculate the weight of the panel was found in the literature review and was about 25 kg/m^2. The density of *Mortar + 30% aerogel* refers to chapter 4.

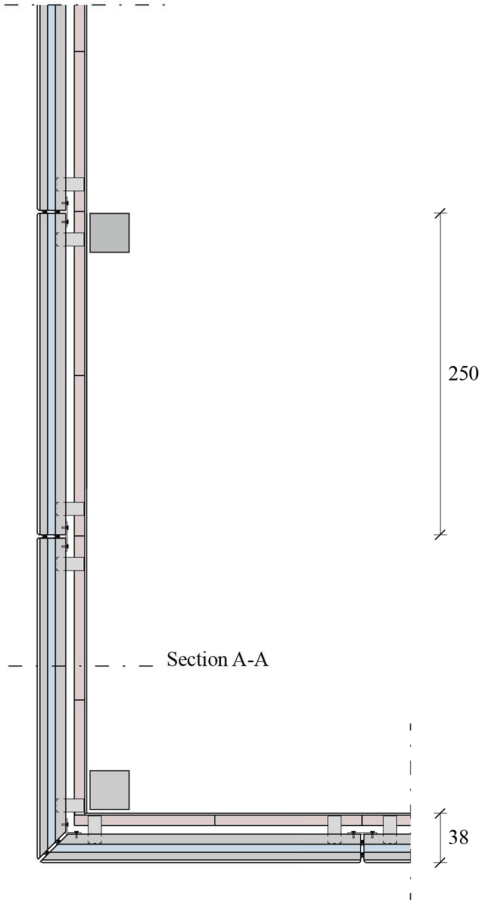

Plan 1:50

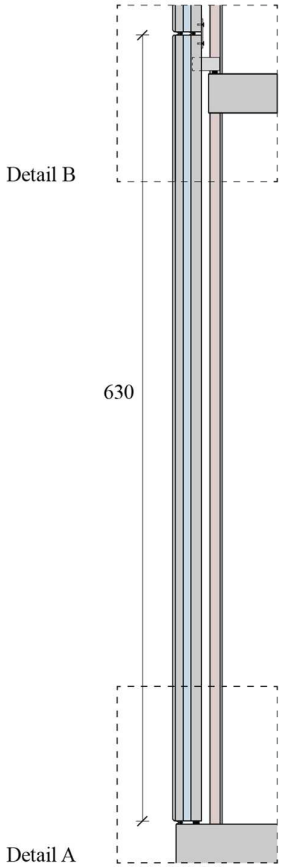

Section A-A 1:50

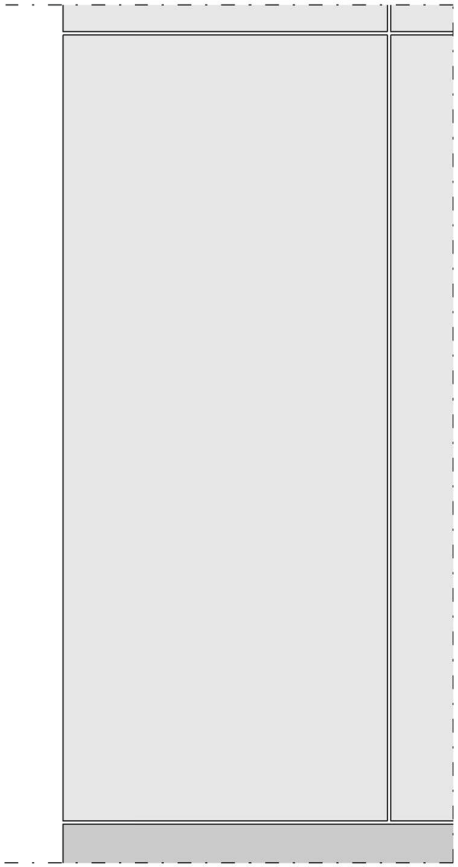

Elevation 1:50

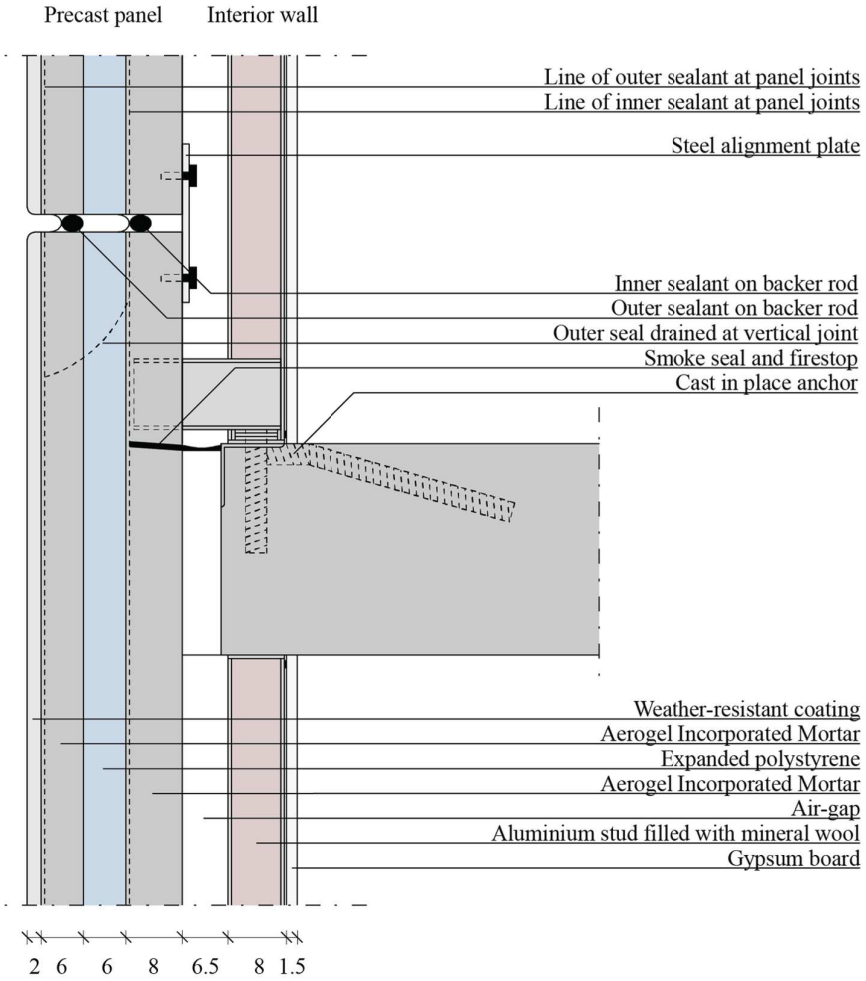

Detail A 1:10

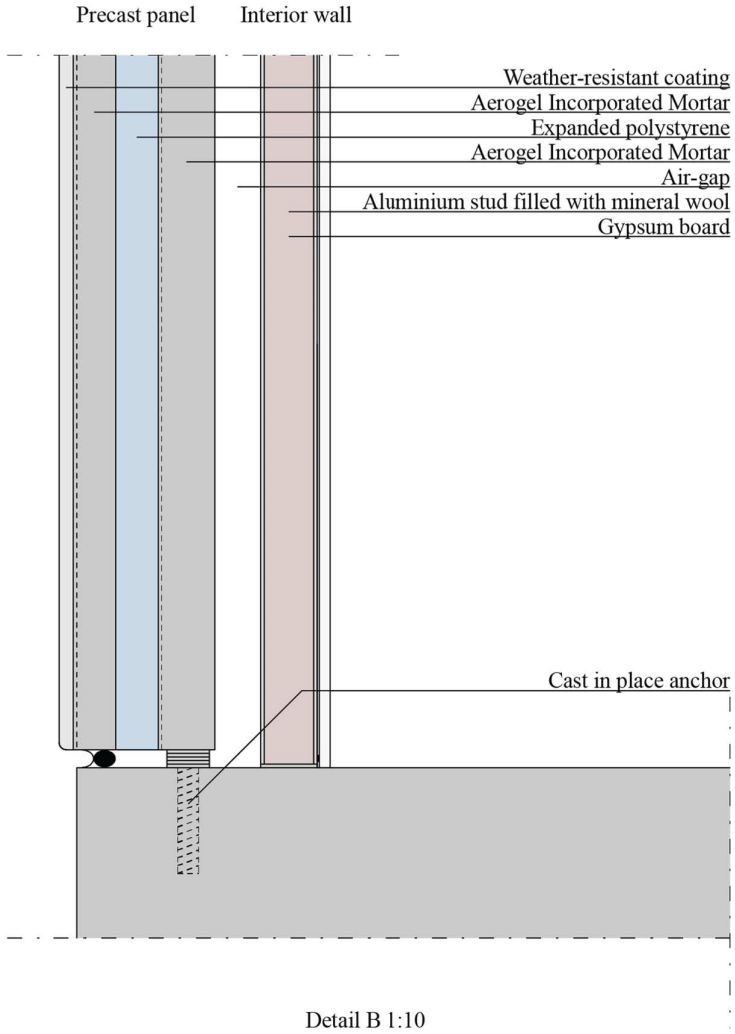

Detail B 1:10

6.4 Hygrothermal modelling of the precast panel

The hygrothermal modelling of the wall was carried out by using *WUFI Pro software*. Two cross sections were studied. *Cross section 1* intersects the mineral wool that fills the aluminium studs and *cross section 2* intersects the aluminium studs that represent the thermal bridges. *Cross section 2* is the worst scenario since it crosses the few centimetres of the stud webs. The monitoring positions were placed between each layer in order to obtain the values of temperature, relative humidity, and water content, as presented in Fig. 53.

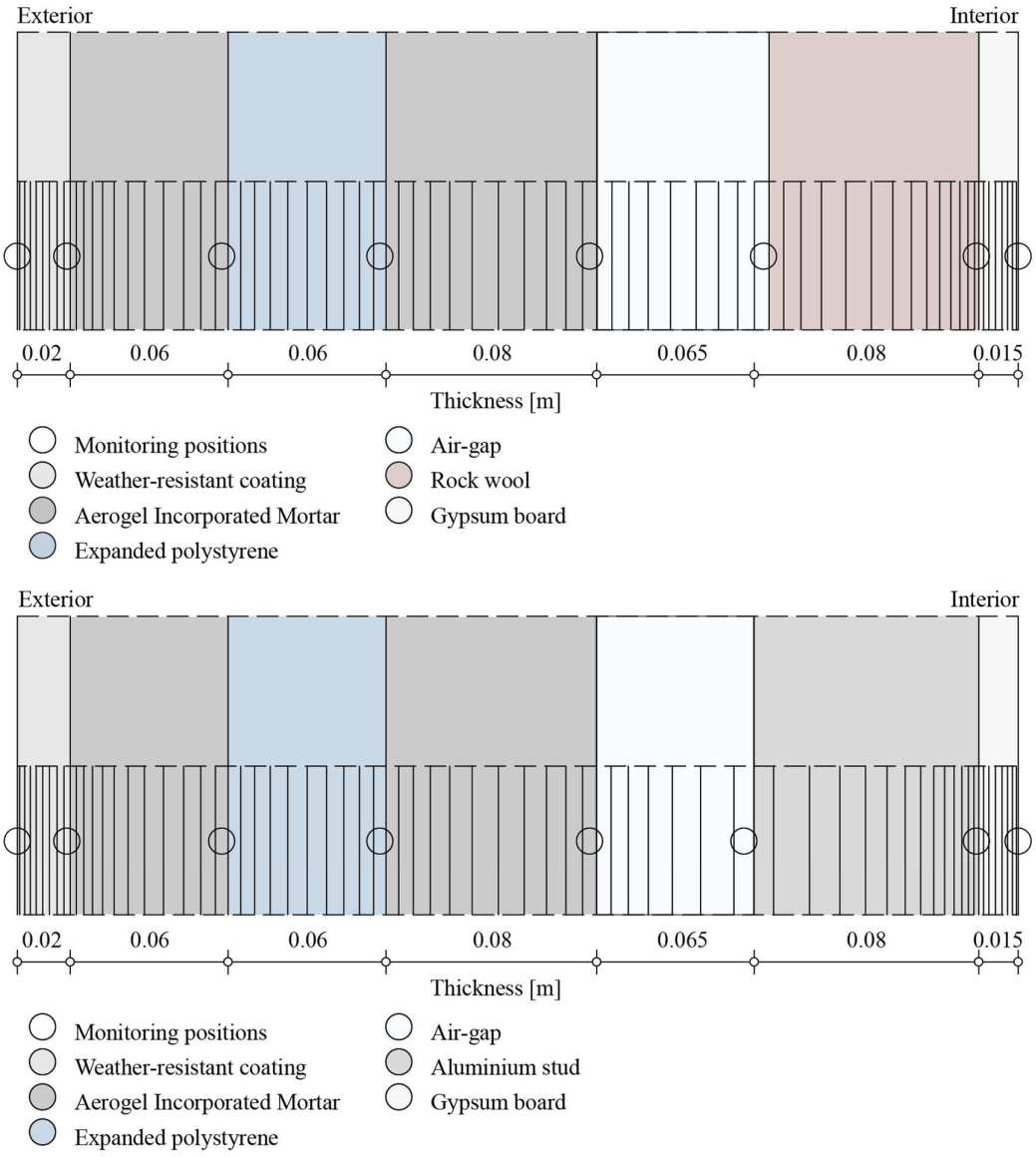

Fig. 53. Modelling of the precast panel in WUFI Pro.

The material properties were taken from the test results of this study and the database of WUFI, which refers to many commercialized products. In the case of the AIM, the thermal conductivity and the density were entered by hand whereas the porosity and the thermal capacity were taken from the material database. As stated in chapter 5.2, it was not possible to calculate an accurate value of water vapor permeability and hence, a diffusion resistance factor. Therefore, the water vapour diffusion resistance (WVDR) was taken from the material database as well. Table 36 summarizes the properties of the materials utilized in the precast panel and involved in the simulation.

Table 36. Properties of the material utilized in the precast panel.

Material	Bulk density [kg/m^3]	Porosity [m^3/m^3]	Specific heat capacity [J/kgK]	Thermal conductivity [W/mK]	WVDR
Weather-resistant coating	1900	0.24	850	0.8	25
AIM	1230	0.27	850	0.149	19.99
EPS	15	0.95	1500	0.04	30
Air-gap layer	1.3	0.999	1000	0.94	0.07
Gypsum board	850	0.65	850	0.2	8.3
Aluminium stud	2690	0.25	917	240	0
Mineral wool	60	0.95	850	0.04	1.3

The calculation period lasted two years. The test results of the second year are presented in the next chapter. The wall orientation was set to the west and its inclination to 90°. The outdoor and indoor air temperature and relative humidity are presented in Fig. 54 and Fig. 55, respectively. The outdoor climate was set in Toronto, which latitude and longitude are 43.67° and 79.6°, respectively. The rain load and the solar radiation are presented in Fig. 56 and Fig. 57. The indoor climate was defined according to the *EN15026/WTA 6-2*. The air temperature was set to 20 °C when the outdoor temperature was below 10 °C, and to 25 °C when the outdoor temperature was higher than 20 °C. When the outdoor temperature was between 10 °C and 20 °C the indoor temperature was linearly increased from 20 °C to 25 °C. Finally, the relative humidity was set to a medium moisture load.

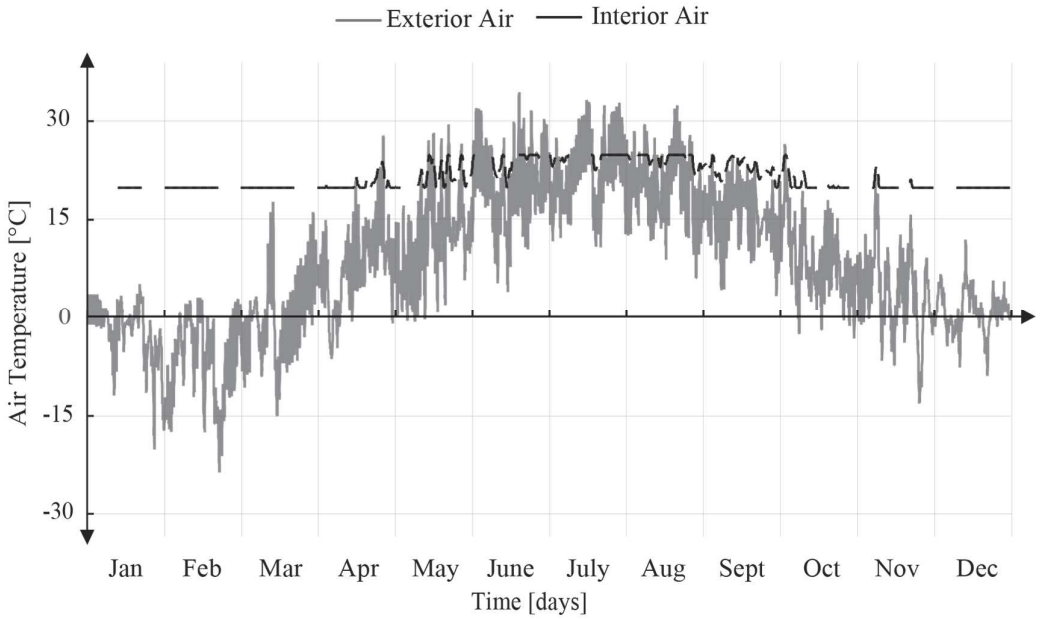

Fig. 54. Indoor and outdoor air temperature in Toronto.

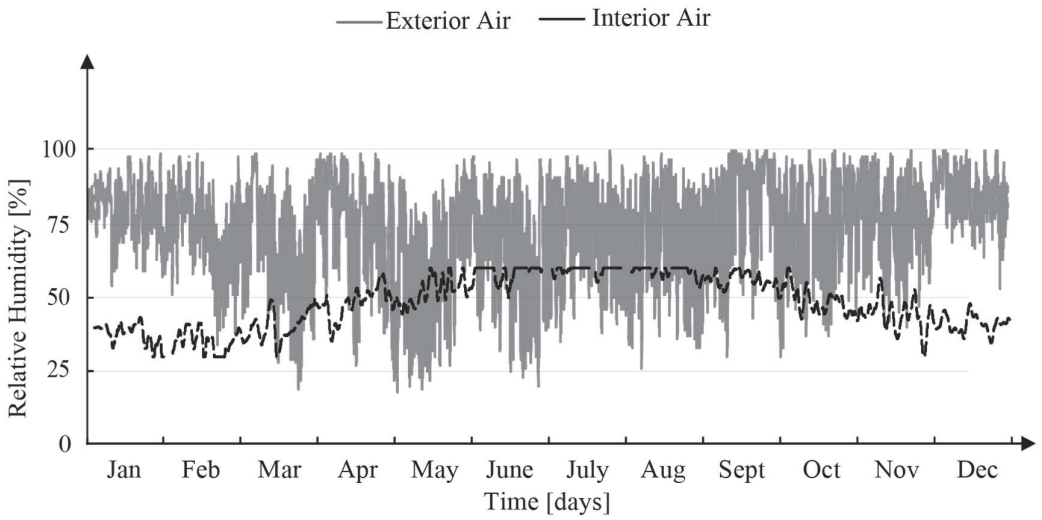

Fig. 55. Indoor and outdoor relative humidity in Toronto.

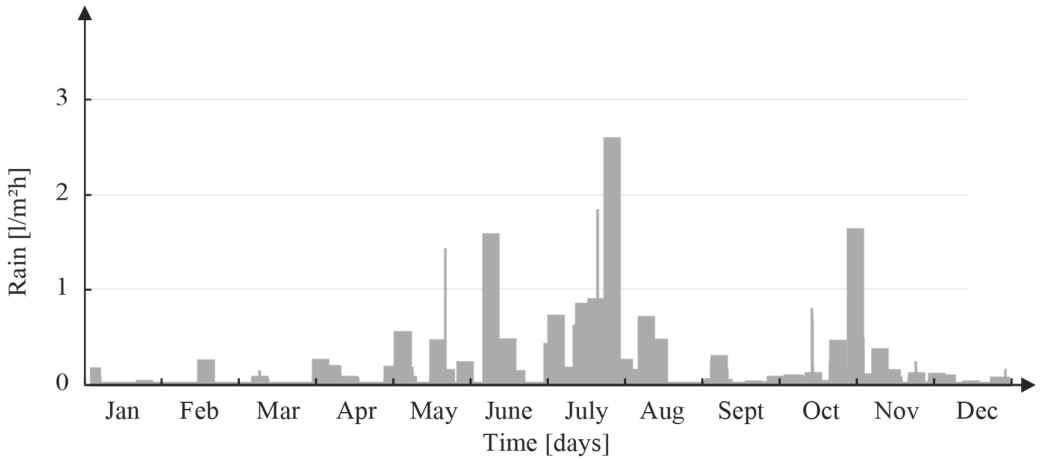

Fig. 56. Rain load in Toronto.

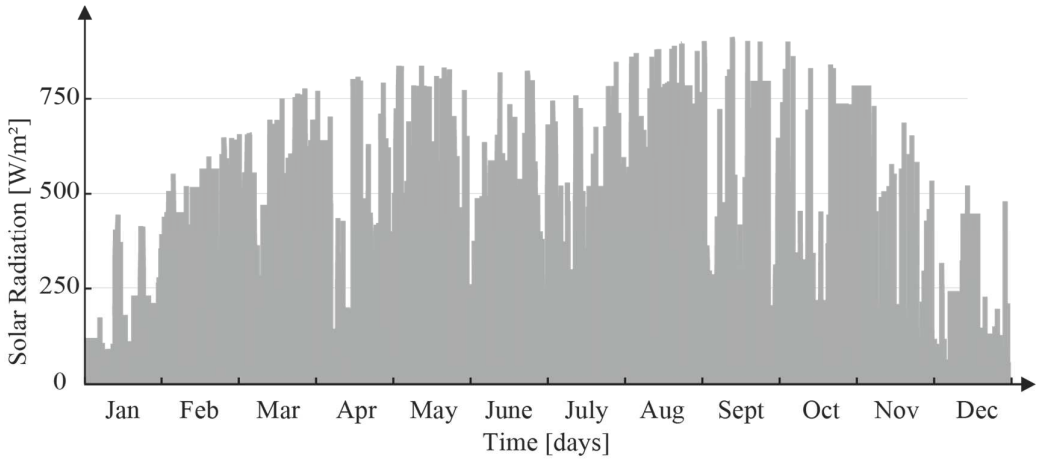

Fig. 57. Solar radiation in Toronto.

6.5 Results of hygrothermal analysis

The calculated U-value of the precast Aerogel Incorporated Mortar panel was 0.46 W/m^{2}K. On the other hand, the U-value of the precast concrete panel used as a benchmark was 0.56 W/m^{2}K. The U-value of the entire wall, calculated considering the precast Aerogel Incorporated Mortar panel and the interior wall, was 0.23 W/m^{2}K. These values are discussed in chapter 6.6.

The relative humidity and the air temperature between each layer of the two cross sections presented in chapter 6.4 are plotted in the following graphs and discussed in chapter 6.6. The graphs of the water content are presented in Appendix 6.

Fig. 58 shows the air temperature between the layers of *cross section 1*. In each layer, the temperature reached the maximum value in August. The exterior surface experienced a maximum temperature of about 45 °C. Between the EPS and the interior layer of AIM, the highest temperature dropped to 30 °C. The inner layer of AIM reduced the temperature a few degrees more whereas the temperature of the interior surface was the same of the indoor climate data.

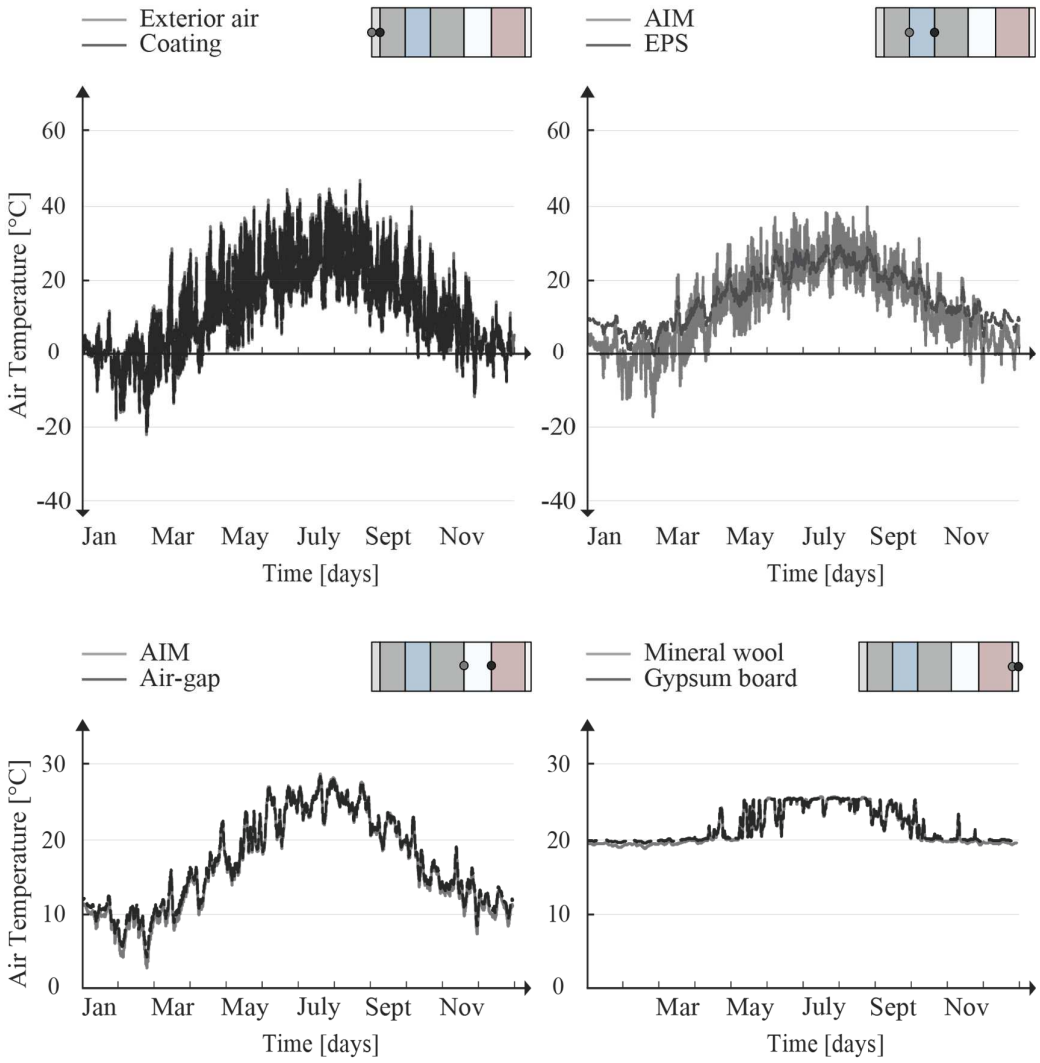

Fig. 58. Air temperature in the proposed panel, *cross section 1*.

Fig. 59 shows the air temperature between the layers of *cross section 2*. The first two graphs are similar to the ones of *cross section 1*. The third and fourth graphs present similar curves. The curves plotted in the third graph are more flat compared to the corresponding ones of *cross section 1* and range from about 15 °C to 25 °C.

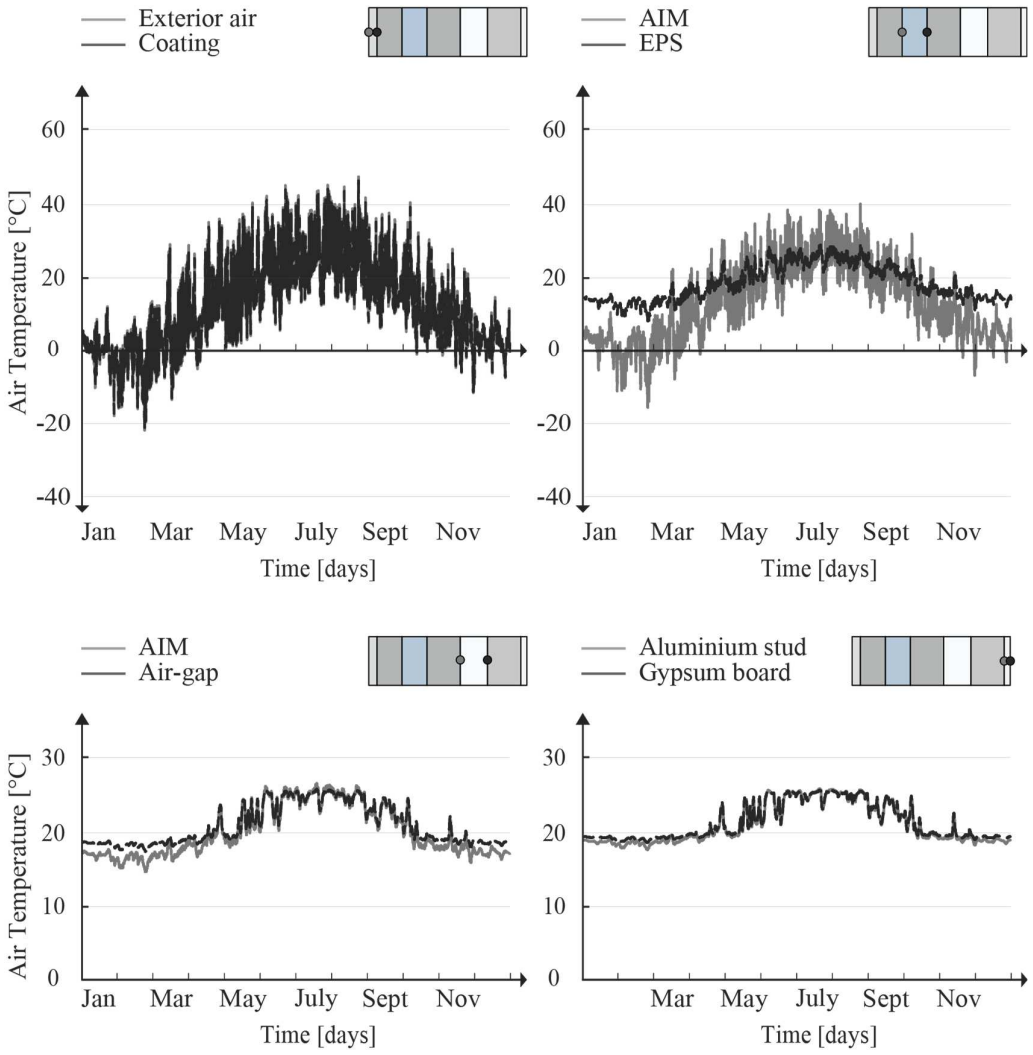

Fig. 59. Air temperature in the proposed panel, *cross section 2*.

Fig. 60 shows the relative humidity between the layers of *cross section 1*. The relative humidity reached a value of 100% on the exterior surface in conjunction with the main rainfall events. Between the weather-resistant coating and the external layer of AIM, the highest value of relative humidity was about 75% and was experienced in January. Between the AIM and the EPS, the relative humidity reached a highest value of about 80% in March. Between the EPS and the interior layer of AIM, it did not experience values greater than 70%. Between the interior layer of AIM and the air-gap it presented a pick of relative humidity of about 75% in January, then it slightly decreased until July and increased again from August. Finally, the mineral wool and the gypsum board had similar relative humidity and the highest value of about 60% was experienced during the summer.

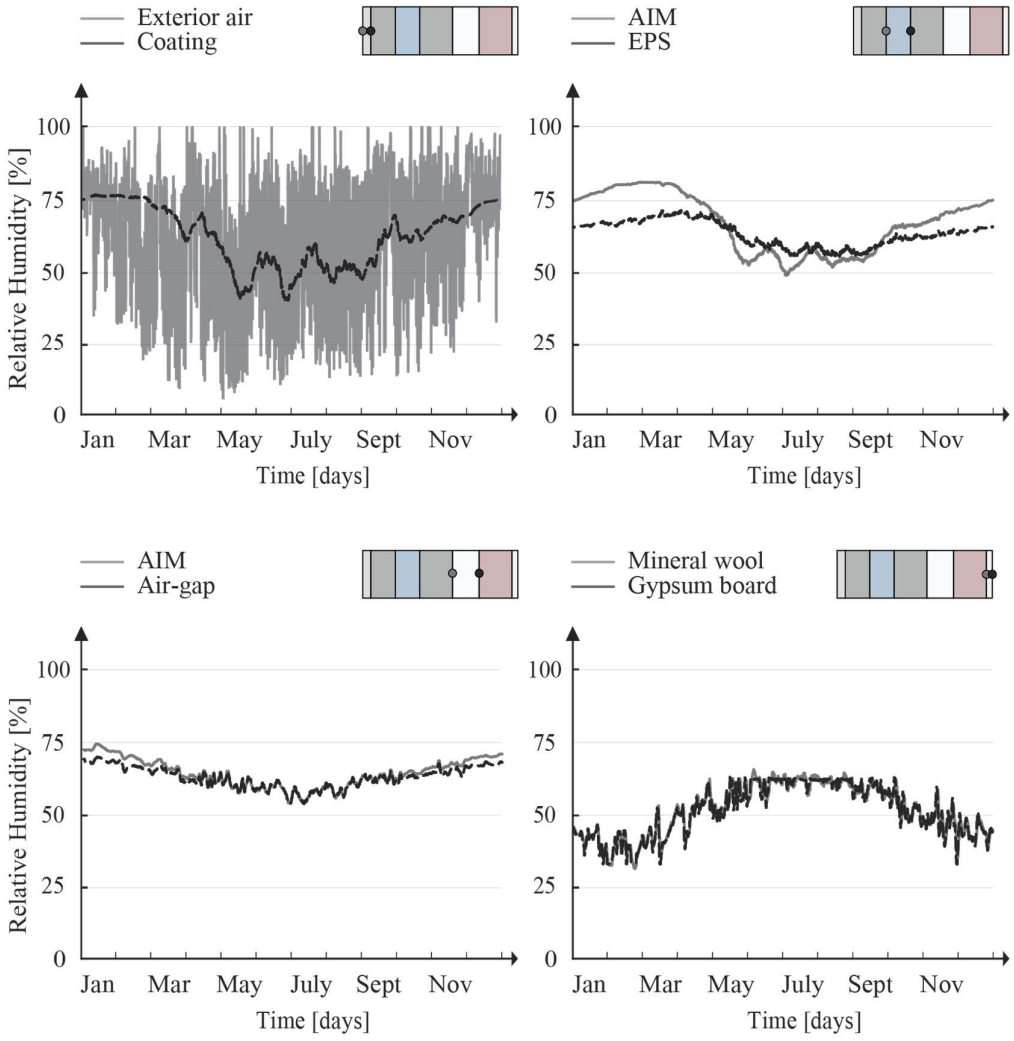

Fig. 60. Relative humidity in the proposed panel, *cross section 1*.

Fig. 61 shows the relative humidity between the layers of *cross section 2*. The results were similar to the ones of *cross section 1*. The relative humidity between the EPS and the interior layer of AIM was lower than the one of the *cross section 1* during the winter. Similarly, it was lower between the AIM layer and the air-gap as well as between the air-gap and the aluminium stud. Finally, the curves of relative humidity plotted in the fourth graph were similar to the ones of *cross section 1*.

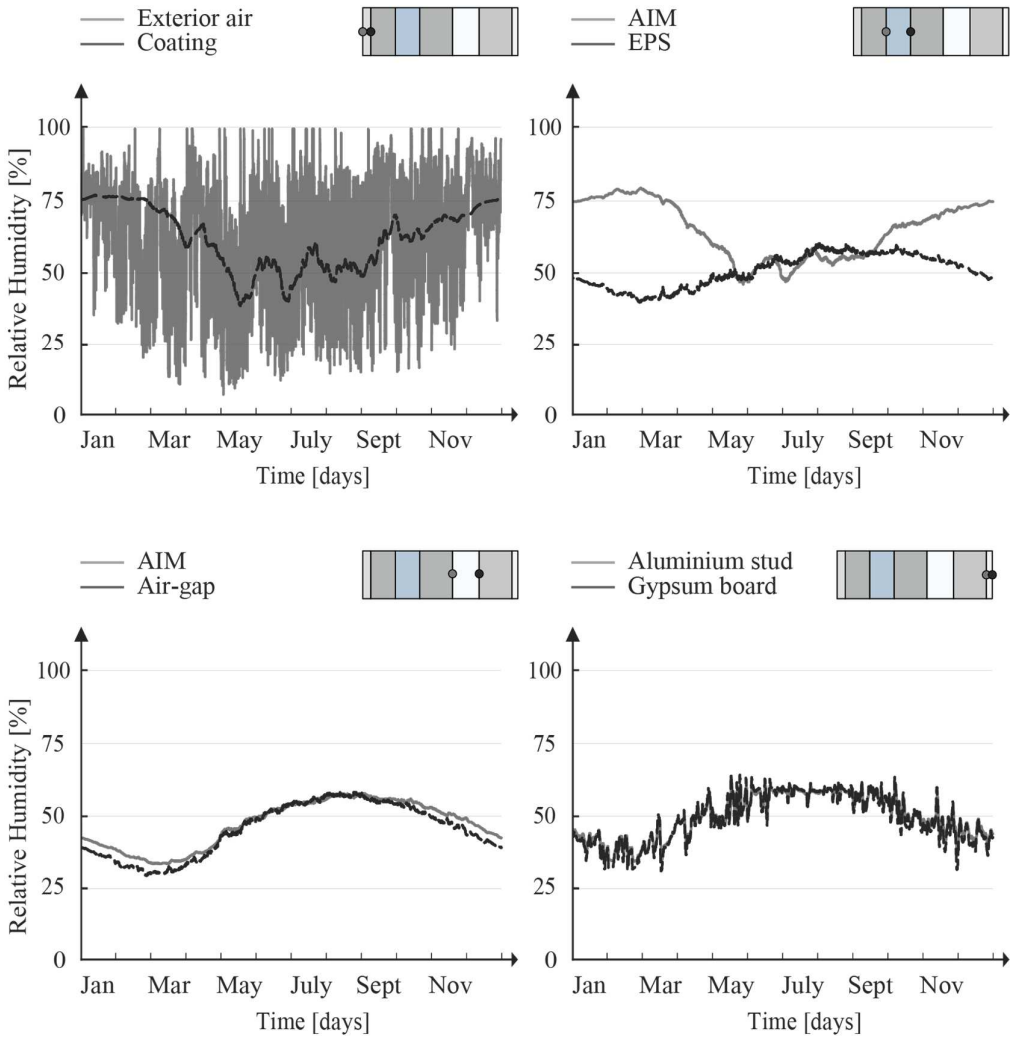

Fig. 61. Relative humidity in the proposed panel, *cross section 2*.

6.6 Discussion of the hygrothermal results

The U-value of the precast panel was reduced by 18% using Aerogel Incorporated Mortar instead concrete C12/15. It achieved an excellent performance with the proposed interior wall. The U-value of the entire wall halved from 0.46 W/m^2K to 0.23 W/m^2K and was reduced by 32% compared to the most performing panels commercialized, which generally have a U-value of about 0.34 W/m^2K. On the other hand, the entire wall resulted in being thick and the interior wall compromised the precast nature of the proposed panel.

The temperatures between the layers of both the cross sections showed that the expanded polystyrene stopped the most of the heat and stabilized the temperature inside the panel. On the other hand, the drop of the temperature due to the presence of the Aerogel Incorporated Mortar was below the expectative. Moreover, the aluminium studs did not represent an issue as thermal bridges. In fact, as stated before, the heat has been stopped by the external layer of expanded polystyrene. The relative humidity did not present any issue and was generally below the 80%, as the graphs show. In the *cross section 2*, it reached a value around 90% in the external level of AIM in March. However, it did not reach the value that leads to the condensation of the water, which is normally considered above 94÷95%. Finally, the water content did not represent an issue as well. It was kept below the 15% in the interior layers and only reached the 50% in the weather-resistant layer, in conjunction with the main rainfall events.

Design and detailing panels require a lot of work. Many aspects of the proposed panel must be still studied or improved. For example, the structural design was not considered. Steel bars were not designed and their effects on the hygrothermal analysis were neglected. Moreover, the compressive strength of the AIM precast panel was lower than the one of the commercialized panels. However, solutions such as fiberglass reinforcements or amphiphilic materials could improve the compressive strength. Finally, a more detailed analysis can be done considering more properties of the materials involved in the simulations. For instance, the porosity, the diffusion resistance factor, and the thermal capacity could be entered by hand instead of being taken from similar materials collected in the material database.

Conclusions

The use of efficient insulating materials reduces the heat losses through the envelopes and allow energy savings in buildings. Many efforts have been done to develop highly insulating materials and reduce the thermal transmittance of envelopes.

Aerogels are nano insulation materials and have a thermal conductivity at an ambient pressure of 0.013÷0.014 W/mK. Aerogel-based products are used in roofs, facades, and windows due to their thermal and optical performances. For example, opaque aerogel panels and blankets are used as insulation layers for building walls and transparent aerogels are employed in glazing windows. However, aerogels are still expensive as the high costs of production and traditional materials still dominate the market, since they have better performances per unit cost. Hence, many current studies on aerogels work toward reduced production costs and optimized applications in buildings.

In the present research, aerogel-based renders are presented. Mixtures of Aerogel Incorporated Plaster and Aerogel Incorporated Mortar were prepared and tested in the laboratories of the Ryerson University. The thermal conductivity of the mixtures was tested by means of a heat flow meter apparatus. Moreover, the mechanical strength and the permeability of Aerogel Incorporated Mortars were tested. Overall, 16 different mixtures and 142 samples were examined.

The preparation of the samples of *Aerogel Incorporated Plaster* involved two different types of hydraulic lime, to which aerogel was added. Also, some samples of plaster were cast by using a hydraulic lime that already contained particles of aerogel. Overall, 11 mixtures and 77 samples of Aerogel Incorporated Plasters were cast and tested. The aerogel permitted to reduce the thermal conductivity by more than 80%. The lowest value of thermal conductivity was about 0.028 W/mK. According to Buratti et al. [10], Aerogel Incorporated Plasters are not only insulating but also transpiring. However, the permeability of the samples of Aerogel Incorporated Plasters was not tested and further studies must investigate it. An important aspect of this research is that Aerogel Incorporated Plasters could be an unobtrusive and sustainable solution for conservation and retrofitting of Italian listed buildings. In fact, they would permit to achieve lower servicing costs and energy savings. Moreover, they could be used for non-planar surfaces, which are common situations in old buildings.

The mixtures of *Aerogel Incorporated Mortar* were designed along with the Civil Department at Ryerson University, which gave support for preparing the mix designs. The proposed

mixtures can be widely improved and represent a path that leads to the production of *Aerogel Incorporated Concrete*. However, it seemed to be more logical to proceed adding to the mixtures, only fine aggregates and produce mortars. Adding coarse aggregates would have required to play around with one more parameter as well as prepare and test much more mixtures. Overall, 5 mixtures and 65 samples of Aerogel Incorporated Mortar were prepared. While the control mixture of mortar had a thermal conductivity of 0.28 W/mK and a compressive strength of 50.3 MPa, the mixture of mortar with an addition of 36 vol.% of aerogel halved the thermal conductivity to 0.14 W/mK and reduced the compressive strength to 4.1 MPa. Also, the density almost halved from 2066 kg/m^3 to 1229 kg/m^3, which is an important result since a lightweight material comports lower dead loads to the structure. However, the samples of Aerogel Incorporated Mortar presented low compressive strengths. Hence, a way forward should study how to incorporate amphiphilic materials or fibres in the mixtures. Moreover, this study attempted to go further and fill certain gaps, such as the definition of the permeability of Aerogel Incorporated Mortars. Only preliminary and qualitative results were achieved and showed that the material does not seem to be permeable. However, it is necessary to understand if the low permeability was due to the presence of the aerogel or to the compactness of the samples caused by the presence of only fine aggregates. A quantitative analysis with the aim to define the exact value of permeability must be done in future studies. Similarly, other important properties must be investigated, such as the porosity and the thermal capacity.

Finally, the application of Aerogel Incorporated Mortars to the case study of a precast panel is presented in chapter 6. It was one of the applications of Aerogel Incorporated Mortars among other suitable solutions, such as screeds and interior walls between different environments. The thermal transmittance of the proposed panel was reduced by 18% compared to the commercialized panels, which suggested that energy savings and reduced costs during the lifetime of the building could be achieved. On the other hand, it would be possible to maintain the thermal performance of standard panels while reducing the thickness of the wall and achieving space saving, that is more square footage. The hygrothermal analysis of the panel was done by using the *WUFI Pro software*. The temperature and the relative humidity between each layer of the panel as well as the water content of the materials were considered in the analysis. The test results indicated that there are no issues related to condensation of water or water transport.

References

[1] T. Herzog, “World Greenhouse Gas Emissions in 2005,” *World Resour. Inst.*, 2009.

[2] E. Cuce, P. M. Cuce, C. J. Wood, and S. B. Riffat, “Toward aerogel based thermal superinsulation in buildings: A comprehensive review,” *Renew. Sustain. Energy Rev.*, vol. 34, pp. 273–299, 2014.

[3] E. Cuce, P. M. Cuce, C. J. Wood, and S. B. Riffat, “Optimizing insulation thickness and analysing environmental impacts of aerogel-based thermal superinsulation in buildings,” *Energy Build.*, vol. 77, pp. 28–39, 2014.

[4] N. Caldeira, K. J. Atul, and M. I. Hoffert, “Climate Sensitivity Uncertainty and the Need for Energy Without CO2 Emission,” vol. 299, no. 5615, pp. 2052–2054, 2003.

[5] U. Berardi, “A cross-country comparison of the building energy consumptions and their trends,” *Resour. Conserv. Recycl.*, no. April, 2016.

[6] R. Baetens, B. P. Jelle, and A. Gustavsen, “Aerogel insulation for building applications: A state-of-the-art review,” *Energy Build.*, vol. 43, pp. 761–769, 2010.

[7] B. P. Jelle, “Traditional, state-of-the-art and future thermal building insulation materials and solutions - Properties, requirements and possibilities,” *Energy Build.*, vol. 43, no. 10, pp. 2549–2563, 2011.

[8] B. P. Jelle, A. Gustavsen, and R. Baetens, “The path to the high performance thermal building insulation materials and solutions of tomorrow,” *J. Build. Phys.*, vol. 34, no. 2, pp. 99–123, 2016.

[9] A. V. Rao and S. D. Bhagat, “Synthesis and physical properties of TEOS-based silica aerogels prepared by two step (acid-base) sol-gel process,” *Solid State Sci.*, vol. 6, no. 9, pp. 945–952, 2004.

[10] C. Buratti, E. Moretti, and E. Belloni, “Aerogel Plasters for Building Energy Efficiency,” vol. Nano and B, no. 2, pp. 17–40, 2016.

[11] I. Najjar, “Aerogel – A Promising Building Material for Sustainable Buildings,” *Am.*

J. Chem. Sci., vol. 2, no. 3, pp. 4–10, 2012.

[12] N. Shukla, A. Fallahi, and J. Kosny, "Aerogel thermal insulation - Technology review and cost study for building enclosure applications," *ASHRAE Trans.*, vol. 120, no. 1, pp. 294–307, 2014.

[13] A. Soleimani Dorcheh and M. H. Abbasi, "Silica aerogel; synthesis, properties and characterization," *J. Mater. Process. Technol.*, vol. 199, no. 1, pp. 10–26, 2008.

[14] G. Wei, Y. Liu, X. Zhang, F. Yu, and X. Du, "Thermal conductivities study on silica aerogel and its composite insulation materials," *Int. J. Heat Mass Transf.*, vol. 54, no. 11–12, pp. 2355–2366, 2011.

[15] S. Hæreid, E. Nilsen, and M. A. Einarsrud, "Properties of silica gels aged in TEOS," *J. Non. Cryst. Solids*, vol. 204, pp. 228–234, 1996.

[16] S. S. Kistler, "Coherent expanded aerogels," *J. Phys. Chem.*, vol. 1, pp. 52–64, 1931.

[17] "ASTM D3766 Standard Terminology Relating to Catalysts and Catalysis," vol. 8, pp. 26–27, 2012.

[18] T. Gao, B. P. Jelle, A. Gustavsen, and S. Jacobsen, "Aerogel-incorporated concrete: An experimental study," *Constr. Build. Mater.*, vol. 52, pp. 130–136, 2014.

[19] L. W. Hrubesh, "Aerogel applications," *J. Non. Cryst. Solids*, vol. 225, pp. 335–342, 1998.

[20] T. Woignier and J. Phalippou, "Skeletal density of silica aerogels," vol. 93, no. 1, pp. 17–21, 1987.

[21] A. V. Rao, G. M. Pajonk, S. D. Bhagat, and P. Barboux, "Comparative studies on the surface chemical modification of silica aerogels based on various organosilane compounds of the type RnSiX4−n," *J. Non. Cryst. Solids*, vol. 350, pp. 216–223, 2004.

[22] G. Biesmans, D. Randall, E. Francais, and M. Perrut, "Polyurethane-based organic aerogels' thermal performance," *J. Non. Cryst. Solids*, vol. 225, pp. 36–40, 1998.

[23] J. K. Lee, G. L. Gould, and W. Rhine, "Polyurea based aerogel for a high performance thermal insulation material," *J. Sol-Gel Sci. Technol.*, vol. 49, no. 2, pp. 209–220, 2009.

[24] M. Reim, G. Reichenauer, A. Beck, and J. Fricke, "Silica-aerogel granulate –

Structural, optical and thermal properties," *J. Non. Cryst. Solids*, vol. 350, pp. 358–363, 2004.

[25] A. C. Pierre and A. Rigacci, "SiO2 Aerogels," vol. Aerogels H, no. 2, pp. 21–45, 2011.

[26] I. Adachi, S. Fratina, Y. Unno, and S. Yamamoto, "Study of highly transparent silica aerogel as a RICH radiator," *Nucl. Instruments Methods Phys. Res.*, vol. 553, no. 1, pp. 146–151, 2005.

[27] J. Lefebvre, A. Leblanc, B. Genestie, T. Chartier, and A. Lavie, "Acoustic properties of aerogel encapsulated by macroporous cellulose," in *23rd international congress on sound and vibration, Athens*, 2016.

[28] M. Schmidt and F. Schwertfeger, "Applications for silica aerogel products," *J. Non. Cryst. Solids*, vol. 225, pp. 364–368, 1998.

[29] R. Merget, T. Bauer, R. Breitstadt, and T. Bruening, "Health hazards due to the inhalation of amorphous silica.," *Arch. Toxicol.*, vol. 75, no. 11–12, pp. 625–634, 2002.

[30] "Aspen Aerogels Industrial Aerogel Insulation." [Online]. Available: http://www.aerogel.com/products-and-solutions/overview/#Refining.

[31] M. Koebel, A. Rigacci, and P. Achard, "Aerogel-based thermal superinsulation: An overview," *J. Sol-Gel Sci. Technol.*, vol. 63, no. 3, pp. 315–339, 2012.

[32] M. Ibrahim, P. H. Biwole, P. Achard, E. Wurtz, and G. Ansart, "Building envelope with a new aerogel-based insulating rendering: Experimental and numerical study, cost analysis, and thickness optimization," *Appl. Energy*, vol. 159, pp. 490–501, 2015.

[33] S. Ng, B. P. Jelle, L. I. C. Sandberg, T. Gao, and O. H. Wallevik, "Experimental investigations of aerogel-incorporated ultra-high performance concrete," *Constr. Build. Mater.*, vol. 77, pp. 307–316, 2015.

[34] C. Buratti, E. Moretti, E. Belloni, and F. Agosti, "Development of innovative aerogel based plasters: Preliminary thermal and acoustic performance evaluation," *Sustain.*, vol. 6, no. 9, pp. 5839–5852, 2014.

[35] S. Kim, J. Seo, J. Cha, and S. Kim, "Chemical retreating for gel-typed aerogel and insulation performance of cement containing aerogel," *Constr. Build. Mater.*, vol. 40, pp. 501–505, 2013.

[36] S. Fickler, B. Milow, L. Ratke, M. Schnellenbach-Held, and T. Welsch, “Development of High Performance Aerogel Concrete,” *Energy Procedia*, vol. 78, pp. 406–411, 2015.

[37] L. Ratke, “Herstellung und Eigenschaften eines neuen Leichtbetons: Aerogelbeton,” *Beton- und Stahlbetonbau*, vol. 103, no. 4, pp. 236–243, 2008.

[38] Cabot, “Product data sheet Cabot Aerogel Particles P300,” 2013. [Online]. Available: http://www.cabotcorp.com/~/media/product-documents/datasheets/datasheet-aerogel-p300pdf.pdf.

[39] U. Berardi, “The development of a monolithic aerogel glazed window for an energy retrofitting project,” *Appl. Energy*, vol. 154, no. June, pp. 603–615, 2015.

[40] Fixit AG, “Product data sheet Fixit 222 aerogel high-performance insulating plaster,” 2013. [Online]. Available: http://www.fixit.ch/aerogel/pdf/Fixit_222_Aerogel_Verarbeitungsrichtlinien_A4_EN.pdf.

[41] CHIRAEMA s.r.l., “Product data sheet Calce idraulica.” [Online]. Available: http://www.chiraema.it/genera_pdf.php?idp=34.

[42] TransMineral USA Inc., “Product data sheet Saint Astier.” [Online]. Available: http://www.limes.us/wp-content/uploads/pdfs/NHL35-data.pdf.

[43] “CAN/CSA-A3001-13 - Cementitious Materials Used in Concrete,” 2014.

[44] CRH Canada Group Inc., “Product data sheet of Anlegg cement.”

[45] LafargeHolcim, “Report data sheet of the aggregates.” .

[46] “ASTM C260 / C260M - 10a (2016) Standard Specification for Air- Entraining Admixtures for Concrete,” *ASTM Int.*, vol. 04.02 Conc, 2016.

[47] “ASTM C518-15 - Standard test method for steady-state thermal transmission properties by means of the heat flow meter apparatus,” *ASTM Int.*, vol. ASTM Volum, 2015.

[48] “ASTM C1017 / C1017M - 13e1 - Standard Specification for Chemical Admixtures for Use in Producing Flowing Concrete,” *ASTM Int.*, vol. 04.02 Conc, 2013.

[49] “ASTM C109/C109M - Standard Test Method for Compressive Strength of Hydraulic

Cement Mortars," *ASTM Int.*, vol. 4.

[50] Netzsch Group, "Product data sheet heat flow meter thermal conductivity instrumentation." [Online]. Available: https://www.netzsch-thermal-analysis.com/en/products-solutions/thermal-diffusivity-conductivity/hfm-436-lambda/.

[51] S. Arabuli, V. Vlasenko, A. Havelka, and Z. Kus, "Analysis of modern methods for measuring vapor permeability properties of textiles," *Proc. 7th Int. Conf.*, pp. 1–6, 2010.

[52] Fraunhofer-Gesellschaft, "WUFI manual," 2016.

[53] "Hepworth Art Gallery in Wakefield (UK) designed by David Chipperfield." [Online]. Available: https://davidchipperfield.com/project/the_hepworth_wakefield.

Appendix

Appendix 1: weight and density of the samples of plaster

Table 37. Weight and density of the samples of plaster.

Sample	Dry weight [g]	Dry density [kg/m^3]
Pure Fixit #1	98	217.78
Pure Fixit #2	120	266.67
Pure Fixit #3	100	222.22
Pure Fixit #4	94	208.89
Pure Fixit #5	116	257.78
Pure Fixit #6	116	257.78
Pure Fixit #7	116	257.78
Fixit + 15% aerogel #1	92	204.44
Fixit + 15% aerogel #2	94	208.89
Fixit + 15% aerogel #3	92	204.44
Fixit + 15% aerogel #4	94	208.89
Fixit + 15% aerogel #5	88	195.56
Fixit + 15% aerogel #6	90	200.00
Fixit + 15% aerogel #7	92	204.44
Fixit + 25% aerogel #1	88	195.56
Fixit + 25% aerogel #2	90	200.00
Fixit + 25% aerogel #3	90	200.00
Fixit + 25% aerogel #4	90	200.00
Fixit + 25% aerogel #5	88	195.56
Fixit + 25% aerogel #6	92	204.44
Pure Calce Idraulica #1	478	1062.22
Pure Calce Idraulica #2	468	1040.00
Pure Calce Idraulica #3	520	1155.56
Pure Calce Idraulica #4	526	1168.89
Pure Calce Idraulica #5	524	1164.44

Pure Calce Idraulica #6	498	1106.67
Pure Calce Idraulica #7	482	1071.11
Calce Idraulica + 25% aerogel #1	346	768.89
Calce Idraulica + 25% aerogel #2	324	720.00
Calce Idraulica + 25% aerogel #3	310	688.89
Calce Idraulica + 25% aerogel #4	348	773.33
Calce Idraulica + 25% aerogel #5	346	768.89
Calce Idraulica + 25% aerogel #6	312	693.33
Calce Idraulica + 50% aerogel #1	226	502.22
Calce Idraulica + 50% aerogel #2	226	502.22
Calce Idraulica + 50% aerogel #3	230	511.11
Calce Idraulica + 50% aerogel #4	226	502.22
Calce Idraulica + 50% aerogel #5	220	488.89
Calce Idraulica + 50% aerogel #6	222	493.33
Calce Idraulica + 50% aerogel #7	228	506.67
Calce Idraulica + 70% aerogel #1	116	257.78
Calce Idraulica + 70% aerogel #2	120	266.67
Calce Idraulica + 70% aerogel #3	116	257.78
Pure Saint Astier Plaster #1	370	822.22
Pure Saint Astier Plaster #2	356	791.11
Pure Saint Astier Plaster #3	588	1306.67
Pure Saint Astier Plaster #4	524	1164.44
Pure Saint Astier Plaster #5	564	1253.33
Pure Saint Astier Plaster #6	584	1297.78
Pure Saint Astier Plaster #7	514	1142.22
Saint Astier + 25% aerogel #1	334	742.22
Saint Astier + 25% aerogel #2	318	706.67
Saint Astier + 25% aerogel #3	318	706.67
Saint Astier + 25% aerogel #4	326	724.44
Saint Astier + 25% aerogel #5	324	720.00
Saint Astier + 25% aerogel #6	330	733.33
Saint Astier + 50% aerogel #1	232	515.56
Saint Astier + 50% aerogel #2	242	537.78
Saint Astier + 50% aerogel #3	230	511.11
Saint Astier + 50% aerogel #4	230	511.11

Saint Astier + 50% aerogel #5	230	511.11
Saint Astier + 50% aerogel #6	228	506.67
Saint Astier + 50% aerogel #7	238	528.89
Saint Astier + 70% aerogel #1	140	311.11
Saint Astier + 70% aerogel #2	136	302.22
Saint Astier + 70% aerogel #3	138	306.67

Appendix 2: thermal properties of the samples of plaster

Table 38. Characterization of the samples of plaster at 23.9 °C.

Sample	*Pure Fixit #2*		
Date	December 12th, 2016		
Mean temperature [˚C]	11.12	20.50	30.01
Delta [˚C]	20.25	20.11	19.94
Thermal Conductivity [W/mK]	0.0321	0.0326	0.0332
Thermal Resistance [m^2K/W]	0.6416	0.6343	0.6245
Thickness [cm]	2.060	2.067	2.073
Temperature Gradient [K/m]	982.86	972.80	961.76
Test duration [hh:mm]	01:23	00:55	00:55
Mean thermal conductivity at 23.9 °C [W/mK]		0.0328	
Mean thermal resistance at 23.9 °C [m^2K/W]		0.6316	
Mean thickness at 23.9 °C [cm]		2.0666	

Sample	*Pure Fixit #3*		
Date	December 20th, 2016		
Mean temperature [˚C]	9.52	18.73	30.40
Delta [˚C]	20.09	19.95	19.93
Thermal Conductivity [W/mK]	0.0309	0.0315	0.0322
Thermal Resistance [m^2K/W]	0.6639	0.6532	0.6406
Thickness [cm]	2.0525	2.0572	2.0619
Temperature Gradient [K/m]	978.75	969.74	966.50
Test duration [hh:mm]	01:20	00:59	01:08
Mean thermal conductivity at 23.9 °C [W/mK]		0.0317	
Mean thermal resistance at 23.9 °C [m^2K/W]		0.6472	
Mean thickness at 23.9 °C [cm]		0.0579	

Sample	*Fixit + 15% aerogel #1*		
Date	November 30th, 2016		
Mean temperature [˚C]	10.40	19.74	29.15
Delta [˚C]	19.79	19.65	19.46
Thermal Conductivity [W/mK]	0.0269	0.0274	0.0280
Thermal Resistance [m^2K/W]	0.7852	0.7722	0.7582
Thickness [cm]	2.114	2.119	2.124
Temperature Gradient [K/m]	936.22	927.26	916.21
Test duration [hh:mm]	01:38	00:58	00:55
Mean thermal conductivity at 23.9 °C [W/mK]		0.0277	
Mean thermal resistance at 23.9 °C [m^2K/W]		0.7665	
Mean thickness at 23.9 °C [cm]		2.1196	

Sample	*Fixit + 15% aerogel #4*		
Date	December 2nd, 2016		
Mean temperature [˚C]	10.02	19.35	28.78
Delta [˚C]	20.82	20.70	20.50
Thermal Conductivity [W/mK]	0.0267	0.0272	0.0278
Thermal Resistance [m^2K/W]	0.7757	0.7641	0.7501
Thickness [cm]	2.075	2.080	2.088
Temperature Gradient [K/m]	1003.59	994.71	982.04
Test duration [hh:mm]	01:16	00:55	00:57
Mean thermal conductivity at 23.9 °C [W/mK]		0.0275	
Mean thermal resistance at 23.9 °C [m^2K/W]		0.7584	
Mean thickness at 23.9 °C [cm]		2.0809	

Sample	*Fixit + 25% aerogel #1*		
Date	December 12th, 2016		
Mean temperature [˚C]	11.21	20.5	30.01
Delta [˚C]	20.33	20.19	20.00
Thermal Conductivity [W/mK]	0.0269	0.0273	0.0278
Thermal Resistance [m^2K/W]	0.7586	0.7487	0.7359
Thickness [cm]	2.0377	2.0425	2.0480
Temperature Gradient [K/m]	997.44	988.70	976.70
Test duration [hh:mm]	01:21	00:58	00:59
Mean thermal conductivity at 23.9 °C [W/mK]		0.0275	
Mean thermal resistance at 23.9 °C [m^2K/W]		0.7451	
Mean thickness at 23.9 °C [cm]		2.0423	

Sample	*Fixit + 25% aerogel #2*		
Date	December 2nd, 2016		
Mean temperature [˚C]	10.11	10.11	10.11
Delta [˚C]	20.82	20.82	20.82
Thermal Conductivity [W/mK]	0.0267	0.0267	0.0267
Thermal Resistance [m^2K/W]	0.7692	0.7692	0.7692
Thickness [cm]	2.050	2.050	2.050
Temperature Gradient [K/m]	1015.41	1015.41	1015.41
Test duration [hh:mm]	01:23	01:23	01:23
Mean thermal conductivity at 23.9 °C [W/mK]		0.0275	
Mean thermal resistance at 23.9 °C [m^2K/W]		0.7518	
Mean thickness at 23.9 °C [cm]		2.0552	

Sample	*Pure Calce Idraulica #3*		
Date	December 20th, 2016		
Mean temperature [˚C]	10.22	18.44	30.23
Delta [˚C]	20.02	20.07	20.00
Thermal Conductivity [W/mK]	0.1755	0.1783	0.1824
Thermal Resistance [m^2K/W]	0.1210	0.1194	0.1172
Thickness [cm]	2.1243	2.1291	2.1378
Temperature Gradient [K/m]	942.36	942.79	935.43
Test duration [hh:mm]	01:29	01:26	01:23
Mean thermal conductivity at 23.9 °C [W/mK]		0.1792	
Mean thermal resistance at 23.9 °C [m^2K/W]		0.1183	
Mean thickness at 23.9 °C [cm]		2.1300	

Sample	*Pure Calce Idraulica #7*		
Date	December 6th, 2016		
Mean temperature [˚C]	11.38	20.78	30.23
Delta [˚C]	18.47	18.30	18.09
Thermal Conductivity [W/mK]	0.1331	0.1379	0.1420
Thermal Resistance [m^2K/W]	0.1634	0.1580	0.1537
Thickness [cm]	2.176	2.179	2.183
Temperature Gradient [K/m]	849.16	840.15	828.77
Test duration [hh:mm]	01:29	01:29	01:26
Mean thermal conductivity at 23.9 °C [W/mK]		0.1398	
Mean thermal resistance at 23.9 °C [m^2K/W]		0.1532	
Mean thickness at 23.9 °C [cm]		2.1785	

Sample	*Calce Idraulica + 25% aerogel #1*		
Date	November 30th, 2016		
Mean temperature [˚C]	11.58	21.82	30.07
Delta [˚C]	19.89	19.91	20.03
Thermal Conductivity [W/mK]	0.1115	0.1139	0.1162
Thermal Resistance [m^2K/W]	0.1917	0.1881	0.1847
Thickness [cm]	2.137	2.142	2.146
Temperature Gradient [K/m]	930.80	929.23	933.28
Test duration [hh:mm]	00:58	00:55	01:20
Mean thermal conductivity at 23.9 °C [W/mK]		0.1157	
Mean thermal resistance at 23.9 °C [m^2K/W]		0.1874	
Mean thickness at 23.9 °C [cm]		2.1415	

Sample	*Calce Idraulica + 25% aerogel #3*		
Date	November 30th, 2016		
Mean temperature [˚C]	9.00	20.13	30.6
Delta [˚C]	19.99	20.04	19.90
Thermal Conductivity [W/mK]	0.1107	0.1124	0.1174
Thermal Resistance [m^2K/W]	0.1761	0.1740	0.1670
Thickness [cm]	1.949	1.955	1.961
Temperature Gradient [K/m]	1025.59	1024.96	1014.75
Test duration [hh:mm]	01:09	01:31	00:30
Mean thermal conductivity at 23.9 °C [W/mK]		0.1145	
Mean thermal resistance at 23.9 °C [m^2K/W]		0.1733	
Mean thickness at 23.9 °C [cm]		1.9551	

Sample	*Calce Idraulica + 50% aerogel #5*		
Date	December 21st, 2016		
Mean temperature [˚C]	8.18	20.95	30.43
Delta [˚C]	20.23	19.91	19.71
Thermal Conductivity [W/mK]	0.0673	0.0687	0.0694
Thermal Resistance [m^2K/W]	0.3009	0.2907	0.2939
Thickness [cm]	2.0242	1.9957	2.0387
Temperature Gradient [K/m]	999.20	979.48	966.71
Test duration [hh:mm]	01:08	01:12	00:54
Mean thermal conductivity at 23.9 °C [W/mK]		0.0688	
Mean thermal resistance at 23.9 °C [m^2K/W]		0.2883	
Mean thickness at 23.9 °C [cm]		1.9978	

Sample	*Calce Idraulica + 50% aerogel #6*		
Date	December 8th, 2016		
Mean temperature [˚C]	9.34	21.34	30.73
Delta [˚C]	20.00	19.89	19.71
Thermal Conductivity [W/mK]	0.0672	0.0683	0.0692
Thermal Resistance [m^2K/W]	0.3042	0.3002	0.2975
Thickness [cm]	2.044	2.051	2.057
Temperature Gradient [K/m]	978.12	969.35	957.88
Test duration [hh:mm]	01:17	01:02	00:44
Mean thermal conductivity at 23.9 °C [W/mK]		0.0686	
Mean thermal resistance at 23.9 °C [m^2K/W]		0.2994	
Mean thickness at 23.9 °C [cm]		2.0507	

Sample	*Calce Idraulica + 70% aerogel #n1*		
Date	December 13th, 2016		
Mean temperature [˚C]	9.37	18.61	30.14
Delta [˚C]	20.09	19.96	19.93
Thermal Conductivity [W/mK]	0.0301	0.0305	0.0311
Thermal Resistance [m^2K/W]	0.6598	0.6522	0.6414
Thickness [cm]	1.988	1.991	1.996
Temperature Gradient [K/m]	1010.45	1002.59	998.39
Test duration [hh:mm]	01:23	01:00	01:17
Mean thermal conductivity at 23.9 °C [W/mK]		0.0309	
Mean thermal resistance at 23.9 °C [m^2K/W]		0.6478	
Mean thickness at 23.9 °C [cm]		1.9915	

Sample	*Calce Idraulica + 70% aerogel #2*		
Date	December 12th, 2016		
Mean temperature [˚C]	9.16	18.42	30.06
Delta [˚C]	20.09	19.96	19.95
Thermal Conductivity [W/mK]	0.0300	0.0308	0.0317
Thermal Resistance [m^2K/W]	0.6624	0.6468	0.6313
Thickness [cm]	1.990	1.995	2.0000
Temperature Gradient [K/m]	1009.5	1000.79	997.26
Test duration [hh:mm]	01:11	01:50	01:36
Mean thermal conductivity at 23.9 °C [W/mK]		0.0312	
Mean thermal resistance at 23.9 °C [m^2K/W]		0.6375	
Mean thickness at 23.9 °C [cm]		1.9954	

Sample	*Pure Saint Astier Plaster #1*		
Date	December 20th, 2016		
Mean temperature [˚C]	10.13	20.30	30.43
Delta [˚C]	19.79	20.03	20.04
Thermal Conductivity [W/mK]	0.1895	0.1942	0.1988
Thermal Resistance [m^2K/W]	0.1105	0.1082	0.1061
Thickness [cm]	2.0943	2.1015	2.1089
Temperature Gradient [K/m]	944.79	953.25	950.36
Test duration [hh:mm]	01:44	01:55	01:48
Mean thermal conductivity at 23.9 °C [W/mK]		0.1969	
Mean thermal resistance at 23.9 °C [m^2K/W]		0.1074	
Mean thickness at 23.9 °C [cm]		2.1013	

Sample	*Pure Saint Astier Plaster #2*		
Date	December 15th, 2016		
Mean temperature [˚C]	10.11	20.38	30.34
Delta [˚C]	19.78	20.06	20.07
Thermal Conductivity [W/mK]	0.1774	0.1827	0.1875
Thermal Resistance [m^2K/W]	0.1212	0.1180	2.0.1153
Thickness [cm]	2.1501	2.1559	2.1611
Temperature Gradient [K/m]	919.87	930.68	928.61
Test duration [hh:mm]	01:50	01:56	01:56
Mean thermal conductivity at 23.9 °C [W/mK]		0.1844	
Mean thermal resistance at 23.9 °C [m^2K/W]		0.1169	
Mean thickness at 23.9 °C [cm]		2.1556	

Sample	*Saint Astier + 25% aerogel #1*		
Date	November 4th, 2016		
Mean temperature [˚C]	10.75	20.05	31.45
Delta [˚C]	19.70	19.57	19.83
Thermal Conductivity [W/mK]	0.1187	0.1206	0.1228
Thermal Resistance [m^2K/W]	0.1782	0.1757	0.1731
Thickness [cm]	2.115	2.120	2.126
Temperature Gradient [K/m]	931.75	922.92	932.85
Test duration [hh:mm]	00:48	00:43	00:47
Mean thermal conductivity at 23.9 °C [W/mK]		0.1214	
Mean thermal resistance at 23.9 °C [m^2K/W]		0.1747	
Mean thickness at 23.9 °C [cm]		2.1202	

Sample	*Saint Astier + 25% aerogel #6*		
Date	December 1st, 2016		
Mean temperature [˚C]	8.46	21.32	30.74
Delta [˚C]	20.05	19.89	19.72
Thermal Conductivity [W/mK]	0.1135	0.1154	0.1168
Thermal Resistance [m^2K/W]	0.1878	0.1852	0.1835
Thickness [cm]	2.131	2.138	2.144
Temperature Gradient [K/m]	940.81	930.31	919.69
Test duration [hh:mm]	01:06	01:07	00:50
Mean thermal conductivity at 23.9 °C [W/mK]		0.1170	
Mean thermal resistance at 23.9 °C [m^2K/W]		0.1847	
Mean thickness at 23.9 °C [cm]		2.1373	

Sample	*Saint Astier + 50% aerogel #1*		
Date	December 21st, 2016		
Mean temperature [˚C]	9.65	18.87	30.41
Delta [˚C]	20.07	19.95	19.92
Thermal Conductivity [W/mK]	0.0688	0.0699	0.0710
Thermal Resistance [m^2K/W]	0.3040	0.2998	0.2957
Thickness [cm]	2.0913	2.0955	2.1009
Temperature Gradient [K/m]	959.51	952.04	948.11
Test duration [hh:mm]	01:13	01:06	01:22
Mean thermal conductivity at 23.9 °C [W/mK]		0.0702	
Mean thermal resistance at 23.9 °C [m^2K/W]		0.2976	
Mean thickness at 23.9 °C [cm]		2.0960	

Sample	*Saint Astier + 50% aerogel #6*		
Date	December 4th, 2016		
Mean temperature [˚C]	9.63	20.75	30.77
Delta [˚C]	20.12	19.97	19.97
Thermal Conductivity [W/mK]	0.1114	0.1131	0.1148
Thermal Resistance [m^2K/W]	0.1805	0.1783	0.1761
Thickness [cm]	2.010	2.017	2.022
Temperature Gradient [K/m]	1001.03	990.14	987.72
Test duration [hh:mm]	01:26	01:24	01:16
Mean thermal conductivity at 23.9 °C [W/mK]		0.1146	
Mean thermal resistance at 23.9 °C [m^2K/W]		0.1777	
Mean thickness at 23.9 °C [cm]		2.0165	

Sample	*Saint Astier + 70% aerogel #1*		
Date	December 8th, 2016		
Mean temperature [˚C]	11.4	20.79	30.32
Delta [˚C]	19.84	19.69	19.51
Thermal Conductivity [W/mK]	0.0352	0.0356	0.0361
Thermal Resistance [m^2K/W]	0.5765	0.5719	0.5656
Thickness [cm]	2.0289	2.0352	2.0414
Temperature Gradient [K/m]	978.04	967.26	955.87
Test duration [hh:mm]	01:34	00:52	00:59
Mean thermal conductivity at 23.9 °C [W/mK]		0.0358	
Mean thermal resistance at 23.9 °C [m^2K/W]		0.5703	
Mean thickness at 23.9 °C [cm]		2.0346	

Sample	*Saint Astier + 70% aerogel #2*		
Date	December 19th, 2016		
Mean temperature [˚C]	9.14	20.24	29.82
Delta [˚C]	20.14	19.94	19.75
Thermal Conductivity [W/mK]	0.0348	0.0350	0.0356
Thermal Resistance [m^2K/W]	0.5823	0.5747	0.5671
Thickness [cm]	2.0281	2.0130	2.0173
Temperature Gradient [K/m]	1003.19	990.57	979.21
Test duration [hh:mm]	01:29	01:15	00:58
Mean thermal conductivity at 23.9 °C [W/mK]		0.0354	
Mean thermal resistance at 23.9 °C [m^2K/W]		0.5722	
Mean thickness at 23.9 °C [cm]		2.0134	

Appendix 3: weight and density of the samples of mortar

Table 39. Weight of the samples of mortar.

Sample	Weight day 7 [g]	Weight day 28 [g]	Weight dry [g]
Standard mortar c[1]*#4*	304	-	-
Standard mortar c#5	304	-	-
Standard mortar c#6	305	-	-
Standard mortar c#7	-	309	-
Standard mortar c#8	-	306	-
Standard mortar c#9	-	309	-
Standard mortar p[2]*#1*	-	-	1056
Standard mortar p#2	-	-	1058
Standard mortar p#3	-	-	1056
Standard mortar p#4	-	-	1072
Mortar + air entraining c#4	268	-	-
Mortar + air entraining c#5	262	-	-
Mortar + air entraining c#6	266	-	-
Mortar + air entraining c#7	-	266	-
Mortar + air entraining c#8	-	265	-
Mortar + air entraining c#9	-	266	-
Mortar + air entraining p#1	-	-	922
Mortar + air entraining p#2	-	-	928
Mortar + air entraining p#3	-	-	926
Mortar + air entraining p#4	-	-	928
Mortar + 30% aerogel c#4	221	-	-
Mortar + 30% aerogel c#5	223	-	-
Mortar + 30% aerogel c#6	220	-	-
Mortar + 30% aerogel c#7	-	223	-
Mortar + 30% aerogel c#8	-	223	-
Mortar + 30% aerogel c#9	-	227	-
Mortar + 30% aerogel p#1	-	-	702
Mortar + 30% aerogel p#2	-	-	682
Mortar + 30% aerogel p#3	-	-	672
Mortar + 30% aerogel p#4	-	-	684

[1] cube
[2] parallelepipeds

Mortar + 33% aerogel c#4	199	-	-
Mortar + 33% aerogel c#5	208	-	-
Mortar + 33% aerogel c#6	205	-	-
Mortar + 33% aerogel c#7	-	216	-
Mortar + 33% aerogel c#8	-	212	-
Mortar + 33% aerogel c#9	-	207	-
Mortar + 33% aerogel p#1	-	-	766
Mortar + 33% aerogel p#2	-	-	736
Mortar + 33% aerogel p#3	-	-	726
Mortar + 33% aerogel p#4	-	-	738
Mortar + 36% aerogel c#4	183	-	-
Mortar + 36% aerogel c#5	186	-	-
Mortar + 36% aerogel c#6	177	-	-
Mortar + 36% aerogel c#7	-	192	-
Mortar + 36% aerogel c#8	-	197	-
Mortar + 36% aerogel c#9	-	192	-
Mortar + 36% aerogel p#1	-	-	712
Mortar + 36% aerogel p#2	-	-	746
Mortar + 36% aerogel p#3	-	-	718
Mortar + 36% aerogel p#4	-	-	730

Table 40. Density of the samples of mortar.

Sample	Density day 7 [kg/m^3]	Density day 28 [kg/m^3]	Density dry [kg/m^3]
Standard mortar c#4	2315.24	-	-
Standard mortar c#5	2317.83	-	-
Standard mortar c#6	2327.60	-	-
Standard mortar c#7	-	2354.37	-
Standard mortar c#8	-	2333.17	-
Standard mortar c#9	-	2359.71	-
Standard mortar p#1	-	-	2057.08
Standard mortar p#2	-	-	2060.98
Standard mortar p#3	-	-	2057.08
Standard mortar p#4	-	-	2088.25
Mortar + air entraining c#4	2044.45	-	-
Mortar + air entraining c#5	2001.96	-	-

Mortar + air entraining c#6	2029.34	-	-
Mortar + air entraining c#7	-	2031.10	-
Mortar + air entraining c#8	-	2022.56	-
Mortar + air entraining c#9	-	2027.59	-
Mortar + air entraining p#1	-	-	1796.05
Mortar + air entraining p#2	-	-	1807.74
Mortar + air entraining p#3	-	-	1803.85
Mortar + air entraining p#4	-	-	1807.74
Mortar + 30% aerogel c#4	1684.94	-	-
Mortar + 30% aerogel c#5	1701.95	-	-
Mortar + 30% aerogel c#6	1678.92	-	-
Mortar + 30% aerogel c#7	-	1704.62	-
Mortar + 30% aerogel c#8	-	1702.26	-
Mortar + 30% aerogel c#9	-	1733.99	-
Mortar + 30% aerogel p#1	-	-	1527.23
Mortar + 30% aerogel p#2	-	-	1523.33
Mortar + 30% aerogel p#3	-	-	1558.40
Mortar + 30% aerogel p#4	-	-	1519.44
Mortar + 33% aerogel c#4	1515.45	-	-
Mortar + 33% aerogel c#5	1582.96	-	-
Mortar + 33% aerogel c#6	1560.68	-	-
Mortar + 33% aerogel c#7	-	1645.58	-
Mortar + 33% aerogel c#8	-	1617.89	-
Mortar + 33% aerogel c#9	-	1577.23	-
Mortar + 33% aerogel p#1	-	-	1367.49
Mortar + 33% aerogel p#2	-	-	1328.53
Mortar + 33% aerogel p#3	-	-	1309.05
Mortar + 33% aerogel p#4	-	-	1332.43
Mortar + 36% aerogel c#4	355.63	-	-
Mortar + 36% aerogel c#5	362.72	-	-
Mortar + 36% aerogel c#6	344.13	-	-
Mortar + 36% aerogel c#7	-	1466.86	-
Mortar + 36% aerogel c#8	-	1500.35	-
Mortar + 36% aerogel c#9	-	1466.78	-
Mortar + 36% aerogel p#1	-	-	1262.30

Mortar + 36% aerogel p#2	-	-	1199.97
Mortar + 36% aerogel p#3	-	-	1219.45
Mortar + 36% aerogel p#4	-	-	1235.03

Appendix 4: compressive strength of the samples of mortar

Table 41. Compressive strength of the samples of mortar.

Sample	Compressive Strength [MPa]		
	Day 1	Day 7	Day 28
Standard mortar c#1	20.77	-	-
Standard mortar c#2	17.22	-	-
Standard mortar c#3	21.48	-	-
Standard mortar c#4	-	50.635	-
Standard mortar c#5	-	50.580	-
Standard mortar c#6	-	47.843	-
Standard mortar c#7	-	-	52.579
Standard mortar c#8	-	-	52.063
Standard mortar c#9	-	-	46.264
Mortar + air entraining c#1	19.195	-	-
Mortar + air entraining c#2	18.402	-	-
Mortar + air entraining c#3	15.982	-	-
Mortar + air entraining c#4	-	17.782	-
Mortar + air entraining c#5	-	22.298	-
Mortar + air entraining c#6	-	23.622	-
Mortar + air entraining c#7	-	-	25.007
Mortar + air entraining c#8	-	-	23.911
Mortar + air entraining c#9	-	-	26.359
Mortar + 30% aerogel c#1	5.530	-	-
Mortar + 30% aerogel c#2	5.537	-	-
Mortar + 30% aerogel c#3	5.681	-	-
Mortar + 30% aerogel c#4	-	9.701	-
Mortar + 30% aerogel c#5	-	9.598	-
Mortar + 30% aerogel c#6	-	10.566	-
Mortar + 30% aerogel c#7	-	-	11.590
Mortar + 30% aerogel c#8	-	-	11.420
Mortar + 30% aerogel c#9	-	-	10.540
Mortar + 33% aerogel c#1	2.799	-	-
Mortar + 33% aerogel c#2	2.296	-	-
Mortar + 33% aerogel c#3	2.365	-	-

Mortar + 33% aerogel c#4	-	4.854	-
Mortar + 33% aerogel c#5	-	5.109	-
Mortar + 33% aerogel c#6	-	4.606	-
Mortar + 33% aerogel c#7	-	-	m.v.[1]
Mortar + 33% aerogel c#8	-	-	5.179
Mortar + 33% aerogel c#9	-	-	5.109
Mortar + 36% aerogel c#1	0.800	-	-
Mortar + 36% aerogel c#2	0.986	-	-
Mortar + 36% aerogel c#3	m.v.[1]	-	-
Mortar + 36% aerogel c#4	-	3.282	-
Mortar + 36% aerogel c#5	-	2.751	-
Mortar + 36% aerogel c#6	-	3.048	-
Mortar + 36% aerogel c#7	-	-	4.323
Mortar + 36% aerogel c#8	-	-	4.426
Mortar + 36% aerogel c#9	-	-	3.578

[1] Missing values

Appendix 5: thermal properties of the samples of mortar

Table 42. Characterization of the samples of mortar at 23.9 °C.

Sample	*Standard mortar p#1*		
Date	December 10th, 2016		
Mean temperature [˚C]	10.50	18.27	28.27
Delta [˚C]	19.91	20.04	20.08
Thermal Conductivity [W/mK]	0.2766	0.2842	0.2966
Thermal Resistance [m^2K/W]	0.0609	0.0789	0.0758
Thickness [cm]	1.6845	2.2423	2.2480
Temperature Gradient [K/m]	889.88	893.93	893.15
Test duration [hh:mm]	01:35	01:25	01:28
Mean thermal conductivity at 23.9 °C [W/mK]		0.2907	
Mean thermal resistance at 23.9 °C [m^2K/W]		0.0771	
Mean thickness at 23.9 °C [cm]		2.2455	

Sample	*Standard mortar p#3*		
Date	December 13th, 2016		
Mean temperature [˚C]	11.68	20.95	30.43
Delta [˚C]	20.03	19.82	19.50
Thermal Conductivity [W/mK]	0.2665	0.2756	0.2860
Thermal Resistance [m^2K/W]	0.0841	0.0815	0.0788
Thickness [cm]	2.2412	2.2469	2.2520
Temperature Gradient [K/m]	893.60	882.12	865.74
Test duration [hh:mm]	01:57	01:51	01:54
Mean thermal conductivity at 23.9 °C [W/mK]		0.2781	
Mean thermal resistance at 23.9 °C [m^2K/W]		0.0807	
Mean thickness at 23.9 °C [cm]		2.2485	

Sample	*Mortar + air entraining p#1*		
Date	December 17th, 2016		
Mean temperature [˚C]	11.75	21.00	30.48
Delta [˚C]	20.37	20.18	19.93
Thermal Conductivity [W/mK]	0.2383	0.2457	0.2539
Thermal Resistance [m^2K/W]	0.0978	0.0950	0.0922
Thickness [cm]	2.3295	2.3346	2.3405
Temperature Gradient [K/m]	874.51	864.26	851.53
Test duration [hh:mm]	01:51	01:41	01:45
Mean thermal conductivity at 23.9 °C [W/mK]		0.2475	
Mean thermal resistance at 23.9 °C [m^2K/W]		0.0942	
Mean thickness at 23.9 °C [cm]		2.3364	

Sample	*Mortar + air entraining p#3*		
Date	December 10th, 2016		
Mean temperature [˚C]	10.32	20.50	29.90
Delta [˚C]	19.62	19.85	19.58
Thermal Conductivity [W/mK]	0.2429	0.2529	0.2618
Thermal Resistance [m^2K/W]	0.0948	0.0912	0.0883
Thickness [cm]	2.3014	2.3061	2.3110
Temperature Gradient [K/m]	852.40	860.64	847.39
Test duration [hh:mm]	01:58	02:16	01:44
Mean thermal conductivity at 23.9 °C [W/mK]		0.2568	
Mean thermal resistance at 23.9 °C [m^2K/W]		0.0900	
Mean thickness at 23.9 °C [cm]		2.3079	

Sample	*Mortar + 30% aerogel p#1*		
Date	December 16th, 2016		
Mean temperature [˚C]	8.94	20.89	31.55
Delta [˚C]	20.2	20.03	19.85
Thermal Conductivity [W/mK]	0.2408	0.2538	0.2645
Thermal Resistance [m^2K/W]	0.0926	0.0882	0.0849
Thickness [cm]	2.2308	2.2379	2.2456
Temperature Gradient [K/m]	905.36	894.85	884.07
Test duration [hh:mm]	00:38	01:15	00:42
Mean thermal conductivity at 23.9 °C [W/mK]		0.2555	
Mean thermal resistance at 23.9 °C [m^2K/W]		0.0871	
Mean thickness at 23.9 °C [cm]		2.2401	

Sample	*Mortar + 30% aerogel p#4*		
Date	December 5th, 2016		
Mean temperature [˚C]	9.66	20.33	31.37
Delta [˚C]	19.99	19.89	19.76
Thermal Conductivity [W/mK]	0.2009	0.2285	0.2166
Thermal Resistance [m^2K/W]	0.1148	0.1012	0.1071
Thickness [cm]	2.3061	2.3125	2.3188
Temperature Gradient [K/m]	866.60	859.95	851.99
Test duration [hh:mm]	02:44	00:37	01:34
Mean thermal conductivity at 23.9 °C [W/mK]		0.2174	
Mean thermal resistance at 23.9 °C [m^2K/W]		0.0966	
Mean thickness at 23.9 °C [cm]		2.3146	

Sample	*Mortar + 33% aerogel p#1*		
Date	December 16th, 2016		
Mean temperature [˚C]	10.81	20.55	30.54
Delta [˚C]	19.84	19.86	19.89
Thermal Conductivity [W/mK]	0.2083	0.2140	0.2191
Thermal Resistance [m^2K/W]	0.1071	0.1045	0.1024
Thickness [cm]	2.2308	2.2370	2.2435
Temperature Gradient [K/m]	889.49	887.89	886.74
Test duration [hh:mm]	02:39	01:50	01:54
Mean thermal conductivity at 23.9 °C [W/mK]		0.2144	
Mean thermal resistance at 23.9 °C [m^2K/W]		0.1037	
Mean thickness at 23.9 °C [cm]		2.2392	

Sample	*Mortar + 33% aerogel p#3*		
Date	December 6th, 2016		
Mean temperature [˚C]	10.24	19.64	29.00
Delta [˚C]	19.79	19.64	19.40
Thermal Conductivity [W/mK]	0.1790	0.1844	0.1899
Thermal Resistance [m^2K/W]	0.1249	0.1215	0.1183
Thickness [cm]	2.2366	2.2410	2.2465
Temperature Gradient [K/m]	884.76	876.26	863.62
Test duration [hh:mm]	02:15	01:37	01:36
Mean thermal conductivity at 23.9 °C [W/mK]		0.1874	
Mean thermal resistance at 23.9 °C [m^2K/W]		0.1200	
Mean thickness at 23.9 °C [cm]		2.2435	

Sample	*Mortar + 36% aerogel p#1*		
Date	December 17th, 2016		
Mean temperature [˚C]	11.59	20.85	30.36
Delta [˚C]	21.47	21.32	21.10
Thermal Conductivity [W/mK]	0.1444	0.1479	0.1513
Thermal Resistance [m^2K/W]	0.1550	0.1517	0.1488
Thickness [cm]	2.2385	2.2442	2.2519
Temperature Gradient [K/m]	958.93	949.88	937.15
Test duration [hh:mm]	01:41	01:36	01:33
Mean thermal conductivity at 23.9 °C [W/mK]		0.1498	
Mean thermal resistance at 23.9 °C [m^2K/W]		0.1516	
Mean thickness at 23.9 °C [cm]		2.2466	

Sample	*Mortar + 36% aerogel p#4*		
Date	December 7th, 2016		
Mean temperature [˚C]	10.11	19.49	28.95
Delta [˚C]	20.00	19.83	19.64
Thermal Conductivity [W/mK]	0.1419	0.1454	0.1488
Thermal Resistance [m^2K/W]	0.1580	0.1546	0.1516
Thickness [cm]	2.2418	2.2489	2.2553
Temperature Gradient [K/m]	891.99	881.91	870.63
Test duration [hh:mm]	02:24	01:39	01:35
Mean thermal conductivity at 23.9 °C [W/mK]		0.1477	
Mean thermal resistance at 23.9 °C [m^2K/W]		0.1531	
Mean thickness at 23.9 °C [cm]		2.2519	

Appendix 6: water content in the proposed precast panel

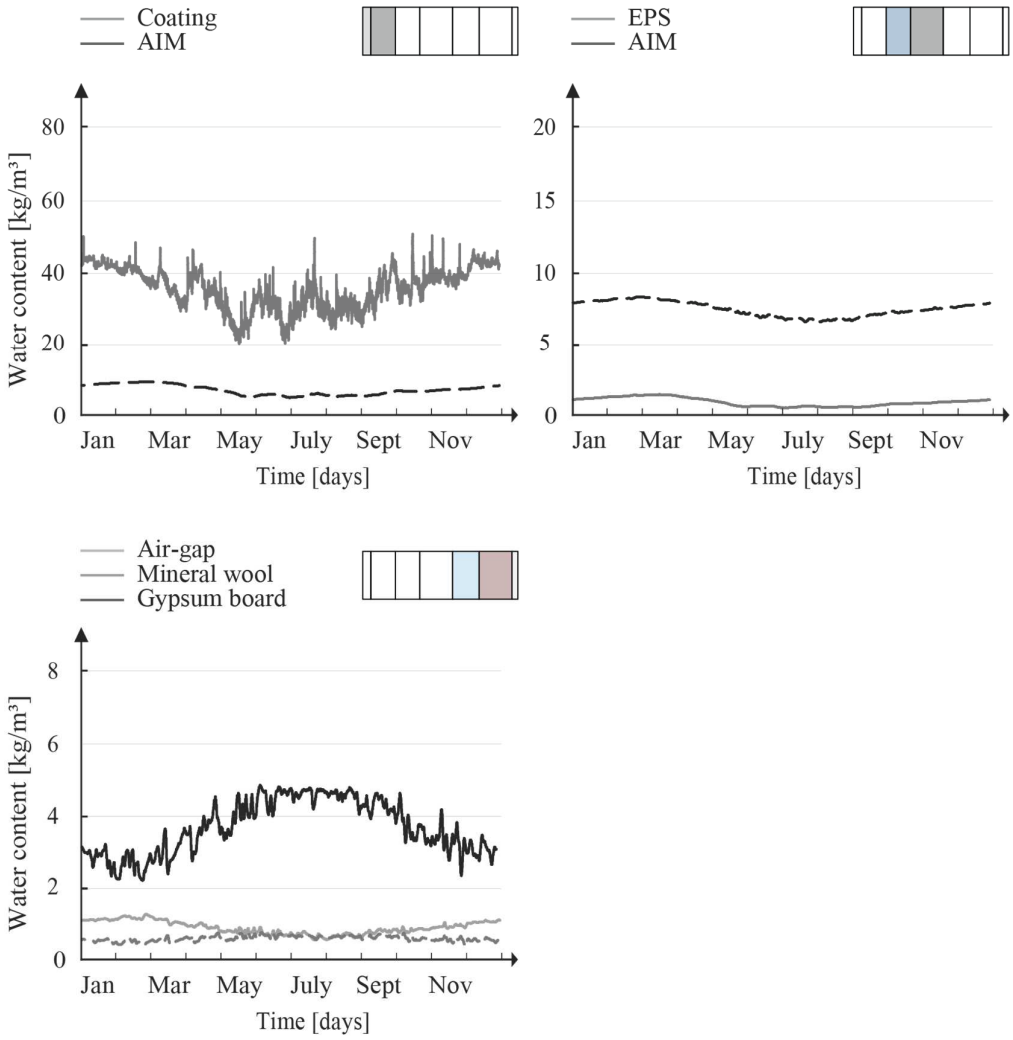

Fig. 62. Water content in the proposed precast panel, *cross section 1*.

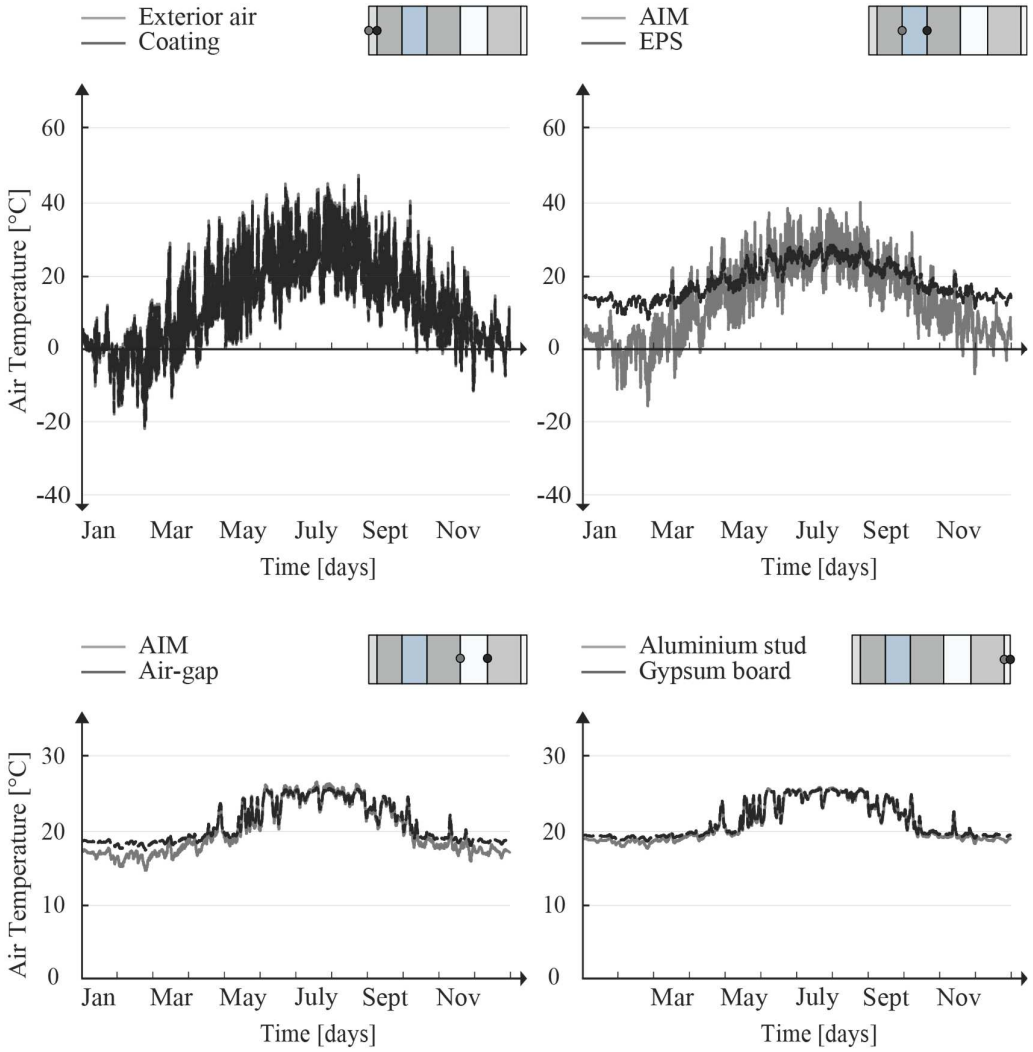

Fig. 63. Water content in the proposed precast panel, *cross section 2*.